

**Temporal Geochemical Variation Within the Koolau Shield:  
A Trace Element Perspective.**

**Shichun Huang\* (huangs@mit.edu)**

**and**

**Frederick A. Frey (fafrey@mit.edu)**

Department of Earth, Atmospheric and Planetary Sciences  
Massachusetts Institute of Technology

Corresponding author: Shichun Huang  
54-1210 EAPS  
77 Mass Ave  
Cambridge, MA 02139  
Tel: 617-253-2869  
Fax: 617-253-7102

Main text: 5,921 words  
Abstract: 159 words  
Table: 4  
Figure: 16

**Submitted to Contributions of Mineralogy and Petrology, September 22nd, 2004**

**Abstract:**

The subaerial surface of Koolau volcano is composed of Makapuu-stage shield lavas which define the well known, distinctive endmember composition for Hawaiian shield lavas, known as the Koolau component. From ~300 m to 470 m below this surface, drilling and coring by the Koolau Scientific Drilling Project shows that the Koolau shield lavas transitioned to a composition similar to Mauna Loa lavas; these Koolau lavas form the Kalihi-stage of the Koolau shield.

Among all Koolau shield lavas and within the Makapuu- and Kalihi-stages, there are strong correlations between the compositional parameters,  $\text{SiO}_2$  content (adjusted to be in equilibrium with  $\text{Fo}_{90}$  olivine), Sr/Nb, La/Nb and Th/La, with radiogenic isotope ratios of Nd, Hf and Pb. These trends show that as the shield aged there was an increasing role for a marine sediment component accompanied by  $\text{SiO}_2$ -rich (dacite) melt. Therefore a recycled oceanic crust component was increasingly important as the Koolau shield moved away from the hotspot and encountered lower temperature.

## 1.Introduction:

Although shield-stage lavas of Hawaiian volcanoes are derived from the Hawaiian hotspot, commonly inferred to be a mantle plume, many Hawaiian shields are distinct in major and trace element abundances, as well as isotopic ratios. Some of these geochemical differences may be related to melting processes, but there is no doubt that the mantle source for Hawaiian shield lavas is geochemically heterogeneous. Compositions of lavas collected from subaerial exposures of the Koolau shield on Oahu define an extreme. They are characterized by relatively high  $\text{SiO}_2$  content,  $\text{SiO}_2/\text{Fe}_2\text{O}_3^*$ ,  $\text{Al}_2\text{O}_3/\text{CaO}$ ,  $\text{La}/\text{Nb}$ ,  $\text{Sr}/\text{Nb}$ ,  $^{87}\text{Sr}/^{86}\text{Sr}$ ,  $^{187}\text{Os}/^{188}\text{Os}$ ,  $\delta^{18}\text{O}$  and low total iron and CaO contents,  $^{143}\text{Nd}/^{144}\text{Nd}$ ,  $^{176}\text{Hf}/^{177}\text{Hf}$  and  $^{206}\text{Pb}/^{204}\text{Pb}$  (e.g., *Frey et al., 1994; Roden et al., 1994; Lassiter and Hauri, 1998; Blichert-Toft et al., 1999*). These geochemical characteristics have provided support for recycled oceanic crust, including sediments, in the source of Koolau lavas.

It is also well established that there are important temporal geochemical changes within individual Hawaiian shields. At some shields there are large variations, e.g., Mauna Loa (*Rhodes and Hart, 1995; Kurz et al., 1995*), whereas at others, such as Mauna Kea, the temporal changes are relatively subtle (e.g., *Special Section of Hawaii Scientific Drilling Project in J. Geophys. Res., 1996 Vol. 101, pp11,593-pp11,864; Theme of Hawaii Scientific Drilling Project in Geochem. Geophys. Geosyst. 2003*). Hence, an important question is – **Does the entire Koolau shield have the end-member geochemical characteristics manifested by the subaerially exposed lavas?** Studies of lavas recovered from a highway (H3) tunnel (*Jackson et al., 1999*) and from the submarine landslide blocks (*Shinozaki et al., 2002; Tanaka et al., 2002*) indicate that the

geochemical characteristics of older Koolau lavas may not be similar to the surface Koolau lavas. Specifically, *Tanaka et al. (2002)* argue for a temporal transition from Mauna Kea-like to Mauna Loa-like to Koolau-like with decreasing age. However, determining the origin and relative age of lavas from landslide blocks is difficult. A more direct approach to determining temporal geochemical variations in Koolau shield lavas is drilling and coring. This goal was achieved by the Koolau Scientific Drilling Project (KSDP) which deepened and cored a ~351 m water well to a depth of ~679 m (*Haskins and Garcia, 2004*). The upper 351 m were rotary drilled and only rock chips are available, whereas nearly continuous core was recovered from the lower 328 m using a diamond drill bit. This core samples 103 subaerially erupted lava flows and one sedimentary unit. Based on petrography and compositions of whole-rocks and glasses, *Haskins and Garcia (2004)* conclude that the distinctive geochemical features of uppermost Koolau lavas (hereafter referenced as Makapuu-stage lavas) **‘form a veneer only 175-250 m thick at the drill site’**. This veneer overlies lavas with Mauna Loa-like major element compositions which *Haskins and Garcia (2004)* call the Kalihi-stage of the Koolau shield.

As part of a team effort studying the KSDP core, we report 26 trace element abundances in 91 KSDP core samples (Table 1a) analyzed by inductively coupled plasma mass spectrometry (ICP-MS); see Appendix A2 of *Huang and Frey (2003)* for procedures and discussion of accuracy and precision. We use these data, in conjunction with major element compositions and Nd-Hf-Pb isotopic ratios (*Haskins and Garcia, 2004; Fekiacova et al., in prep.; Salters et al., in prep.*), to understand the temporal evolution of Koolau shield lavas.

Makapuu-stage lavas have been studied by *Frey et al. (1994)*, who used X-ray fluorescence (XRF) and instrumental neutron activation (INAA) to obtain trace element data. In order to minimize bias caused by using different analytical methods, we re-analyzed by ICP-MS 15 Makapuu-stage lavas which have been analyzed for Sr-Nd-Pb isotopic ratios (*Roden et al., 1994*) and major and trace elements (*Frey et al., 1994*) (Table 1b).

## **2. Results: Incompatible Elements**

Abundances of incompatible elements that are immobile during alteration, such as Nb, La, Zr and Yb, are positively correlated with Th abundance for both Makapuu-stage lavas and Kalihi-stage lavas (Fig. 1a-e). Trends are linear for highly incompatible elements (Th vs La and Nb, Fig. 1a, 1b), and become convex upwards as the incompatibility of the element on the vertical axis decreases (e.g., Th vs Yb in Fig. 1d). Pb, Ba, Sr and Rb abundances are generally correlated with Th abundance; however, these trends are more scattered (Fig. 1e-h). Some of this scatter, e.g., to relative low Rb abundance, is caused by altered samples. There are significant differences between Makapuu-stage and Kalihi-stage lavas; at a given Th abundance Makapuu-stage lavas have higher La and Sr abundances than Kalihi-stage lavas (Fig. 1a, 1g).

Fig. 2 shows the primitive mantle normalized trace element abundances of Makapuu-stage and Kalihi-stage lavas. Both lava suites have been adjusted to be in equilibrium with mantle olivine composition ( $Fo_{90}$ ) to minimize the effect of crystal fractionation. The most obvious difference between the two lava suites is the relative Sr enrichment in the Makapuu-stage lavas. In contrast to the large variations in highly

incompatible elements, abundances of heavy rare earth elements are nearly constant in both Makapuu-stage and Kalihi-stage lavas (Fig. 2).

### **3. Discussion:**

#### **3.1 Effects of Post-Magmatic Alteration on Lava Compositions**

It is well established that  $K_2O/P_2O_5$  and Ba/Rb are sensitive indicators of alteration in subaerially erupted Hawaiian lavas; with increasing extents of alteration,  $K_2O/P_2O_5$  decreases and Ba/Rb increases (e.g., *Feigenson et al., 1983; Frey et al., 1991, 1994; Yang et al., 1996; Huang and Frey, 2003*). In Kalihi-stage lavas, Ba/Rb is negatively correlated with  $K_2O/P_2O_5$  and positively correlated with Loss on Ignition (L.O.I.), respectively (Fig. 3a, b), thereby reflecting K and Rb loss during post-magmatic alteration.

Sr/Nd versus  $K_2O/P_2O_5$  does not form an obvious trend (Fig. 3c); but Sr/Nd ranges to lower values at high L.O.I. (>1%) (Fig. 3d). Hence, we infer that Sr was also lost during post-magmatic alteration in these highly altered samples. Nevertheless, at a given  $K_2O/P_2O_5$  or MgO content, most Makapuu-stage lavas have higher Sr/Nd than Kalihi-stage lavas (Fig. 3c), and all have higher Sr/Nb (Fig. 4a; Fig. 6a of *Haskins and Garcia, 2004*). Therefore, the higher Sr abundance in Makapuu-stage lavas (Figs 1g, 2) is not a result of alteration or plagioclase control.

#### **3.2 The Transition from Makapuu-Stage to Kalihi-Stage Lavas: Timing and Role of Recycled Marine Sediment in the Source of Koolau Lavas**

*Haskins and Garcia* (Fig. 10, 2004) used  $Al_2O_3/CaO$  to define a change from the Makapuu-stage ( $Al_2O_3/CaO > 1.45$ ) to Kalihi-stage ( $Al_2O_3/CaO < 1.45$ ) within the

uppermost 250 m of the KSDP hole. There is, however, considerable structure in the downhole variation of  $\text{Al}_2\text{O}_3/\text{CaO}$  within the KSDP drill core. Within the upper part of the KSDP core, at a depth level inferred to be Kalihi-stage lavas, there are two groups of lavas which have  $\text{Al}_2\text{O}_3/\text{CaO}$  near this boundary. Units 4, 5, 6 and 9, 10, 12 have  $\text{Al}_2\text{O}_3/\text{CaO} = 1.42$  to 1.44 (Fig. 5a). Deeper in the core, Unit 70 has  $\text{Al}_2\text{O}_3/\text{CaO} = 1.43$  and Unit 88 has a ratio of 1.54, but among Kalihi-stage lavas, Unit 88 has the highest L.O.I. (3.65%, Fig. 3d) and it probably lost CaO during alteration.

The presence of orthopyroxene is a diagnostic petrographic characteristic of Makapuu-stage lavas (Frey *et al.*, 1994), but orthopyroxene also occurs in KSDP cored lavas classified as Kalihi-stage lavas, that is, orthopyroxene occurs in 6 of the uppermost 11 lava flows, including Units 9, 10 and 12 with high  $\text{Al}_2\text{O}_3/\text{CaO}$ , is absent in the underlying 44 lava flows, and is sporadically present in 7 of the lowermost 35 lava flows (Table 2 of Haskins and Garcia, 2004).

Surface Koolau lavas, i.e., Makapuu-stage lavas, are distinguished from other Hawaiian shield lavas by their relatively high La/Nb and Sr/Nb (Fig. 11 of Frey *et al.*, 1994; Fig. 13b of Huang and Frey, 2003). A distinct difference between Makapuu-stage and Kalihi-stage lavas in La/Nb and Sr/Nb is apparent in Fig. 4a where the lower ratios of the Kalihi-stage lavas overlap with the Mauna Loa field. These differences are not a function of MgO content (Fig. 4b, c). In detail, however, Units 4, 5 and 6 of the KSDP core overlap with Makapuu-stage lavas in Sr/Nb and Units 4, 6, 14, 73 and 81 overlap in La/Nb (Fig. 5).

An objective is to use trace element geochemistry to understand the transition from Kalihi-stage to Makapuu-stage compositions. In particular to address the question –

was the transition abrupt or gradual? As shown in Fig. 5, within the uppermost 32 m of the KSDP core, classed as Kalihi-stage by *Haskins and Garcia (2004)*, there are six flows (Units 4, 5, 6, 9, 10 and 12) with geochemical characteristics that are transitional between Makapuu-stage and Kalihi-stage groups. Also, La/Nb and Sr/Nb generally increase upwards from an elevation of ~470 m below sea level, but there are high frequency variations superimposed on these general trends. There is no indication that there was an abrupt change to the distinctive Makapuu-stage composition within the KSDP core. Rather the Makapuu-stage geochemical signature gradually appears towards the top of the core and is most evident in two groups, Units 4, 5, 6, and Units 9, 10, 12.

What is the source of the distinctive Makapuu-stage geochemical signature? Depth profiles of  $^{208}\text{Pb}/^{206}\text{Pb}$ ,  $^{143}\text{Nd}/^{144}\text{Nd}$  and  $^{176}\text{Hf}/^{177}\text{Hf}$  (*Fekiacova et al., in prep.; Salters et al., in prep.*) are similar to those of La/Nb and Sr/Nb. Consequently, Makapuu-stage and Kalihi-stage lavas form trends in La/Nb versus  $^{208}\text{Pb}/^{206}\text{Pb}$ ,  $^{143}\text{Nd}/^{144}\text{Nd}$  and  $^{176}\text{Hf}/^{177}\text{Hf}$  plots (Fig. 6a-c). Koolau lavas (Makapuu-stage and Kalihi-stage) also form trends in Th/La versus  $^{208}\text{Pb}/^{206}\text{Pb}$ ,  $^{143}\text{Nd}/^{144}\text{Nd}$  and  $^{176}\text{Hf}/^{177}\text{Hf}$  plots (Fig. 6d-f). Clearly, they were derived from a heterogeneous source containing two geochemically distinct components. One component is like Mauna Loa lavas (Fig. 6a, c). The characteristics of Makapuu-stage lavas, high La/Nb, high  $^{176}\text{Hf}/^{177}\text{Hf}$  at a given  $^{143}\text{Nd}/^{144}\text{Nd}$  and relatively high  $^{187}\text{Os}/^{188}\text{Os}$  and  $\delta^{18}\text{O}$ , have been proposed as recycled sediment signatures (*Lassiter and Hauri, 1998; Jackson et al., 1999; Blichert-Toft et al., 1999; Huang and Frey, 2003*). Since marine sediments typically have higher  $^{232}\text{Th}/^{238}\text{U}$  and lower  $^{238}\text{U}/^{204}\text{Pb}$  than primitive mantle values (e.g., Figs 11 and 12 of *Ben Othman et al., 1989*), ancient recycled sediments are characterized by relatively low  $^{206}\text{Pb}/^{204}\text{Pb}$  and

high  $^{208}\text{Pb}/^{204}\text{Pb}$  at a given  $^{206}\text{Pb}/^{204}\text{Pb}$ , i.e., high  $^{208*}\text{Pb}/^{206*}\text{Pb}$ . Therefore, these extreme geochemical characteristics of Makapuu-stage lavas are consistent with ancient recycled marine sediment in their source. The correlations in Figs 4 and 6 require that this component also has high Sr/Nb ( $>55$ ) and low Th/La ( $<0.05$ ). We ask – Are these characteristics of marine sediment? Carbonate-rich sediment has high Sr/Nb (*Plank and Langmuir, 1998*; Fig. 7a). Marine sediments range widely in Th/La; terrigenous sediment is characterized by high Th/La ( $>0.2$ ) and slowly deposited metalliferous and phosphate-rich sediment are characterized by low Th/La ( $<0.2$ ) (Fig. 2 of *Plank, in press*; Fig. 7b). In particular, the pelagic carbonate section of Guatemala sediments which is rich in biogenic apatite has extremely low Th/La ( $\sim 0.02$ ) (Table 1 of *Plank and Langmuir, 1998*). Can such a sediment also explain the Makapuu-stage characteristic of high  $^{176}\text{Hf}/^{177}\text{Hf}$  at a given  $^{143}\text{Nd}/^{144}\text{Nd}$  (Fig. 7c)? Rare earth elements are compatible in apatite; consequently, apatite-rich sediment is characterized by high Lu/Hf. Time-integrated high Lu/Hf leads to high  $^{176}\text{Hf}/^{177}\text{Hf}$  at a given  $^{143}\text{Nd}/^{144}\text{Nd}$ . For example, the carbonate section at Guatemala section has Lu/Hf = 1.4 and Sm/Nd = 0.25 (Table 1 of *Plank and Langmuir, 1998*). A mixture of 3% 2Ga sediment with such Lu/Hf and Sm/Nd ratios and 97% primitive mantle has  $\epsilon_{\text{Nd}} = -2.7$  and  $\epsilon_{\text{Hf}} = 4.4$ , which are appropriate as an end-member component for Makapuu-stage lavas (Table 2; Fig. 7c). Therefore, we infer that the distinctive Makapuu-stage composition is consistent with sampling a recycled pelagic carbonate and apatite-rich sediment.

Compared with MORB and OIB, marine sediments are generally characterized by low Ce/Pb and Nb/U ratios (e.g., *Hofmann, 1997*). Specifically, the carbonate section at Guatemala has Ce/Pb = 0.8 and Nb/U = 2.9 (Table 1 of *Plank and Langmuir, 1998*).

However, unaltered Makapuu-stage lavas ( $1.2 < K_2O/P_2O_5 < 2.2$ ) have  $Ce/Pb = 23 \pm 3$  ( $2\sigma$ ) and  $Nb/U = 52 \pm 12$ , which are similar to those in unaltered Kalihi-stage lavas ( $Ce/Pb = 23 \pm 5$  and  $Nb/U = 50 \pm 6$ ) and oceanic basalt in general (Hofmann, 1997). Moreover,  $Ce/Pb$  (Fig. 6g-i) and  $Nb/U$  (not shown) are not correlated with isotopic ratios. A possible explanation is that subducted marine sediment was modified in the subduction zone by loss of the mobile elements, such as Pb and U; consequently, their low  $Ce/Pb$  and  $Nb/U$  signature was lost (e.g., *Ben Othman et al., 1989; Stracke et al., 2003*). On the other hand, since REE, Th and Hf are immobile, this process may not significantly fractionate these elements, and some sedimentary signatures such as high  $La/Nb$  and  $Lu/Hf$  were preserved. This inference is consistent with the evidence, low  $H_2O/Ce$  and  $\delta D$ , that the Koolau (Makapuu) component was dehydrated (*Dixon and Clague, 2001; Hauri, 2002*).

With decreasing age, there was a greater proportion of a recycled sedimentary component in the source of Koolau lavas, but the proportion of this component in the source did not change abruptly (Fig. 5) or systematically with time in the Kalihi-stage (Fig. 5) or Makapuu-stage (*Frey et al., 1994; Roden et al., 1994*). This inference of a gradual transition from Kalihi-stage geochemical characteristics contrasts with that of *Shinozaki et al. (2002)*, *Takahashi and Nakajima (2002)* and *Tanaka et al. (2002)* who described the transition from Mauna Loa-like composition (Kalihi-stage) to Makapuu-stage composition as “very sharp and abrupt” occurring over an interval of ~10 m in subaerial outcrops on the Nuuanu Pali. We note, however, that their data form linear trends overlapping with the trends defined by KSDP and Makapuu-stage lavas in  $La/Nb$  vs  $Sr/Nb$ ,  $^{143}Nd/^{144}Nd$  and  $^{208}Pb/^{206}Pb$  plots (Fig. 8). In detail, the Nuuanu landslide samples overlap with the Kalihi-stage field; the submarine Oahu North and subaerial

Makapuu samples overlap with the Makapuu-stage field; and the lavas from Nuuanu Pali straddle the boundaries between Kalihi-stage and Makapuu-stage lavas (Fig. 8). Consequently, we argue for a gradual, rather than abrupt, transition between Kalihi-stage and Makapuu-stage volcanism (Figs 5 and 8).

### **3.3 Relative Role of Garnet Pyroxenite/Eclogite and Peridotite as Sources for Koolau Lavas: Trace Element Constraints**

After Koolau whole rock compositions are adjusted to be in equilibrium with a common mantle olivine composition ( $Fo_{90}$ ), the abundance of heavy rare earth elements are much less variable than those of highly incompatible elements (Fig. 2). This result reflects garnet as a residual mineral during partial melting (*Hofmann et al., 1984*). Compared with other Hawaiian shield lavas, Makapuu-stage lavas at a given MgO content have lower Sc, Y and Yb abundances, a result interpreted to reflect a larger proportion of residual garnet during generation of Makapuu-stage lavas (*Budahn and Schmitt, 1985; Frey et al., 1994; Jackson et al., 1999*). This observation is confirmed by our ICP-MS data of Makapuu-stage lavas (Fig. 9). Kalihi-stage lavas have higher Sc, Y and Yb abundances than Makapuu-stage lavas, and overlap with (Sc) or are on the lower part of (Y and Yb) the fields defined by Mauna Kea and Mauna Loa lavas (Fig. 9a-d). Among these elements, Sc is the best discriminant between Makapuu-stage and Kalihi-stage lavas. This may reflect the greater compatibility of Sc, relative to Y and Yb, in both garnet and clinopyroxene (e.g., *Pertermann et al., 2004*).

The variable presence of a sedimentary component in Koolau lavas is consistent with garnet pyroxenite, formed from recycled oceanic crust, as a source component. In subsequent discussion, we use garnet pyroxenite as a general rock name that includes

eclogite. Hence the source of Koolau lavas may have been peridotite with embedded garnet pyroxenite heterogeneities. How does melting of such a mixed source precede? Since the solidi of most garnet pyroxenites are lower than those of peridotite (e.g., *Hirschmann and Stolper, 1996*), one modeling approach is to create a modified peridotite source by fertilizing the unmelted peridotite with partial melt of garnet pyroxenite to form a modified garnet peridotite source. This process is consistent with the experiments by *Yaxley and Green (1998)* and was used by *Sobolev et al. (2000)* to model the origin of melt inclusions in olivine in Mauna Loa lavas.

Koolau data consistent with variable partial melting of a garnet peridotite source are the correlated variations in ratios that are controlled by residual garnet, such as La/Yb, Sc/Y and Tb/Yb, in Kalihi-stage and Makapuu-stage lavas (Fig. 10). The La/Yb-Sc/Y, La/Yb-Zr/Yb and La/Yb-Tb/Yb trends can be explained by partial melting of a garnet peridotite, with uniform La/Yb, Sc/Y, Zr/Yb and Tb/Yb (Fig. 10). These ratios may have been similar in the sources of Kalihi-stage and Makapuu-stage lavas because adding 3% carbonate-apatite-rich sediment into the proposed source for Kalihi-stage lavas markedly increases La/Nb from 0.95 to 1.5, Sr/Nb from 40 to 102 and decreases Th/La from 0.07 to 0.05, but only changes La/Yb by <50%, and Sc/Y, Zr/Yb and Tb/Yb by <15% (Table 3a). In contrast, La/Yb, Sc/Y, Zr/Yb and Tb/Yb in Makapuu-stage and Kalihi-stage lavas vary by a factor of >2, ~1.7, >2 and ~1.2, respectively (Fig. 10). The inference is that Makapuu-stage lavas were derived by lower extents of melting than Kalihi-stage lavas. Consequently, they equilibrated with a larger amount of residual garnet.

Although we are confident that abundance ratios sensitive to control by residual garnet were controlled by the melting process, the simple model of variable extents of

partial melting of garnet peridotite is not viable. *Eggins (1992)* and *Wagner and Grove (1998)* showed that the estimated primary magma compositions for Hawaiian shield lavas, and especially Makapuu-stage lavas (*Hauri, 1996*), are not in equilibrium with garnet peridotite. More complex models are required.

One possibility is mixing of melts derived from garnet peridotite and garnet pyroxenite. However, La/Yb is not correlated with Sr-Nd-Pb isotopic ratios (Fig. 6j-l); therefore, the trends formed by Koolau lavas in Fig. 10 are not magma mixing trends. Rather we infer that they reflect both partial melting and magma mixing processes. That is, the transition from Kalihi-stage to Makapuu-stage was accompanied by decreasing melting extent and an increasing proportion of a garnet pyroxenite melt component. In this scenario a complexity is that melts of garnet pyroxenite are very reactive with peridotite and require transport in isolated channels (e.g., *Yaxley and Green, 1998; Takahashi and Nakajima, 2002; Kogiso et al., 2004*). That is, the SiO<sub>2</sub>-rich melts derived by partial melting of quartz eclogite and some garnet pyroxenites react with peridotite and convert olivine to orthopyroxene (e.g., *Yaxley and Green, 1998; Takahashi and Nakajima, 2002*). It is possible that the orthopyroxene band formed between SiO<sub>2</sub>-rich and peridotite precludes further reaction. Consequently, there is a possibility that SiO<sub>2</sub>-rich melts ascend to a magma chamber or even to the Earth's surface. The presence of adakite, which is proposed as partial melt of subducting oceanic crust (e.g., *Yogodzinski et al., 1995*), provides evidence for this possibility. Since melts of garnet pyroxenite have been proposed to be a significant (*Hauri, 1996*) or even dominant component (*Takahashi and Nakajima, 2002*) for the Makapuu-stage of Koolau, we ask – Is it possible to use

trace element abundances to distinguish between garnet pyroxenite and garnet peridotite as sources for Makapuu-stage lavas?

Based on experiments in the CMAS (CaO, MgO, Al<sub>2</sub>O<sub>3</sub> and SiO<sub>2</sub>) system, *van Westrenen et al.* (Fig. 5d, 2001) proposed that Zr/Yb can be used to distinguish between melts derived from garnet pyroxenite and garnet peridotite. This discriminant arises because  $D_{Zr}^{garnet/melt} > 1$  for the Ca-rich garnet in garnet pyroxenite, and consequently  $D_{Zr}$  is similar to  $D_{Yb}$ , but  $D_{Zr}^{garnet/melt} < D_{Yb}^{garnet/melt}$  for the Mg-rich garnet in garnet peridotite. However, recent experimental results for more complex compositional systems, notably including Ti, show that Zr is not compatible in Ca-rich garnet (*Pertermann et al.*, 2004). Rather than Zr/Yb, they propose Zr/Hf as a discriminant for distinguishing residual eclogite (high clinopyroxene/garnet ratio) from residual garnet peridotite (low clinopyroxene/garnet ratio) (Fig. 10 of *Pertermann et al.*, 2004). The suitability of Zr/Hf as a discriminant arises because: (1)  $(K_D)_{Zr/Hf}$  for clinopyroxene/melt is ~0.5 whereas it is ~1 for garnet/melt; and (2) the very different clinopyroxene/garnet ratios for eclogite and garnet peridotite used by *Pertermann et al.* (2004). However clinopyroxene/garnet ratios in peridotite are very dependent upon pressure and temperature (e.g., Walter, 1998), and may overlap with the ratios in eclogite; therefore, we suggest that Zr/Hf is not a reliable discriminant (Fig. 11). Moreover, Fig. 10 of *Pertermann et al.* (2004) is misleading because as Koolau lavas they include data from both tholeiitic Koolau shield stage lavas and highly alkalic rejuvenated stage lavas erupted onto the Koolau shield (i.e., the Honolulu Volcanics). If only Koolau shield lavas are plotted, it is intriguing that Kalihi-stage and Makapuu-stage lavas define different trends (Fig. 11). If this difference is

substantiated with more high quality data, it requires a higher clinopyroxene/garnet ratio in the residue of Makapuu-stage lavas.

### **3.4 Relative Role of Garnet Pyroxenite/Eclogite and Peridotite as Sources for Koolau Lavas: Major Element Constraints**

An early hypothesis for explaining the distinctive major element composition of Makapuu-stage lavas, i.e., relatively high SiO<sub>2</sub> and low total iron and CaO contents, was melt segregation at relatively low pressure (*Frey et al., 1994; Putirka, 1999*). However, *Hauri (1996)* noted problems with this interpretation. Namely the high SiO<sub>2</sub> content of Makapuu-stage lavas requires melt segregation at depths of 30-45 km, less than the thickness of Hawaiian lithosphere (*Li et al., 2004*). Also at low pressure, the experimental total iron contents are lower than observed (Fig. 2 of *Hauri, 1996*). He proposed an alternative hypothesis that the distinctive Makapuu-stage composition reflects SiO<sub>2</sub>-rich partial melts derived from a garnet pyroxenite component in the plume.

Based on melt-peridotite reactions first discussed in *Kelemen (1986)*, a third alternative for generating relatively high SiO<sub>2</sub> content was proposed by *Stolper et al. (2004)* for the High-SiO<sub>2</sub> Group Mauna Kea lavas recovered in Phase 2 of the Hawaii Scientific Drilling Project (HSDP). Specifically, melt generated from peridotite (relatively low SiO<sub>2</sub> content) reacts with an overlying residual peridotite by assimilating orthopyroxene, clinopyroxene and crystallizing olivine thereby increasing the SiO<sub>2</sub> content in the melt. This reaction is similar to the models proposed by *Eggins (1992)* and *Wagner and Grove (1998)* to explain the high MgO Kilauea glasses. No attempt has yet been made to explain incompatible element abundance and isotopic ratios of HSDP lavas by this process. In addition, since Ni is much more compatible in olivine than other

phases, this process will simultaneously increase SiO<sub>2</sub> content and decrease Ni content. Using mineral and melt compositions given in Table 3 of *Stolper et al. (2004)* and Equation 39 of *Beattie et al. (1991)*, we obtain that  $D_{\text{Ni}}^{\text{olivine/melt}}=6.59$  and  $D_{\text{Ni}}^{\text{orthopyroxene/melt}}=1.92$ . Since  $D_{\text{Ni}}^{\text{clinopyroxene/orthopyroxene}}<0.5$  (e.g, Table 2 of *Seitz et al., 1999*), we take  $D_{\text{Ni}}^{\text{clinopyroxene/melt}}=0.96$  as a maximum estimate. Consequently, the reaction (Fit A) given in Table 3 of *Stolper et al. (2004)* predicts that Ni content in High-SiO<sub>2</sub> Mauna Kea Group lavas should be ~70% of that in Low-SiO<sub>2</sub> Mauna Kea Group lavas. However, this is not observed in HSDP2 whole rocks (Fig. 5f of *Huang and Frey, 2003*).

With respect to Koolau lavas, the reaction proposed by *Stolper et al. (2004)* does not significantly affect CaO and Al<sub>2</sub>O<sub>3</sub> contents (see their Fig. 18). Therefore, this process does not explain the low CaO and high Al<sub>2</sub>O<sub>3</sub>/CaO of Makapuu-stage lavas (Fig. 11 of *Frey et al., 1994*; Fig. 10 of *Haskins and Garcia, 2004*). In addition, *Garcia (2002)* noted the unusually high Ni contents of olivine in Koolau lavas and in detail Makapuu-stage lavas have higher Ni contents than Kalihi-stage lavas (Fig. 9e). Consequently, the melt-rock reaction fails to explain important compositional features (low CaO and high Ni) of Makapuu-stage lavas. Therefore, this model is not suitable for explaining the SiO<sub>2</sub> difference between Makapuu-stage and Kalihi-stage lavas.

*Sobolev et al. (submitted)* suggest that high Ni content may be associated with SiO<sub>2</sub>-rich melt. They speculate that partial melt of garnet pyroxenite reacts with peridotite, replaces olivine with orthopyroxene, and generates secondary garnet pyroxenite (e.g., *Yaxley and Green, 1998*). Consequently, this reaction lowers the bulk solid/melt partition coefficient of Ni because of the low olivine proportion in this secondary garnet pyroxenite; therefore, partial melt of this garnet pyroxenite is characterized by high SiO<sub>2</sub>

and Ni contents. Hence, the high SiO<sub>2</sub> and Ni contents in Makapuu-stage lavas (Fig. 9e) are consistent with the hypothesis that these lavas contain a larger proportion of SiO<sub>2</sub>-rich melt derived from garnet pyroxenite.

To further evaluate the role of melt derived from garnet pyroxenite in controlling major element compositions of Koolau lavas, the Makapuu-stage and Kalihi-stage lavas, with K<sub>2</sub>O/P<sub>2</sub>O<sub>5</sub>>1.2 and MgO>6.5%, were adjusted to be in equilibrium with Fo<sub>90</sub> olivine, which is the highest Fo olivine found in Makapuu-stage lavas (*Norman and Garcia, 1999; Garcia, 2002*), by adding or subtracting equilibrium olivine in 0.1% steps assuming (Fe/Mg)<sub>olivine</sub>/(Fe/Mg)<sub>melt</sub>=0.30. After this adjustment, there is still considerable variation in major element composition of Makapuu-stage and Kalihi-stage lavas (Fig. 12). Surprisingly, SiO<sub>2</sub> content does not distinguish Makapuu-stage and Kalihi-stage lavas. Some Kalihi-stage lavas, Units 6, 9 and 10, also have high SiO<sub>2</sub> content (Fig. 12a). These three units, along with samples from Units 4, 5 and 12 which are altered and not plotted in Fig. 12, also have the distinctive high Sr/Nb, a characteristic of Makapuu-stage lavas (Fig. 5c). The best discriminant between Makapuu-stage and Kalihi-stage lavas is CaO content (Fig. 12d; Fig. 5 of *Haskins and Garcia; 2004*). Note, however, that Kalihi-stage Units 6, 9 and 10 with relatively high SiO<sub>2</sub> and Sr/Nb have lower CaO than most Kalihi-stage lavas (Fig. 12d).

Olivine adjusted SiO<sub>2</sub> content is correlated with Nd-Hf-Pb isotopic ratios, but Makapuu-stage and Kalihi-stage lavas form subparallel trends (Fig. 13). Because Kalihi-stage lavas define linear trends in plots of 1/[Nd] vs <sup>143</sup>Nd/<sup>144</sup>Nd and 1/[Hf] vs <sup>176</sup>Hf/<sup>177</sup>Hf (Fig. 14), we concur with *Hauri (1996)* that the SiO<sub>2</sub>-isotopic trends (Fig. 13) are mixing lines. That is, the large variations in olivine adjusted major element contents are not

artifacts of olivine adjustment, and the inverse MgO-SiO<sub>2</sub> trend (Fig. 12a) is inferred to arise from source heterogeneity. A possible interpretation for the subparallel trends in Fig. 13 is that both Makapuu-stage and Kalihi-stage lavas contain varying proportions of a SiO<sub>2</sub>-rich component derived from garnet pyroxenite but that the Makapuu-stage lavas contain more of an isotopically distinctive sedimentary component. Interestingly, in an olivine adjusted SiO<sub>2</sub>-<sup>143</sup>Nd/<sup>144</sup>Nd plot, the averages of Hawaiian shields or stratigraphic sections (from Table 1 of *Hauri, 1996*) largely overlap with Koolau lavas (Makapuu-stage and Kalihi-stage lavas) (Fig. 13c), implying that a single shield (Koolau) may sample all the source components contributing to Hawaiian shields.

The calculated dacitic magma of *Hauri (1996)* has an unusual composition in having quite high MgO (6%) for its high SiO<sub>2</sub> content (64%). No experimentally derived melt of eclogite/garnet pyroxenite has these characteristics; in fact, *Pertermann and Hirschmann (2003)* concluded that “no eclogitic partial melt has been identified that is capable of explaining all of compositional features of the exotic Koolau component”. We ask – Is the 6% MgO-64% SiO<sub>2</sub> a robust estimate? A concern about the Hauri compilation of shield lava composition is SiO<sub>2</sub> mobility during alteration. A significant fraction (26%) of lavas in Hauri’s data compilation have K<sub>2</sub>O/P<sub>2</sub>O<sub>5</sub> < 1, and *Frey et al. (1994)* showed that SiO<sub>2</sub> contents are commonly lower in such altered lavas. However, using our alteration discriminant (2.2 > K<sub>2</sub>O/P<sub>2</sub>O<sub>5</sub> > 1.2) leads to similar averages for Makapuu-stage lavas (Table 4).

The mismatch between the 6% MgO-64% SiO<sub>2</sub> composition with partial melts of eclogite/garnet pyroxenite is apparent in Fig. 15a. This discrepancy can be avoided by choosing a more SiO<sub>2</sub>-rich component with <2% MgO. Although such a dacitic

component is consistent with experimentally determined melts of eclogite/garnet pyroxenite, *Pertermann and Hirschmann (2003)* suggest that there are two problems with this interpretation:

- 1 Low degrees of melting are required to create a SiO<sub>2</sub>-rich melt; hence a relatively low temperature is inferred. Although this may be inconsistent within a plume context, the Makapuu-stage lavas formed as Koolau shield volcanism waned; i.e., when the shield was moving off the hotspot and encountering lower temperature.
- 2 Referring to *Norman and Garcia (1999)*, they argue that the trace element features created by residual garnet, e.g., high Sr/Y and Sm/Yb, are absent in Koolau lavas. However, in Figs 2, 9 and 10 we provide evidence for garnet as an important residual phase for Makapuu-stage lavas. Moreover, Fig 6c of *Haskins and Garcia (2004)* also shows that a relatively high Sr/Y in Makapuu-stage lavas is consistent with a dacitic component.

Finally Hawaiian shield lavas define a clear inverse MgO-SiO<sub>2</sub> trend with Makapuu-stage lavas as one extreme (Fig. 15a), but the MgO-CaO plot is scattered (Fig. 15b). Nevertheless, Makapuu-stage lavas are offset to low CaO at a given MgO, and this result is consistent with a low CaO, dacitic component in these lavas (Fig. 15b). Since we argue in **Section 3.2** that Makapuu-stage lavas sampled more of a recycled carbonate-rich sedimentary component, the lower CaO content in Makapuu-stage lavas implies that CaO content is more controlled by the dacitic component.

### **3.5 Temporal Geochemical Variations Within the KSDP core**

The relative ages of lava flows recovered from the KSDP core are constrained; hence, it is possible to use the time-dependent geochemical variations to constrain

temporal changes in the spatial distribution of geochemical heterogeneity and process. In order to remove complications caused by alteration, we consider only unaltered lavas ( $1.2 < K_2O/P_2O_5 < 2.2$  and  $L.O.I. < 0.8$ ) in a time series analysis. We follow the assumption of *Blichert-Toft et al. (2003)* that the resurfacing time was constant, i.e., the time differences between lava flows are equal. The resurfacing time ranges from ~500 years at Kilauea (*Holcomb, 1987*) to ~1400 years at the HSDP 2 drill site (~410 ka for ~300 lava flow units in the Mauna Kea section, *Sharp and Renne, submitted*). Following the method described in *Press et al. (pp. 575-579, 1992)*, we calculate the Lomb normalized periodograms for  $Al_2O_3/CaO$ , Th/La, Sr/Nb, La/Nb, La/Yb and Tb/Yb (Fig. 16). There are two peaks in these periodograms for  $Al_2O_3/CaO$ , Th/La, Sr/Nb and La/Nb: one is at very low frequency (unlabeled) and the other is at around 21 times resurfacing time (Fig. 16a-d). These peaks, except the Th/La peak at very low frequency, are significant at the 95% confidence level. The low frequency peak reflects the long-term secular trend shown in Fig. 5. Fig. 16e shows that, after removal of this secular trend, only the peak at ~21 times resurfacing time exists in the Lomb normalized periodogram for  $Al_2O_3/CaO$ . In contrast, there is only one peak at ~30 times resurfacing time (significant at 95% confidence level) in the Lomb normalized periodograms for La/Yb and Tb/Yb.

Time series analyses show that the variations of  $Al_2O_3/CaO$ , Th/La, Sr/Nb and La/Nb are highly correlated and share a period of ~21 times resurfacing time, which corresponds to 10-29 ka using different (500 and 1400 years) resurfacing times. The correlations among these ratios are consistent with our inference that high  $Al_2O_3/CaO$  arises from partial melting of garnet pyroxenite and the high Sr/Nb, La/Nb with low Th/La arise from a carbonate-apatite-rich sediment component in this garnet pyroxenite.

These variations reflect horizontal (e.g., *DePaolo et al., 2001*) and/or vertical (e.g., see Figs 12 and 13 of *Blichert-Toft et al., 2003*) geochemical heterogeneity with the Hawaiian plume. Considering that the plume upwelling velocity is greater than the plate motion velocity and magma extraction may homogenize the horizontal heterogeneity to some extent, *Blichert-Toft et al. (2003)* imply that the geochemical heterogeneity in lavas reflects vertical heterogeneity within the plume. If the observed variations of  $\text{Al}_2\text{O}_3/\text{CaO}$ ,  $\text{La}/\text{Nb}$ ,  $\text{Sr}/\text{Nb}$  and  $\text{Th}/\text{La}$  in KSDP core reflect the reappearance of a garnet pyroxenite component within the Hawaiian plume, the vertical spacing between two such components is 1-29 km given 10 cm/year and 1 m/year as the lower and upper limits of the plume upwelling velocity (e.g., *Ribe and Christensen, 1999*). This gives the largest estimate of the vertical size of the eclogitic component sampled by KSDP lavas. Using a different approach, *Takahashi and Nakajima (2002)* suggest that the eclogitic component contributing to Makapuu-stage lavas is 10 km in size. However, *Hauri et al. (1994)* show that within a mantle plume, the upwelling velocity is a function of the distance from the center of the plume. That is, the central part of the plume rises much faster than the periphery. Consequently, it is unlikely that the vertical, “pancake”-like heterogeneity shown in Fig. 13 of *Blichert-Toft et al. (2003)* is stable over time. The approach of *Eisele et al. (2003)* for the HSDP drill core at Mauna Kea calculates the spacing of Pb isotopic heterogeneities by integrating over non-linear flow path beneath the HSDP drill site (see their Fig. 13); they infer 21 to 86 km as minimum length scale of these heterogeneity. However, this approach requires information about the distance between the shield and plume center as a function of time. Such information is not available for Koolau.

The lack of a significant peak (at 95% confidence level) at ~21 times resurfacing time in the Lomb normalized periodograms for La/Yb and Tb/Yb implies that these ratios were not affected by the recycled oceanic crust component. That is, La/Yb and Tb/Yb are controlled by the partial melting process, as inferred previously by the lack of correlations between La/Yb and isotopic ratios (Fig. 6j-1). The variations of La/Yb and Tb/Yb, at a period of ~30 times resurfacing time which corresponds to ~15-42 ka, imply that there was substantial variation in melting extent during the shield building stage (Figs 5d and 10). Variable extents of melting during shield construction have also been inferred for Kilauea (*Pietruszka and Garcia, 1999*), Mauna Loa (*Rhodes and Hart, 1995*) and Mauna Kea (*Stolper et al., 2004*).

#### **4. Summary**

Geochemical and petrographic studies of surface lavas erupted on the Koolau shield and drill core from the Koolau Scientific Drilling Project show that the shield lavas changed markedly near the end of shield-building (*Frey et al., 1994; Roden et al., 1994; Jackson et al., 1999; Haskins and Garcia, 2004; this paper*). Specifically, as shield building ended, tholeiitic shield basalt changed gradually from a Mauna Loa-like composition (Kalihi-stage of *Haskins and Garcia, 2004*) to the well known geochemical endmember that characterizes subaerially exposed Koolau lavas (Makapuu-stage of *Haskins and Garcia, 2004*). *Haskins and Garcia (2004)* argue that this transition in lava composition occurred over “the 60-m-thick lava from the H3 tunnel”; consequently, this transition lasted over 2,600–4,600 years assuming a lava accumulation of 13-23 mm per year (*DePaolo and Stolper, 1996*). However, we infer that the transition from typical

Kalihi-stage composition to Makapuu-stage composition began at the elevation of ~470 m below sea level in the KSDP drill hole, and continued to the top of the cored section (Fig. 5). Consequently, we infer that the transition in composition from Kalihi-stage composition to Makapuu-stage composition occurred over at least 170 m which is about three times longer than the estimate of *Haskins and Garcia (2004)*.

The transition from Kalihi-stage to Makapuu-stage lavas reflects changes in source material that presumably occurred as Koolau volcano migrated away from the hotspot:

1. The continuous trends in major element contents (Fig. 12) and trace element ratios controlled by residual garnet (e.g., Sc/Y and La/Yb in Fig. 10) show that with decreasing age a garnet pyroxenite component was increasingly important in generating Koolau shield lavas. This resulted in Makapuu-stage characteristics, such as high SiO<sub>2</sub> and low Sc and CaO contents at a given MgO content, and relatively high La/Yb, Zr/Yb and low Sc/Y. All these features are consistent with an increasing amount of melt (dacite) derived from partial melting of garnet pyroxenite.
2. Makapuu-stage lavas also have relatively high La/Nb, Sr/Nb and low Th/La which are correlated with <sup>143</sup>Nd/<sup>144</sup>Nd, <sup>176</sup>Hf/<sup>177</sup>Hf and <sup>208</sup>Pb/<sup>206</sup>Pb (Fig. 6). These reflect a small amount of ancient recycled pelagic carbonate and apatite-rich sediment in the source of Makapuu-stage lavas. Such sediments occur in the Central America trench (DSDP Site 495, *Plank and Langmuir, 1998*).

**Acknowledgement:**

This research was supported by NSF Grant EAR-0105557. Expenses associated with coring were partially supported by funds from the University of Hawaii, California Institute of Technology, University of California at Berkeley, Massachusetts Institute of Technology, Carnegie Institute of Washington, Max-Planck Institut für Chemie, Woods Hole Oceanographic Institute and Tokyo Institute of Technology. We especially thank M. O. Garcia (University of Hawaii) for his origination and leadership of the KSDP. We thank V. J. M. Salters and Z. Fekiacova for sharing their Nd, Hf and Pb isotopic data for the KSDP samples we studied. We also appreciate the constructive review comments of S. W. Parman, V. J. M. Salters, X, Y and Z. We thank B. Grant, R. Kayser and S. Higgins for their assistance in ICP-MS analysis, and F. Dudas for help in the clean lab.

## References:

- Beattie, P., Ford, C., Russell, D., Partition coefficients for olivine-melt and orthopyroxene-melt system, *Contrib. Mineral. Petrol.*, 109 (2), 212-224, 1991.
- Ben Othman, D., White, W. M., Patchett, J., The geochemistry of marine sediments, island arc magma genesis, and crust-mantle recycling, *Earth Planet Sci Letts.*, 94 (1-2), 1-21, 1989.
- Blichert-Toft, J., Frey, F. A., and Albarede, F., Hf isotope evidence for pelagic sediments in the source of Hawaiian basalts, *Science*, 285 (5429), 879-882, 1999.
- Blundy, J. D., Robinson, J. A. C., and Wood, B. J., Heavy REE are compatible in clinopyroxene on the spinel lherzolite solidus. *Earth Planet. Sci. Lett.*, 160, 493-504, 1998.
- Budahn, J. R., Schmitt, R. A., Petrogenetic modeling of Hawaiian tholeiitic basalts; a geochemical approach, *Geochim. Cosmochim. Acta.*, 49 (1), 67-87, 1985.
- Chen, C.-Y., Frey, F. A., Rhodes, J. M., and Easton, R. M., Temporal geochemical evolution of Kilauea Volcano: Comparison of Hilina and Puna Basalt. in Earth Processes: Reading the isotopic code, *Geophysical Monograph Series*, vol. 95, edited by A. Basu and S. R. Hart, 161-181, AGU, Washington, D.C., 1996.
- Cohen, A. S., O'Nions, R. K., and Kurz, M. D., Chemical and isotopic variations in Mauna Loa tholeiites, *Earth Planet. Sci. Lett.*, 143, 111-124, 1996.
- DePaolo, D. J. and Stolper, E. M., Models of Hawaiian volcano growth and plume structure; implications of results from the Hawaii Scientific Drilling Project, *J. Geophys. Res.*, 101 (5), 11,643-11,654, 1996.
- DePaolo, D., J. Bryce, A. Dodson, D. Shuster, and B. Kennedy, Isotopic evolution of Mauna Loa and the chemical structure of the Hawaiian plume, *Geochem. Geophys. Geosyst.*, 2, doi:10.1029/2000GC000139, 2001.
- Dixon, J. E. and Clague, D. A., Volatiles in basaltic glasses from Loihi Seamount, Hawaii; evidence for a relatively dry plume component, *J. Petrol.*, 42 (3), 627-654, 2001.
- Eggins, S. M., Petrogenesis of Hawaiian tholeiites; 1, Phase equilibria constraints, *Contrib. Mineral. Petrol.*, 110 (2-3), 387-397, 1992.
- Eisele, J., Abouchami, W., Galer, S. J. G. and Hofmann, A. W., The 320 kyr Pb isotope evolution of Mauna Kea lavas recorded in the HSDP-2 drill core, *Geochem. Geophys. Geosyst.*, 4(5), 8710, doi:10.1029/2002GC000339, 2003.

Feigenson, M. D., Hofmann, A. W., Spera, Frank J., Case studies on the origin of basalt; II, The transition from tholeiitic to alkalic volcanism on Kohala Volcano, Hawaii, *Contrib. Mineral. Petrol.*, 84 (4), 390-405, 1983.

Fodor, R. V., Frey, F. A., Bauer, G. R., Clague, D. A., Ages, rare-earth element enrichment, and petrogenesis of tholeiitic and alkalic basalts from Kahoolawe Island, Hawaii, *Contrib. Mineral. Petrol.*, 110, 442-462, 1992.

Frey, F. A., and Clague, D. A., Geochemistry of diverse basalt types from Loihi Seamount, Hawaii; petrogenetic implications. *Earth Planet Sci. Letts.* 66, 337-355, 1983.

Frey, F. A., Garcia, M. O., Wise, W. S., Kennedy, A., Gurriet, P., Albarede, F., The evolution of Mauna Kea volcano, Hawaii: Petrogenesis of tholeiitic and alkalic basalts, *J. Geophys. Res.*, 96, 14,347-14,375, 1991.

Frey, F. A., Garcia, M. O., and Roden, M. F., Geochemical characteristics of Koolau Volcano: Implications of intershield geochemical differences among Hawaiian volcanoes. *Geochim. Cosmochim. Acta.*, 58, 1441-1462, 1994.

Galer, S. J. G., and O'Nions, R. K., Residence time of thorium, uranium and lead in the mantle with implications for mantle convection, *Nature*, 316 (6031), 778-782, 1985.

Garcia, M. O., Jorgenson, B. A., Mahoney, J. J., Ito E., and Irving, A. J., An evaluation of temporal geochemical evolution of Loihii summit lavas: Results from Alvin submersible dives. *J. Geophys. Res.* 98, 535-550, 1993.

Garcia, M. O., Foss, D. J. P., West, H. B. and Mahoney, J. J., Geochemical and isotopic evolution of Loihi Volcano, Hawaii, *J. Petrol.*, 36, 1647-1644, 1995b.

Garcia, M. O., Hulsebosch, T. P., Rhodes, J. M., Olivine-rich submarine basalts from the southwest rift zone of Mauna Loa Volcano; implications for magmatic processes and geochemical evolution, in *Mauna Loa Revealed, Geophysical Monograph Series, vol. 92*, (eds, J.M. Rhodes and J.P. Lockwood) 219-239, AGU, Washington, D.C., 1995a.

Garcia, M. O., Rubin, K. H., Norman, M. D., Rhodes, J. M., Graham, D. W., Muenow, D W., Spencer, K., Petrology and geochronology of basalt breccia from the 1996 earthquake swarm of Loihi Seamount, Hawaii; magmatic history of its 1996 eruption, *Bull. Volcan.*, 59, 577-592, 1998.

Garcia, M. O., Pietruszka, A. J., Rhodes, J. M., Swanson, K., Magmatic processes during the prolonged Pu'u O'o eruption of Kilauea volcano, Hawaii, *J. Petrol*, 41(7), 967-990, 2000.

Garcia, M. O., Giant landslides in the northeast of O'ahu; when, why and how? in *Hawaiian volcanoes; deep underwater perspectives, Geophysical Monograph Series, vol.*

128, (eds, Takahashi, E., Lipman, P. W., Garcia, M. O., Naka, J., Aramaki, S), 221-222, 2002.

Hart, S. R. and Dunn, T., Experimental cpx/melt partitioning of 24 trace elements, *Contrib. Mineral. Petrol.*, 113 (1), 1-8, 1993.

Haskins, E. R., and Garcia M. O., Scientific drilling reveals geochemical heterogeneity within the Ko'olau shield, Hawai'i, *Contrib. Mineral. Petrol.*, 147, 162-188, 2004.

Hauri, E. H., Wagner, T. P., Grove, T. L., Experimental and natural partitioning of Th, U, Pb and other trace elements between garnet, clinopyroxene and basaltic melts, *Chem. Geol.*, 117 (1-4), 149-166, 1994.

Hauri, E. H., Major-element variability in the Hawaiian mantle plume, *Nature* 382, 415-419, 1996.

Hauri, E. H., SIMS analysis of volatiles in silicate glasses; 2, Isotopes and abundances in Hawaiian melt inclusions, *Chem. Geol.*, 183 (1-4), 115-141, 2002.

Hirschmann, M. M., Stolper, E. M., A possible role for garnet pyroxenite in the origin of the "garnet signature" in MORB, *Contrib. Mineral. Petrol.*, 124 (2), 185-208, 1996.

Hofmann, A. W., Feigenson, M. D., Raczek, I., Case studies on the origin of basalt; III, Petrogenesis of the Mauna Ulu eruption, Kilauea, 1969-1971, *Contrib. Mineral. Petrol.*, 88 (1-2), 24-35, 1984.

Hofmann, A. W., Chemical differentiation of the earth: the relationship between mantle, continental crust, and oceanic crust, *Earth Planet. Sci. Lett.* 90, 297-314, 1988.

Hofmann, A. W., Mantle geochemistry; the message from oceanic volcanism, *Nature*, 385 (6613), 219-229, 1997.

Holcomb, R. T., Eruptive history and long-term behavior of Kilauea Volcano, in *Volcanism in Hawaii*, (eds, Decker, R. W., Wright, T. L. and Stauffer, P. H.) U. S. Geological Survey Professional Paper, P 1350, p. 261-350, 1987.

Huang, S. and Frey, F.A., Trace element abundances of Mauna Kea basalt from Phase 2 of the Hawaiian Scientific Drilling Project: Petrogenetic implications of correlations with major element content and isotopic ratios, *Geochem. Geophys., Geosys*, 4(6), 8711, doi, 1029/2002 GC000322, 2003.

Jackson, M. C., Wilmoth, R. A., and Frey, F. A., Geology and petrology of basaltic lavas and dikes of the Koolau Volcano in the Trans-Koolau exploratory tunnels, Oahu, Hawaii. *Bull. Volcan.* 60, 381-401, 1999.

Kelemen, P. B., Assimilation of ultramafic rock in subduction-related magmatic arcs, *J. Geol.*, 94 (6), 829-843, 1986.

Kogiso, T., Hirschmann, M. M., Reiners, P. W., Length scales of mantle heterogeneities and their relationship to ocean island basalt geochemistry, *Geochim. Cosmochim. Acta.*, 68(2), 345-360, doi, 10.1016/S0016-7037(03)00419-8, 2004.

Kurz, M. D., Kenna, T. C., Kammer, D. P., Rhodes, J. M., and Garcia, M. O., Isotopic evolution of Mauna Loa volcano: a view from the submarine southwest rift Mauna Loa: A Decade Volcano, in *Mauna Loa Revealed, Geophysical Monograph Series, vol. 92*, (eds, J.M. Rhodes and J.P. Lockwood) 289-306, AGU, Washington, D.C., 1995.

Lassiter, J. C. and Hauri, E. H., Osmium-isotope variations in Hawaiian lavas: Evidence for recycled oceanic lithosphere in the Hawaiian plume. *Earth Planet Sci Letts.*, 164, 483-496, 1998.

Leeman, W. P., Gerlach, D. C., Garcia, M. O., West, H. B., Geochemical variations in lavas from Kahoolawe volcano, Hawaii: evidence for open system evolution of plume-derived magmas, *Contrib. Mineral. Petrol.*, 116, 62-77, 1994.

Li, X., Kind, R., Yuan, X., Wö lbern I. and & HANKA, W., Rejuvenation of the lithosphere by the Hawaiian plume, *Nature* 427, 827-829 doi:10.1038/nature02349, 2004.

Norman, M. D., and Garcia, M. O., Primitive magmas and source characteristics of the Hawaiian Plume; petrology and geochemistry of shield picrites, *Earth Planet Sci. Letts.*, 168, 27-44, 1999.

Pertermann, M., and Hirschmann, M. M., Trace-element partitioning between vacancy-rich eclogitic clinopyroxene and silicate melt, *Am. Mineral.*, 87, 1265-1376, 2002.

Pertermann, M., and Hirschmann M. M., Anhydrous partial melting experiments on MORB-like eclogite: Phase reactions, phase compositions and mineral-melt partitioning of major elements at 2-3 GPa, *J. Petrol.*, 44(12), 2173-2201, 2003.

Pertermann, M., Hirschmann, M. M., Hametner, K., Gunther, D., Schmidt, M. W., Experimental determination of trace element partitioning between garnet and silica-rich liquid during anhydrous partial melting of MORB-like eclogite, *Geochem. Geophys. Geosyst.*, 5, Q05A01, doi:10.1029/2003GC000638, 2004.

Pietruszka, A. J. and Garcia, M. O., A rapid fluctuation in the mantle source and melting history of Kilauea Volcano inferred from the geochemistry of its historical summit lavas (1790-1982), *J. Petrol.*, 40 (8), 1321-1342, 1999.

Plank, T., and Langmuir, C. H., The chemical composition of subducting sediment and its consequences for the crust and mantle, *Chem. Geol.*, 145 (3-4), 325-394, 1998.

Plank, T., Constraints from Thorium/Lanthanum on Sediment Recycling at Subduction Zones and the Evolution of the Continents, *J. Petrol.*, in press.

Press, W. H., S. A. Teukolsky, W. T. Vetterling, and B. P. Flannery, Numerical Recipes in C, 2nd ed., 994 pp., Cambridge Univ. Press, New York, 1992.

Putirka, K., Melting depths and mantle heterogeneity beneath Hawaii and the East Pacific Rise; constraints from Na/Ti and rare earth element ratios, *J. Geophys. Res.*, 104(2), 2817-2829, 1999.

Quane, S. L., Garcia, M. O., Guillou, H., Hulsebosch, T. P., Magmatic history of the East Rift Zone of Kilauea Volcano, Hawaii based on drill core from SOH 1, *J. Volcanol. Geotherm. Res.*, 102 (3-4), 319-338, 2000.

Rapp, R. P., and Watson, E. B., Dehydration melting of metabasalt at 8-32 kbar; implications for continental growth and crust-mantle recycling, *J. Petrol.*, 36(4), 891-931, 1995.

Rhodes, J. M. and Hart, S. R., Episodic trace element and isotopic variation in historical Mauna Loa lavas, in *Mauna Loa Revealed, Geophysical Monograph Series, vol. 92*, (eds. J.M. Rhodes and J.P. Lockwood) 263-288, AGU, Washington, D.C., 1995.

Rhodes, J. M., Geochemical stratigraphy of lava flows sampled by the Hawaii Scientific Drilling Project, *J. Geophys. Res.* 101, 11,729-11,746, 1996.

Rhodes, J. M., and M. J. Vollinger, Composition of basaltic lavas sampled by phase-2 of the Hawaii Scientific Drilling Project: Geochemical stratigraphy and magma types, *Geochem. Geophys. Geosyst.*, 5, Q03G13, doi:10.1029/2002GC000434, 2004.

Ribe, N. M. and Christensen, U. R., The dynamical origin of Hawaiian volcanism, *Earth Planet. Sci. Lett.*, 171(4), 517-531, 1999.

Roden, M. F., Trull, T., Hart, S. R., and Frey, F. A., New He, Sr, Nd and Pb isotopic constraints on the constitution of the Hawaiian plume: Results from Koolau Volcano, Oahu, Hawaii. *Geochim. Cosmochim. Acta.*, 58, 1431-1440, 1994.

Salters, V. J. M., The generation of mid-ocean ridge basalts from the Hf and Nd isotope perspective. *Earth Planet. Sci. Letts.*, 141, 109-123, 1996.

Salters, V. J. M. and Longhi, J., Trace element partitioning during the initial stages of melting beneath mid-ocean ridges. *Earth Planet. Sci. Letts.*, 166, 15-30, 1999.

Seitz, H.-M., Altherr, R., Ludwig, T., Partitioning of transition elements between orthopyroxene and clinopyroxene in peridotitic and websteritic xenoliths; new empirical geothermometers, *Geochim. Cosmochim. Acta.*, 63 (23-24), 3967-3982, 1999.

Sharp, W. D. and Renne, P. R.,  $^{40}\text{Ar}/^{39}\text{Ar}$  dating of core recovered by the Hawaii Scientific Drilling Project (Phase 2) Hilo, Hawaii, submitted to *Geochem. Geophys. Geosyst.*

Shinozaki, K., Ren, Z.-Y., Takahashi, E., Geochemical and petrological characteristics of Nuuanu and Wailau landslide blocks, in *Hawaiian volcanoes; deep underwater perspectives, Geophysical Monograph Series, vol. 128*, (eds, Takahashi, E., Lipman, P. W., Garcia, M. O., Naka, J., Aramaki, S), 297-310, 2002.

Sobolev, A.V., Hofmann, A.W., and Nikogosian, I. K., Recycled oceanic crust observed in ghost plagioclase within the source of Mauna Loa lavas, *Nature* 404, 986-990, 2000.

Sobolev, A. A., Hofmann, A. W., Sobolev, S. V., Nikogosian, I. K., An olivine free mantle source of Hawaiian shield basalts, *submitted to Nature*.

Stolper, E., Sherman, S., Garcia, M., Baker, M. and Seaman, C., Glass in the submarine section of the HSDP2 drill core, Hilo, Hawaii, *Geochem. Geophys. Geosys*, 5, Q07G15, doi:10.1029/2003GC000553, 2004.

Stracke, A., Bizimis, M., and V. J. M. Salters, Recycling oceanic crust: Quantitative constraints, *Geochem. Geophys. Geosyst.*, 4(3), 8003, doi:10.1029/2001GC000223, 2003.

Takahashi, E., and Nakajima, K., Melting process in the Hawaiian Plume; an experimental study, in *Hawaiian volcanoes; deep underwater perspectives, Geophysical Monograph Series, vol. 128*, (eds, Takahashi, E., Lipman, P. W., Garcia, M. O., Naka, J., Aramaki, S), 403-418, 2002.

Tanaka, R., Nakamura, E., Takahashi, E., Geochemical evolution of Koolau Volcano, Hawaii, in *Hawaiian volcanoes; deep underwater perspectives, Geophysical Monograph Series, vol. 128*, (eds, Takahashi, E., Lipman, P. W., Garcia, M. O., Naka, J., Aramaki, S), 311-332, 2002.

van Westrenen, W., Blundy, J. D., Wood, B. J., High field strength element/rare earth element fractionation during partial melting in the presence of garnet; implications for identification of mantle heterogeneities, *Geochem. Geophys., Geosys*, 2(7), doi:10.1029/2000GC000133, 2001.

Wagner, T. P., and Grove, T. L., Melt/harzburgite reaction in the petrogenesis of tholeiitic magma from Kilauea Volcano, Hawaii, *Contrib. Mineral. Petrol.*, 131 (1), 1-12, 1998.

Walter, M. J., Melting of garnet peridotite and the origin of komatiite and depleted lithosphere, *J. Petrol.*, 39 (1), 29-60, 1998.

Yang, H.-J., Frey, F. A., Rhodes, J. M., and Garcia, M. O., Evolution of Mauna Kea volcano: Inferences from lava compositions recovered in the Hawaii Scientific Drilling Project, *J. Geophys. Res.* 101, 11,747-11,767, 1996

Yaxley G. M. and Green, D. H., Reactions between eclogite and peridotite: mantle refertilisation by subduction of oceanic crust, *Schweiz. Mineral. Petrogr. Mitt.* 78, 243-255, 1998.

Yogodzinski, G. M., Kay, R. W., Volynets, O. N., Koloskov, A. V., Kay, S. M., Magnesian andesite in the western Aleutian Komandorsky region; implications for slab melting and processes in the mantle wedge, *Geol. Soc. Am. Bull.*, 107 (5), 505-519, 1995.

**Figure Caption:**

**Fig. 1.** Th abundance vs selected incompatible element abundances (in ppm).

In this figure and all subsequent figures, all KSDP core samples are included in Kalihi-stage lavas. The Kalihi-stage to Makapuu-stage transition is inferred to be within the overlying rotary drilled interval (see Fig. 10 of Haskins and Garcia, 2004). Most notable are the higher La/Th and Sr/Th of Makapuu-stage lavas. In **panels f-h**, the greater scatter of Ba, Rb and Sr reflects post-magmatic alteration as indicated by altered ( $K_2O/P_2O_5 > 2.2$  or  $< 1.2$  or L.O.I.  $> 0.8\%$ ) lavas. Unit 70 is not an obviously altered sample and high Ba abundance was also obtained by XRF analysis (Table 5 of Haskins and Garcia, 2004). High Ba is associated with highly altered KSDP lavas, especially in the lower part of the core beneath the sandstone unit at 566 m below sea level, such as Unit 87. We infer that the high Ba in Unit 70 is a result of alteration. Units 7 and 40 range to higher Pb abundances, and their high Pb values are confirmed by duplicate analyses. It may reflect Pb contamination during sample collection or sample preparation.

**Fig. 2.** Primitive mantle normalized trace element abundances in Makapuu-stage and Kahili-stage lavas. Primitive mantle values are from Hofmann (1988).

Measured incompatible element abundances in lavas with  $2.2 > K_2O/P_2O_5 > 1.2$  and  $MgO > 6.5\%$  were adjusted by adding or subtracting equilibrium olivine until the whole rock Fe/Mg ratio was in equilibrium with  $Fo_{90}$  olivine (0.1% increments using  $(Fe/Mg)_{\text{olivine}} / (Fe/Mg)_{\text{melt}} = 0.30$ ).

**Fig. 3.** Ba/Rb and Sr/Nd vs  $K_2O/P_2O_5$  and Loss on Ignition (L.O.I.). Highly altered lavas have relatively high L.O.I. and Ba/Rb but low  $K_2O/P_2O_5$ . Sr/Nd also decreases with increasing L.O.I., thereby indicating Sr loss during alteration (**panel d**). However, the offset of Makapuu-stage lavas to high Sr/Th (Fig. 1g) and Sr/Nd (**panel c**) is not correlated with  $K_2O/P_2O_5$ ; hence, relatively high Sr is a magmatic characteristic of Makapuu-stage lavas.

Kalihi-stage lavas: major element and L.O.I. data are from Haskins and Garcia (2004), and trace element data are from this study.

Makapuu-stage lavas: major element data are from Frey et al. (1994), and trace element data are from this study.

**Fig. 4.** Sr/Nb vs La/Nb; and MgO (%) vs Sr/Nb and La/Nb for Makapuu-stage and Kalihi-stage lavas.

In **panel a**, Kalihi-stage lavas are not similar to subaerially exposed Makapuu-stage lavas, but they are within the field defined by Mauna Loa lavas. Specifically, compared with Makapuu-stage lavas, Kalihi-stage lavas have lower La/Nb and Sr/Nb. These differences are not related to MgO content (**panels b and c**).

Following Haskins and Garcia (2004), only relatively unaltered lavas (Kalihi-stage, Makapuu-stage and Mauna Loa lavas) with  $2.2 > K_2O/P_2O_5 > 1.2$  and  $L.O.I. < 0.8\%$  are plotted. The squares are ICP-MS data for Makapuu-stage lavas and open circles are data for Kalihi-stage lavas obtained in this study. Major element data are from Frey et al. (1994) (Makapuu) and Haskins and Garcia (2004) (KSDP), respectively. Fields labeled as “Makapuu-stage Lavas” are defined by XRF and INAA data from Frey et al. (1994). Mauna Loa data are from Garcia et al. (1995a), Rhodes (1995; 1996), Rhodes and Hart

(1995), Cohen et al. (1996), Rhodes and Vollinger (2004), our unpublished INAA data for Mauna Loa section of HSDP2.

**Fig. 5.** Depth profiles of  $\text{Al}_2\text{O}_3/\text{CaO}$ ,  $\text{La}/\text{Nb}$ ,  $\text{Sr}/\text{Nb}$  and  $\text{La}/\text{Yb}$  for KSDP drill hole.

These ratios generally increase upwards from an elevation of ~470 m below sea level, but there are superimposed high frequency variations. Several lavas with geochemical characteristics similar to Makapuu-stage lavas, e.g., high  $\text{Al}_2\text{O}_3/\text{CaO}$ ,  $\text{La}/\text{Nb}$  and  $\text{Sr}/\text{Nb}$ , occur in the interval of 304 to 336 m. In addition, a few lavas at ~525 m have some geochemical characteristics similar to Makapuu-stage lavas. The Makapuu/Kalihi-stage compositional boundary, vertical dashed line, is taken as  $\text{Al}_2\text{O}_3/\text{CaO} = 1.45$  (Haskins and Garcia, 2004),  $\text{La}/\text{Nb} = 1.09$  and  $\text{Sr}/\text{Nb} = 39.4$  (lowest values in Makapuu-stage lavas; Fig. 4).

Following Haskins and Garcia (2004), unaltered lavas are defined as lavas with  $2.2 > \text{K}_2\text{O}/\text{P}_2\text{O}_5 > 1.2$  and  $\text{L.O.I.} < 0.8\%$ .

**Fig. 6 a-f:**  $\text{La}/\text{Nb}$  and  $\text{Th}/\text{La}$  vs  $^{143}\text{Nd}/^{144}\text{Nd}$ ,  $^{176}\text{Hf}/^{177}\text{Hf}$  and  $^{208}\text{Pb}/^{206}\text{Pb}$  for Makapuu-stage and Kalihi-stage lavas.

Kalihi-stage lavas overlap with the field defined by Mauna Loa lavas in **panels a** and **c**. The linear trends in these panels imply that the transition from Kalihi-stage composition to Makapuu-stage composition reflect an increasing role of a sedimentary component in the source. Kalihi-stage Units 6 and 9 near the top of the KSDP core are transitional (i.e., relatively low  $\text{Th}/\text{La}$  and high  $\text{La}/\text{Nb}$ ) to Makapuu-stage characteristics. Labeled Kalihi-

stage Units 8 and 71 also have relatively low Th/La (Unit 71 also has relatively high La/Nb), but their isotopic ratios do not trend to Makapuu-stage field.

**g-i:** Ce/Pb vs  $^{143}\text{Nd}/^{144}\text{Nd}$ ,  $^{176}\text{Hf}/^{177}\text{Hf}$  and  $^{208}\text{Pb}/^{206}\text{Pb}$  for Makapuu-stage and Kalihi-stage lavas. There are no obvious trends and Makapuu-stage and Kalihi-stage lavas have similar Ce/Pb.

**j-l:** La/Yb vs  $^{143}\text{Nd}/^{144}\text{Nd}$ ,  $^{176}\text{Hf}/^{177}\text{Hf}$  and  $^{208}\text{Pb}/^{206}\text{Pb}$  for Makapuu-stage and Kalihi-stage lavas. There are no obvious trends; consequently, we infer that variation in La/Yb reflects the melting process control rather than source heterogeneity.

$^{208}\text{Pb}/^{206}\text{Pb}$  represents the time-integrated  $^{232}\text{Th}/^{238}\text{U}$  since the Earth formation, and is defined as  $[(^{208}\text{Pb}/^{204}\text{Pb})_{\text{sample}} - 29.475] / [(^{206}\text{Pb}/^{204}\text{Pb})_{\text{sample}} - 9.307]$  (Galer and O’Nions, 1985).

Isotopic data for Kalihi-stage lavas are from Salters et al. (in prep.) and Fekiacova et al. (in prep.). Isotopic data for Makapuu-stage lavas are from Roden et al. (1994), Lassiter and Hauri (1998) and Blichert-Toft et al. (1999).

Mauna Loa data are from Rhodes (1995; 1996), Rhodes and Hart (1995), Cohen et al. (1996), Blichert-Toft et al. (2003) and our unpublished INAA data for Mauna Loa section of HSDP 2.

**Fig. 7a-b** Sr/Nb vs La/Nb and Th/La for estimated subducting sediment columns and global subducting sediment (GLOSS) from Plank and Langmuir (1998). Sediments are generally characterized by high La/Nb (>2) and Sr/Nb, but only carbonate and apatite-

rich sediment columns are characterized by high Sr/Nb (>50) and low Th/La (<0.2), such as those at Central America and Colombia.

**Fig. 7c**  $\epsilon_{Nd}$  vs  $\epsilon_{Hf}$  for Hawaiian lavas. Figure is modified from Fig. 2 of Blichert-Toft et al. (1999) by adding new data for KSDP lavas from Salters et al. (in prep.). The pink triangle is calculated by adding 3% of 2 Ga recycled carbonate-apatite-rich sediment to 97% primitive mantle (see Table 2 for details). This mixture is appropriate as an end-member component for Makapuu-stage lavas.

**Fig. 8.** La/Nb vs Sr/Nb,  $^{143}Nd/^{144}Nd$  and  $^{208}Pb/^{206}Pb$  for samples from Koolau shield and Nuuanu landslide blocks studied by Tanaka et al. (2002). Legend indicates stratigraphic sequence inferred in Fig. 2 of Tanaka et al. (2002). Fields labeled as ‘Makapuu-stage’, ‘Kalihi-stage’ and ‘Mauna Loa’ in **panel a.** are the same as these in Fig 4; Kalihi-stage (KSDP) field in **panels b** and **c** is defined by KSDP lavas (this study; Salters et al., in prep.; Fekiacova et al., in prep.); and Makapuu field in **panels b** and **c** is from Fig. 6.

**Fig. 9.** MgO (%) vs Sc, Yb, Y and Ni (all in ppm) for Makapuu-stage and Kalihi-stage lavas.

Fields for Mauna Kea, Mauna Loa and Kilauea lavas are plotted for comparison. Relative to Kalihi-stage, Mauna Loa, Mauna Kea and Kilauea lavas, Makapuu-stage lavas have lower Sc, Y and Yb and higher Ni abundances.

In **panel a, b** and **d**, only our ICP-MS data for Koolau (Makapuu-stage and Kalihi-stage) and Mauna Kea lavas are plotted. Since there are negligible systematic differences

between Sc and Yb abundances determined by INAA and ICP-MS at MIT (e.g., Fig. A5 of Huang and Frey., 2003), **panels a** and **b** also show a field for Mauna Loa lavas (Sc and Yb abundances determined by INAA). However, there is a significant interlab difference in Y abundance determined by ICP-MS at MIT and XRF at University of Massachusetts (Fig. A4 of Huang and Frey., 2003), therefore, **panel c** shows Y data obtained by XRF and **panel d** shows Y data obtained by ICP-MS.

Ni abundances in Koolau, Mauna Kea, Mauna Loa and Kilauea lavas were obtained by XRF from University of Massachusetts.

Data sources: Kalihi-stage lavas: MgO, Ni and Y (XRF) from Haskins and Garcia (2004); Sc-Y(ICP-MS)-Yb: this study.

Makapuu-stage lavas: MgO, Ni and Y (XRF) from Frey et al. (1994); Sc-Y(ICP-MS)-Yb: this study.

Mauna Kea: MgO, Ni and Y(XRF) from Rhodes (1996) and Rhodes and Vollinger (2004); Sc-Y(ICP-MS)-Yb from Huang and Frey (2003).

Mauna Loa: from Garcia et al. (1995a), Rhodes (1995; 1996), Rhodes and Hart (1995), Cohen et al. (1996), Rhodes and Vollinger (2004).

Kilauea: Garcia et al., (2000).

**Fig. 10.** La/Yb vs Sc/Y, Zr/Yb and Tb/Yb for Makapuu-stage and Kalihi-stage lavas.

Fields for Mauna Loa and Makapuu-stage lavas defined by XRF and INAA data are also shown for comparison. Since Tb data obtained by INAA are not very precise (Fig. A5 of Huang and Frey, 2003), the fields for Makapuu-stage lavas and Mauna Loa lavas defined

by INAA data are not plotted in **panel c**. Only lavas with  $2.2 > \text{K}_2\text{O}/\text{P}_2\text{O}_5 > 1.2$  and  $\text{L.O.I.} < 0.8\%$  are plotted.

As discussed in the text, the source of Makapuu-stage lavas included a recycled sedimentary component. We consider this complexity in modeling. First, we calculate the trends formed by Makapuu-stage and Kalihi-stage lavas using a common garnet peridotite source; i.e., with the same Sc/Y, La/Yb and Zr/Yb ratios. These are the melting trajectories labeled as “original source”. Input values for the calculation are in Table 3. Then we add 3% carbonate sediment to this “original source” (Table 3). The melting trajectories labeled as “original source + 3% sediment” are calculated using this sediment enriched source. Less than 3% sediment is sufficient to explain the distinctive features of Makapuu-stage lavas, such as high Sr/Nb, low Th/La and their Nd-Hf isotopic ratios.

**Fig. 11.** Sm/Yb vs Zr/Hf for Makapuu-stage and Kalihi-stage lavas. Melting trajectories of eclogite are taken from Fig. 10 of Pertermann et al. (2004). Melting trajectories for garnet peridotite with variable initial clinopyroxene/garnet ratios use the input parameters in Table 3, with Zr/Hf and Sm/Yb equal to primitive mantle values (Hofmann, 1988). That is, the proportions of olivine and orthopyroxene in garnet peridotite are fixed, and the proportions of clinopyroxene and garnet are variable. The melting trajectories are labeled with % melting and initial clinopyroxene/garnet ratios. Pertermann et al. (2004) noted that the steep trajectories for melting of eclogite (high clinopyroxene/garnet ratio of 82/18 and 75/25) contrast with the nearly horizontal trend for melting of garnet peridotite with clinopyroxene/garnet  $\sim 1$ . They concluded that some Koolau lavas are consistent

with partial melting of garnet-poor eclogite. This conclusion obviously depends upon the clinopyroxene/garnet ratio of the garnet peridotite.

It is important that Makapuu-stage and Kalihi-stage lavas form different trends, but the whole range of Zr/Hf in Koolau lavas is barely beyond analytical uncertainty. The 2- $\sigma$  analytical uncertainties for Zr/Hf and Sm/Yb are from Huang and Frey (2003).

**Fig. 12.** Olivine adjusted major element contents in Makapuu-stage and Kalihi-stage lavas. MgO vs SiO<sub>2</sub>, TiO<sub>2</sub>, Al<sub>2</sub>O<sub>3</sub> and CaO (all in %). Major element contents are adjusted to be in equilibrium with mantle olivine (Fo<sub>90</sub>) by adding or subtracting equilibrium olivine at 0.1% steps assuming (Fe/Mg)<sub>olivine</sub>/(Fe/Mg)<sub>melt</sub>=0.30. Only lavas with 2.2>K<sub>2</sub>O/P<sub>2</sub>O<sub>5</sub>>1.2 and MgO>6.5% are plotted. Note that after olivine adjustment, a large variation in MgO content remains. Units 6, 9 and 10 of Kalihi-stage lavas trend to high SiO<sub>2</sub> content. These three lavas are from the two groups (Units 4, 5, 6 and Units 9, 10, 12) having Makapuu-stage trace element characteristics (e.g., high Sr/Nb in Fig. 5c); the other three lavas from these two groups, Units 4, 5 and 12, are altered lavas and not shown in Fig. 9. Unit 31 has the highest olivine-adjusted MgO content, and is offset from the KSDP trend in most panels. This unit is a picrite and contains 23% olivine phenocrysts.

Data source: Makapuu-stage lavas: Frey et al. (1994); Kalihi-stage lavas: Haskins and Garcia (2004).

**Fig. 13.** Olivine adjusted SiO<sub>2</sub> (%) vs La/Nb, <sup>208</sup>\*Pb/<sup>206</sup>\*Pb, <sup>143</sup>Nd/<sup>144</sup>Nd and <sup>176</sup>Hf/<sup>177</sup>Hf for Makapuu-stage and Kalihi-stage lavas.

These linear trends show that variations in olivine adjusted major element contents are not artifacts of olivine adjustment, but reflect source heterogeneity in major element composition. Surprisingly, Makapuu-stage and Kalihi-stage lavas form subparallel trends in these panels.

Averages of Hawaiian shields or stratigraphic sections (excluding Loihi alkalic section) from Table 1 of Hauri (1996) are shown in **panel c**. Interestingly, these averages largely overlap with Koolau (Makapuu-stage and Kalihi-stage) lavas, implying that the geochemical heterogeneity of Koolau source mimics that seen in all Hawaiian shields.

Data source: See Fig captions of Figs 6 and 9.

**Fig. 14. a.**  $1/[Nd]$  (olivine adjusted abundance) vs  $^{143}Nd/^{144}Nd$ ; **b.**  $1/[Pb]$  (olivine adjusted abundance) vs  $^{208}Pb/^{206}Pb$ ; **c.**  $1/[Hf]$  (olivine adjusted abundance) vs  $^{176}Hf/^{177}Hf$ ; **d.**  $1/[Nb]$  (olivine adjusted abundance) vs  $La/Nb$  for Makapuu-stage and Kalihi-stage lavas. Kalihi-stage lavas form linear trends in **panels a** and **c** which imply mixing lines. Although, Makapuu-stage lavas do not form obvious trends, they are offset from the trends defined by Kalihi-stage lavas.

Data source: See Fig 6 captions.

**Fig. 15** MgO vs SiO<sub>2</sub> and CaO (%).

Makapuu-stage (squares) and Kalihi-stage (open circles) lavas (with  $2.2 > K_2O/P_2O_5 > 1.2$  and  $MgO > 6.5\%$ ) are adjusted to be in equilibrium with Fo<sub>90</sub> olivine. The Hawaiian shield field is defined by olivine adjusted (to be in equilibrium with Fo<sub>90</sub> olivine) compositions (only lavas with  $K_2O/P_2O_5 > 1.2$  and  $MgO > 6.5\%$  are included.).

Three end members (grey solid circles) estimated by Hauri (1996) and partial melts of eclogite (triangles, 2-3 GPa, Rapp and Watson, 1995 and Pertermann and Hirschmann, 2003) are also shown for comparison.

In the MgO-SiO<sub>2</sub> plot, Hawaiian shield lavas define a negative trend with Makapuu-stage lavas as one extreme. Clearly, the negative trend defined by Koolau (Makapuu-stage and Kalihi-stage) lavas points towards low temperature partial melts or hydrous partial melts of eclogite.

In the MgO-CaO plot lavas from all Hawaiian shields do not form a single trend, but the positive trend formed by Makapuu-stage and Kalihi-stage lavas also points towards low temperature partial melts or hydrous partial melts of eclogite.

Hawaiian shield data used in this figure are: Koolau (Frey et al., 1994; Haskins and Garcia, 2004); Mauna Loa (Garcia et al., 1995a; Rhodes, 1995; 1996; Rhodes and Hart, 1995; Rhodes and Vollinger, 2004); Mauna Kea (Rhodes, 1996; Rhodes and Vollinger, 2004; Stolper et al., 2004); Kilauea (Chen et al., 1996; Garcia et al., 2000; Quane et al., 2000); Loihi (Frey and Clague, 1983; Garcia et al., 1993; 1995b; 1998; Norman and Garcia, 1999); Kahoolawe (Fodor et al., 1992; Leeman et al., 1994; our unpublished data).

**Fig. 16** Lomb normalized periodograms of Al<sub>2</sub>O<sub>3</sub>/CaO, Th/La, Sr/Nb, La/Nb, La/Yb and Tb/Yb for KSDP lavas. Only unaltered lavas ( $1.2 < K_2O/P_2O_5 < 2.2$  and  $L.O.I. < 0.8$ ) are included in the analysis. Two confidence level lines (at 50% and 95%) are shown for comparison.

The procedure is given by *Press et al.* (pp575-579, 1992), and Matlab® script Lomb.m (<http://mathforum.org/epigone/comp.soft-sys.matlab/hangdiher/34CED3BF.B95E25AF@spectral-imaging.com>) was used.

In **Panel e**, the long-term secular trend in  $\text{Al}_2\text{O}_3/\text{CaO}$  was removed before we applied the analysis; that is, the  $\text{Al}_2\text{O}_3/\text{CaO}$  vs time trend was fit using a polynomial function ( $n=2$ ), and this trend was subtracted from the measured  $\text{Al}_2\text{O}_3/\text{CaO}$  values. This step removes the very low frequency peak observed in **Panel a** without affecting the peak at  $\sim 21$  times resurfacing time. In addition, this peak is not sensitive to the procedure used for removing the secular trend; e.g., the peak is also present if a  $n=5$  polynomial function is used to remove the secular trend (not shown).

**Table 1a. Trace Element Abundances (in ppm) in KSDP Lavas determined by ICP-MS.**

UNIT	Elev. (m)	rock type	Sc	Rb	Sr	Y	Zr	Nb	Ba	La	Ce	Pr	Nd	Sm	Eu	Gd	Tb	Dy	Ho	Er	Tm	Yb	Lu	Hf	Ta	Pb	Th	U
1	-303.8	picrite	23.3	3.16	249	19.4	95	7.06	69.1	7.18	17.6	2.68	12.8	3.56	1.22	3.87	0.623	3.55	0.698	1.78	0.259	1.49	0.216	2.47	0.474	0.976	0.497	0.136
2	-308.4	picrite	22.2	1.85	225	17.3	85	6.15	60.7	6.17	15.3	2.36	11.2	3.15	1.09	3.45	0.555	3.10	0.617	1.55	0.227	1.34	0.190	2.19	0.410	1.14	0.434	0.123
3	-308.9	picrite	22.6	3.44	250	19.9	98	7.14	66.1	7.53	18.9	2.78	13.1	3.72	1.31	4.05	0.653	3.69	0.705	1.91	0.261	1.54	0.218	2.63	0.489	1.12	0.524	0.152
4	-312.3	ol basalt	25.8	2.38	318	22.8	121	7.61	73.8	8.31	20.6	3.23	15.4	4.40	1.58	4.73	0.755	4.20	0.814	2.07	0.295	1.73	0.246	3.05	0.520	0.936	0.573	0.165
5	-314.4	picrite	22.4	2.71	259	18.9	98	6.29	72.9	6.68	17.4	2.55	12.6	3.60	1.29	3.93	0.636	3.56	0.689	1.78	0.254	1.50	0.210	2.56	0.422	0.828	0.465	0.143
6	-316.6	picrite	21.0	3.55	261	18.9	97	6.28	66.1	6.81	16.8	2.66	12.8	3.66	1.29	3.90	0.623	3.50	0.678	1.75	0.241	1.44	0.203	2.53	0.430	0.795	0.455	0.140
7	-325.0	ol basalt	27.9	4.66	301	23.9	126	8.35	76.6	8.50	21.4	3.36	16.0	4.52	1.59	4.80	0.792	4.33	0.838	2.16	0.301	1.78	0.247	3.25	0.560	1.58	0.571	0.171
8	-329.0	ol basalt	26.6	5.15	304	24.6	125	8.52	79.1	8.78	21.9	3.43	16.4	4.59	1.59	4.98	0.796	4.48	0.868	2.22	0.308	1.80	0.256	3.21	0.558	1.04	0.555	0.173
9	-332.4	ol basalt	26.9	3.46	267	23.4	104	6.85	59.0	7.04	17.3	2.72	13.3	3.96	1.43	4.44	0.726	4.19	0.830	2.12	0.300	1.79	0.257	2.74	0.465	0.744	0.465	0.146
10	-334.2	basalt	27.1	2.25	271	22.7	103	6.98	69.8	6.99	18.1	2.73	13.1	3.93	1.40	4.37	0.736	4.17	0.811	2.07	0.294	1.75	0.252	2.68	0.472	0.836	0.486	0.137
12	-336.0	basalt	26.2	3.59	274	23.3	108	7.27	67.7	7.13	17.9	2.76	13.4	4.00	1.42	4.45	0.728	4.14	0.814	2.08	0.300	1.74	0.248	2.77	0.477	1.06	0.467	0.138
13	-338.0	basalt	29.9	7.15	378	27.8	158	11.4	106	12.1	29.9	4.50	21.2	5.62	1.92	5.81	0.920	5.13	0.970	2.43	0.346	2.02	0.286	3.96	0.729	1.23	0.814	0.247
14	-341.9	ol basalt	30.2	7.03	371	27.1	151	10.8	101	11.7	30.1	4.29	20.4	5.46	1.86	5.70	0.886	4.93	0.957	2.47	0.341	1.99	0.278	3.84	0.701	1.23	0.794	0.241
15	-343.8	ol basalt	27.2	5.30	301	25.0	123	9.69	82.6	9.29	24.0	3.54	16.6	4.63	1.64	5.03	0.823	4.57	0.885	2.30	0.319	1.87	0.270	3.21	0.658	1.23	0.678	0.201
16	-345.5	basalt	30.0	6.79	380	27.5	156	11.9	107	11.9	30.4	4.43	21.6	5.63	1.92	5.82	0.931	5.13	0.990	2.52	0.351	2.01	0.283	4.00	0.801	1.30	0.793	0.243
17	-350.4	basalt	30.0	5.90	346	26.8	142	10.6	91.1	10.2	25.7	3.91	18.5	5.10	1.78	5.51	0.892	5.06	0.976	2.56	0.363	1.99	0.296	3.62	0.727	1.17	0.725	0.220
18	-355.6	ol basalt	29.7	5.95	375	28.1	155	11.4	93.0	11.2	28.8	4.25	20.4	5.56	1.91	5.82	0.935	5.14	0.987	2.52	0.350	2.02	0.287	3.87	0.748	1.17	0.785	0.228
19	-357.8	basalt	30.1	6.43	372	28.0	154	11.5	100	11.4	29.2	4.25	20.9	5.57	1.92	5.83	0.940	5.17	0.992	2.53	0.352	2.06	0.280	3.91	0.761	1.20	0.781	0.239
20	-359.2	picrite	26.1	5.63	312	23.3	129	10.2	90.4	9.74	24.4	3.64	17.1	4.61	1.56	4.84	0.775	4.37	0.818	2.16	0.293	1.71	0.241	3.32	0.671	1.06	0.692	0.203
21	-362.5	basalt	29.0	1.94	340	25.9	147	10.7	93.9	9.70	23.9	3.77	18.1	5.12	1.77	5.33	0.875	4.87	0.927	2.34	0.326	1.93	0.275	3.74	0.707	1.14	0.694	0.209
22	-363.9	basalt	30.0	5.13	346	25.7	135	9.68	82.2	9.10	24.4	3.56	17.5	4.90	1.69	5.14	0.825	4.67	0.910	2.33	0.331	1.90	0.275	3.43	0.643	0.993	0.635	0.198
23	-367.3	basalt	29.2	4.87	339	27.6	140	9.94	92.6	10.3	27.7	3.99	18.9	5.29	1.84	5.67	0.898	5.05	0.967	2.42	0.340	1.98	0.286	3.50	0.652	1.05	0.644	0.200
24	-370.6	basalt	28.5	4.68	330	26.1	133	9.54	81.2	9.62	25.1	3.71	17.8	5.03	1.78	5.40	0.879	4.88	0.948	2.41	0.332	1.94	0.274	3.51	0.640	0.957	0.635	0.197
25	-372.5	basalt	29.3	4.12	335	26.3	137	9.58	83.6	9.47	23.8	3.74	18.0	5.03	1.70	5.37	0.869	4.80	0.936	2.42	0.348	1.94	0.270	3.47	0.630	0.996	0.622	0.197
26	-376.1	basalt	28.8	5.44	336	26.9	141	10.1	82.9	10.2	26.3	4.02	18.9	5.24	1.83	5.63	0.904	5.02	0.954	2.48	0.331	1.99	0.286	3.70	0.673	1.36	0.668	0.210
27	-379.5	basalt	30.6	4.51	355	28.0	147	10.3	93.5	10.4	25.6	4.01	19.3	5.26	1.82	5.67	0.904	5.04	0.974	2.51	0.343	2.01	0.288	3.72	0.674	1.15	0.700	0.217
28	-379.8	basalt	29.7	6.16	342	26.7	145	10.3	92.9	10.2	26.2	3.98	19.1	5.30	1.81	5.60	0.893	5.01	0.967	2.49	0.351	2.02	0.289	3.73	0.682	1.08	0.731	0.230
29	-381.3	picrite	24.6	3.76	289	22.8	121	8.50	88.5	8.78	21.7	3.38	16.2	4.41	1.54	4.65	0.743	4.28	0.804	2.08	0.287	1.68	0.239	3.08	0.567	1.07	0.577	0.182

UNIT	Elev. (m)	rock type	Sc	Rb	Sr	Y	Zr	Nb	Ba	La	Ce	Pr	Nd	Sm	Eu	Gd	Tb	Dy	Ho	Er	Tm	Yb	Lu	Hf	Ta	Pb	Th	U
30	-383.0	basalt	27.6	4.58	306	25.2	128	9.07	93.9	9.36	23.1	3.61	17.2	4.73	1.57	5.06	0.805	4.62	0.878	2.28	0.317	1.84	0.263	3.24	0.590	1.13	0.669	0.209
31	-387.6	picrite	21.6	2.57	248	18.3	100	7.08	64.4	6.97	17.9	2.72	12.9	3.56	1.24	3.77	0.611	3.38	0.643	1.66	0.226	1.35	0.201	2.54	0.468	0.771	0.493	0.147
32	-388.2	picrite	26.7	2.49	298	22.5	123	8.73	83.2	8.71	21.9	3.42	16.4	4.49	1.54	4.72	0.762	4.24	0.816	2.10	0.292	1.69	0.239	3.15	0.575	0.989	0.602	0.170
33	-390.0	nd	30.8	4.22	325	26.5	143	10.4	95.8	9.46	24.4	3.78	17.9	5.00	1.76	5.36	0.860	4.87	0.929	2.43	0.337	2.00	0.280	3.63	0.679	1.20	0.700	0.210
34	-391.4	ol basalt	28.7	3.79	320	25.7	132	9.43	72.6	8.82	23.4	3.57	17.4	4.79	1.69	5.22	0.856	4.74	0.918	2.34	0.326	1.89	0.273	3.42	0.654	0.943	0.627	0.198
35	-392.0	ol basalt	30.4	3.31	323	28.3	141	10.2	87.0	9.50	25.5	3.78	18.1	5.13	1.77	5.49	0.897	5.09	0.985	2.61	0.354	2.08	0.293	3.67	0.672	1.08	0.674	0.219
36	-394.4	ol basalt	29.0	3.12	304	24.8	132	9.40	82.1	8.67	22.1	3.48	16.7	4.65	1.61	5.02	0.795	4.57	0.879	2.25	0.312	1.88	0.265	3.37	0.627	0.966	0.607	0.176
37	-395.8	basalt	30.8	4.68	327	27.0	140	10.2	90.4	9.52	24.3	3.80	18.0	5.06	1.77	5.48	0.880	4.89	0.962	2.43	0.346	1.99	0.286	3.61	0.676	1.22	0.658	0.194
38	-398.6	basalt	30.8	5.02	337	27.1	143	10.6	91.9	9.87	24.5	3.91	18.7	5.17	1.81	5.55	0.893	5.01	0.964	2.49	0.336	2.07	0.287	3.73	0.715	1.10	0.714	0.226
39	-403.9	basalt	31.6	4.74	348	28.2	152	11.1	90.6	9.87	27.0	3.93	19.4	5.42	1.87	5.74	0.917	5.16	1.01	2.57	0.358	2.09	0.294	3.82	0.731	1.14	0.708	0.221
40	-407.6	basalt	31.5	5.10	332	27.9	147	10.8	86.8	10.0	25.4	4.00	19.1	5.22	1.79	5.62	0.916	5.15	0.984	2.52	0.355	2.09	0.289	3.79	0.719	1.63	0.691	0.225
41	-408.8	basalt	31.6	4.70	339	29.8	153	11.0	97.9	10.6	25.5	4.21	20.2	5.63	1.87	6.04	0.974	5.47	1.07	2.75	0.390	2.21	0.316	3.98	0.739	1.12	0.725	0.228
44	-411.2	basalt	31.7	5.19	340	28.3	149	10.8	94.3	10.1	25.9	4.08	19.2	5.37	1.82	5.79	0.928	5.23	1.02	2.62	0.369	2.13	0.308	3.86	0.732	1.14	0.718	0.219
45	-412.3	basalt	27.9	4.80	308	24.9	131	9.25	83.5	9.10	23.1	3.63	17.5	4.72	1.64	5.08	0.819	4.59	0.890	2.30	0.322	1.86	0.257	3.38	0.636	1.01	0.615	0.190
46	-413.6	basalt	29.2	5.21	340	26.1	143	10.3	99.4	10.0	24.9	3.89	18.4	5.07	1.75	5.35	0.859	4.79	0.913	2.40	0.336	1.91	0.277	3.59	0.675	1.16	0.683	0.206
47	-418.8	basalt	31.1	5.37	342	26.5	142	10.3	86.8	9.99	25.0	3.87	18.5	5.10	1.70	5.31	0.856	4.78	0.929	2.42	0.337	1.95	0.277	3.61	0.677	1.10	0.673	0.204
48	-422.7	basalt	30.3	5.70	354	27.1	143	10.7	97.2	10.7	27.7	3.97	19.4	5.27	1.82	5.53	0.889	4.90	0.965	2.46	0.335	1.99	0.273	3.66	0.699	1.21	0.714	0.209
49	-426.1	basalt	32.0	4.71	329	26.1	136	9.77	78.0	9.00	23.3	3.60	17.4	4.84	1.68	5.17	0.839	4.71	0.898	2.33	0.323	1.88	0.278	3.50	0.645	0.979	0.652	0.195
50	-429.7	basalt	27.0	5.05	350	24.0	139	10.5	108	10.4	24.9	3.95	18.6	5.03	1.73	5.17	0.820	4.52	0.853	2.16	0.309	1.78	0.253	3.52	0.685	1.20	0.712	0.208
51	-433.4	basalt	31.6	4.94	350	26.9	143	9.71	90.8	9.77	24.2	3.87	18.6	5.14	1.81	5.51	0.884	4.90	0.937	2.44	0.328	1.96	0.279	3.60	0.647	1.02	0.642	0.199
52	-438.9	ol basalt	27.2	4.67	315	24.3	130	9.81	88.8	9.56	24.0	3.64	17.0	4.73	1.60	5.05	0.795	4.53	0.888	2.24	0.318	1.82	0.264	3.34	0.671	1.07	0.691	0.195
53	-440.4	ol basalt	25.8	5.37	299	23.0	124	9.57	93.4	8.84	22.3	3.31	15.9	4.41	1.55	4.74	0.753	4.30	0.831	2.12	0.295	1.75	0.249	3.21	0.640	1.10	0.656	0.193
54	-443.7	basalt	29.7	5.65	362	28.0	152	12.1	106	11.9	27.9	4.42	20.5	5.48	1.89	5.84	0.909	5.14	0.970	2.49	0.350	1.99	0.283	3.90	0.791	1.20	0.818	0.231
55	-445.7	basalt	31.9	3.17	372	27.5	158	12.8	109	11.1	28.4	4.38	20.7	5.62	1.96	5.89	0.928	5.20	0.987	2.44	0.356	2.06	0.290	4.01	0.828	1.23	0.867	0.221
56	-448.8	basalt	30.3	4.62	368	27.3	148	11.9	99.8	11.1	27.8	4.21	19.9	5.36	1.86	5.57	0.893	4.94	0.963	2.42	0.341	1.98	0.283	3.78	0.766	1.11	0.809	0.230
57	-453.2	basalt	29.5	5.06	353	27.4	153	12.2	108	11.1	27.9	4.28	20.2	5.45	1.90	5.68	0.930	5.03	0.972	2.50	0.342	2.02	0.285	3.90	0.799	1.16	0.830	0.221
59	-456.1	basalt	30.0	6.71	353	27.6	151	12.3	109	11.1	27.9	4.23	19.9	5.47	1.91	5.67	0.929	5.06	0.987	2.47	0.351	2.07	0.291	3.83	0.788	1.19	0.823	0.251
60	-464.6	basalt	30.6	2.78	366	30.3	165	13.6	115	12.2	29.7	4.54	21.5	5.77	1.96	6.20	0.998	5.50	1.07	2.75	0.382	2.18	0.315	4.10	0.878	1.19	0.876	0.191
61	-469.3	basalt	29.3	6.12	350	27.9	144	12.0	101	10.6	27.7	4.05	18.8	5.20	1.80	5.57	0.897	5.04	0.969	2.49	0.348	2.02	0.286	3.67	0.786	1.12	0.796	0.226
62	-476.4	basalt	28.9	5.71	324	25.2	130	11.04	97.3	9.61	25.0	3.65	17.1	4.66	1.63	5.02	0.817	4.61	0.889	2.33	0.323	1.85	0.261	3.27	0.700	0.991	0.698	0.199

UNIT	Elev. (m)	rock type	Sc	Rb	Sr	Y	Zr	Nb	Ba	La	Ce	Pr	Nd	Sm	Eu	Gd	Tb	Dy	Ho	Er	Tm	Yb	Lu	Hf	Ta	Pb	Th	U
63	-482.1	basalt	30.2	7.06	338	28.0	146	12.3	105	10.9	27.0	4.10	19.0	5.20	1.76	5.63	0.906	5.07	0.990	2.57	0.363	2.09	0.304	3.71	0.809	1.14	0.835	0.249
64	-493.4	ol basalt	26.3	3.45	252	21.6	99	6.87	61.3	6.59	17.3	2.57	12.6	3.69	1.32	4.13	0.669	3.92	0.748	2.01	0.276	1.63	0.236	2.56	0.463	0.802	0.444	0.132
65	-495.9	basalt	27.5	4.98	293	24.6	123	8.61	74.6	8.28	21.2	3.32	16.0	4.51	1.60	4.90	0.785	4.45	0.870	2.27	0.310	1.83	0.271	3.14	0.567	0.862	0.547	0.171
66	-506.9	basalt	29.3	5.73	318	25.0	131	9.98	82.7	9.20	23.3	3.60	17.1	4.68	1.64	5.11	0.804	4.54	0.892	2.27	0.324	1.88	0.267	3.37	0.656	1.05	0.630	0.191
67	-511.1	ol basalt	26.7	4.26	286	23.4	118	8.27	66.0	7.74	19.8	3.10	14.7	4.24	1.49	4.66	0.741	4.32	0.832	2.14	0.299	1.77	0.251	3.00	0.551	0.803	0.522	0.150
68	-514.2	ol basalt	28.1	3.53	316	24.5	128	8.86	73.8	8.78	22.5	3.41	16.1	4.54	1.58	5.00	0.800	4.56	0.869	2.26	0.314	1.79	0.255	3.26	0.599	0.951	0.607	0.172
69	-521.8	basalt	28.5	4.69	304	26.7	126	8.78	80.5	8.84	20.5	3.41	16.6	4.75	1.68	5.33	0.865	4.81	0.924	2.38	0.333	1.93	0.280	3.29	0.579	0.886	0.553	0.172
70	-526.0	basalt	29.0	2.70	300	24.1	124	8.61	185	8.20	19.0	3.16	15.3	4.48	1.60	4.84	0.787	4.40	0.848	2.15	0.305	1.77	0.248	3.15	0.555	0.885	0.552	0.190
71	-526.5	basalt	29.5	4.36	314	26.4	131	9.17	85.3	9.63	20.1	3.63	17.6	4.90	1.75	5.37	0.853	4.74	0.910	2.28	0.316	1.84	0.269	3.32	0.595	1.01	0.588	0.175
72	-533.7	basalt	30.0	3.81	322	27.0	135	9.65	80.9	9.34	23.9	3.61	17.5	4.82	1.70	5.36	0.880	4.85	0.951	2.45	0.339	1.94	0.279	3.41	0.648	1.06	0.608	0.182
73	-535.2	basalt	30.0	3.60	335	28.5	143	9.87	104	10.8	25.2	4.09	19.5	5.36	1.86	5.83	0.926	5.13	0.999	2.51	0.359	1.97	0.283	3.59	0.661	1.09	0.649	0.181
74	-537.9	basalt	29.8	4.11	320	26.5	133	9.24	95.6	9.20	22.6	3.50	17.0	4.76	1.69	5.21	0.839	4.69	0.907	2.34	0.314	1.88	0.264	3.45	0.613	1.00	0.638	0.172
75	-544.9	basalt	29.1	5.43	311	26.9	139	9.52	81.7	9.42	23.9	3.72	18.0	5.04	1.76	5.48	0.891	4.96	0.976	2.48	0.353	2.03	0.291	3.59	0.643	0.984	0.643	0.203
76	-550.3	basalt	32.0	2.40	305	24.8	140	9.68	84.0	8.72	22.4	3.74	18.3	5.13	1.82	5.38	0.849	4.70	0.898	2.23	0.307	1.78	0.255	3.64	0.669	0.948	0.609	0.186
81	-556.4	basalt	30.6	5.69	318	27.7	141	9.88	133	11.1	23.2	4.25	20.1	5.46	1.88	5.81	0.926	5.11	0.966	2.41	0.346	1.96	0.284	3.54	0.654	1.09	0.620	0.383
82	-558.7	basalt	31.8	2.38	325	29.5	144	10.2	73.3	10.5	24.9	4.11	19.7	5.38	1.88	5.88	0.952	5.27	1.03	2.63	0.374	2.14	0.300	3.72	0.684	1.00	0.648	0.180
83	-562.0	basalt	29.9	2.91	323	28.8	141	9.96	68.4	9.98	24.4	3.83	18.4	5.19	1.82	5.64	0.916	5.14	1.01	2.58	0.362	2.11	0.311	3.61	0.685	0.990	0.640	0.259
85	-564.8	ol basalt	29.0	3.12	283	27.1	135	11.3	114	11.5	26.8	4.22	19.6	5.09	1.73	5.47	0.858	4.93	0.946	2.48	0.344	1.97	0.286	3.36	0.734	1.59	0.748	0.213
87	-566.2	basalt	31.9	8.22	171	24.7	148	12.6	267	9.23	27.8	3.53	16.1	4.46	1.56	4.75	0.805	4.50	0.875	2.22	0.327	1.90	0.267	3.77	0.817	1.74	0.843	0.223
88	-569.4	ol basalt	24.9	2.42	212	21.4	104	8.68	81.6	8.72	21.1	3.15	14.5	3.92	1.37	4.24	0.685	3.87	0.753	1.95	0.274	1.64	0.233	2.73	0.589	0.947	0.631	0.117
91	-573.7	basalt	31.3	2.87	357	28.0	163	14.3	128	14.8	37.1	5.06	22.4	5.72	1.95	5.82	0.933	5.18	0.991	2.58	0.351	2.05	0.291	4.13	0.954	1.59	1.09	0.252
92	-581.7	picrite	21.5	2.10	191	18.7	94	7.89	207	7.40	18.0	2.71	12.8	3.46	1.16	3.77	0.604	3.43	0.650	1.66	0.231	1.33	0.189	2.38	0.531	1.08	0.486	0.122
93	-586.4	basalt	31.3	2.16	324	27.4	140	9.97	90.0	9.28	24.2	3.79	18.5	5.18	1.80	5.61	0.896	5.16	0.990	2.57	0.358	2.08	0.297	3.63	0.684	1.14	0.629	0.186
94	-590.4	basalt	30.3	1.44	330	27.3	129	8.86	68.0	9.04	22.5	3.55	17.3	4.88	1.72	5.37	0.854	4.81	0.943	2.41	0.337	1.98	0.282	3.30	0.604	1.05	0.544	0.157
95	-593.7	basalt	29.9	1.75	317	25.5	129	9.10	64.6	8.62	21.9	3.47	16.8	4.79	1.69	5.18	0.862	4.76	0.917	2.33	0.325	1.95	0.275	3.33	0.612	0.882	0.572	0.168
96	-596.0	basalt	30.3	1.40	316	24.1	116	8.23	64.3	7.92	19.8	3.14	15.3	4.34	1.55	4.70	0.762	4.27	0.832	2.13	0.309	1.79	0.256	2.99	0.545	1.12	0.510	0.160
97	-597.7	picrite	27.3	2.24	236	23.5	121	9.91	84.2	8.62	22.9	3.37	16.2	4.43	1.54	4.82	0.777	4.28	0.830	2.14	0.294	1.72	0.241	3.20	0.671	0.872	0.602	0.171
98	-600.3	basalt	31.8	2.07	294	27.4	134	10.8	83.9	9.05	23.4	3.65	17.5	4.95	1.75	5.51	0.891	5.01	0.989	2.51	0.359	2.06	0.292	3.54	0.720	0.989	0.638	0.158
100	-606.3	basalt	32.6	3.70	308	28.3	141	10.4	64.7	9.22	23.9	3.73	17.8	5.02	1.78	5.54	0.911	5.06	1.00	2.59	0.361	2.05	0.294	3.61	0.684	1.08	0.668	0.220
101	-622.3	basalt	30.6	3.03	295	24.0	120	8.97	49.5	8.23	21.3	3.29	15.7	4.23	1.48	4.72	0.752	4.33	0.841	2.19	0.305	1.74	0.254	3.05	0.607	0.835	0.539	0.162
102	-625.5	ol basalt	30.8	3.86	289	25.3	124	9.66	60.3	8.69	23.5	3.48	16.4	4.52	1.60	5.01	0.821	4.59	0.912	2.34	0.327	1.89	0.272	3.29	0.649	0.869	0.589	0.196
103	-627.8	basalt	32.5	3.32	311	28.0	135	10.3	66.3	9.53	25.7	3.70	17.5	4.87	1.68	5.38	0.892	4.96	0.982	2.53	0.354	2.07	0.293	3.47	0.686	0.925	0.641	0.203

**Table 1b. Trace Element Abundances (in ppm) in Makapuu-stage Lavas.**

Sample <sup>(1)</sup>	Sc	Rb	Sr	Y	Zr	Nb	Ba	La	Ce	Pr	Nd	Sm	Eu	Tb	Dy	Ho	Er	Tm	Yb	Lu	Hf	Ta	Pb	Th	U
KOO-1	26.5	5.79	416	24.0	151	8.13	83.8	10.7	26.2	4.15	19.6	5.21	1.74	0.803	4.42	0.831	2.11	0.304	1.67	0.240	3.56	0.560	1.20	0.611	0.181
KOO-7	25.7	6.24	411	25.5	139	9.05	81.5	10.3	25.0	4.25	20.0	5.27	1.77	0.847	4.69	0.891	2.31	0.340	1.85	0.263	3.73	0.633	1.16	0.592	0.175
KOO-8	24.9	7.17	480	25.5	154	9.42	112	12.1	30.7	4.48	21.0	5.35	1.78	0.822	4.51	0.853	2.20	0.312	1.72	0.238	3.62	0.628	1.28	0.674	0.200
KOO-9	22.7	2.10	280	22.2	99	5.06	49.5	6.00	15.5	2.36	12.0	3.79	1.34	0.682	3.94	0.751	1.99	0.297	1.61	0.233	2.52	0.351	0.709	0.362	0.102
KOO-10	23.1	3.07	340	21.0	117	6.80	61.7	7.88	20.0	3.06	15.1	4.27	1.45	0.687	3.83	0.730	1.87	0.274	1.50	0.218	2.90	0.469	0.968	0.474	0.125
KOO-15	25.5	1.50	377	28.4	148	8.71	103	12.2	27.9	4.48	21.3	5.53	1.85	0.885	4.98	0.975	2.46	0.354	2.00	0.278	3.64	0.579	1.10	0.662	0.146
KOO-16	25.9	0.74	372	29.0	140	8.65	67.8	10.3	25.5	3.96	19.2	5.36	1.84	0.923	5.21	0.999	2.58	0.382	2.05	0.287	3.57	0.609	1.06	0.600	0.139
KOO-17A	19.2	0.23	276	19.5	101	5.64	40.3	7.72	18.2	2.85	13.3	3.39	1.13	0.538	3.00	0.597	1.55	0.225	1.23	0.173	2.36	0.387	0.743	0.388	0.075
KOO-20	28.8	7.26	454	26.4	171	10.7	110	13.2	33.3	4.90	23.2	5.96	1.95	0.916	5.03	0.954	2.42	0.350	1.96	0.275	4.09	0.713	1.43	0.756	0.194
KOO-26	26.6	1.87	345	25.0	115	6.80	61.8	8.44	20.6	3.14	15.2	4.29	1.49	0.747	4.29	0.841	2.16	0.317	1.76	0.247	2.87	0.465	0.954	0.497	0.125
KOO-29	26.5	3.10	440	26.2	161	9.08	75.1	10.9	26.8	4.30	20.8	5.62	1.88	0.887	4.89	0.926	2.34	0.341	1.89	0.269	3.78	0.610	1.19	0.679	0.141
KOO-30	25.2	3.13	438	23.5	152	10.3	73.9	16.3	39.6	5.46	23.4	5.42	1.73	0.779	4.25	0.814	2.06	0.297	1.65	0.232	3.67	0.667	1.91	0.881	0.164
KOO-31	-	2.99	409	24.0	152	8.80	71.0	10.7	27.8	4.10	19.7	5.25	1.75	0.815	4.50	0.855	2.14	0.309	1.74	0.243	3.55	0.577	0.951	0.543	0.133
KOO-48	25.5	4.81	435	27.0	142	9.86	103	11.9	30.4	4.62	21.5	5.54	1.85	0.872	4.85	0.923	2.39	0.348	1.90	0.268	3.63	0.658	1.21	0.673	0.168
KOO-50	26.1	0.20	398	29.3	144	9.44	78.4	12.2	27.3	4.44	20.9	5.48	1.87	0.901	5.03	0.993	2.56	0.370	2.02	0.283	3.45	0.607	1.15	0.660	0.123

(1) For sample locations see Frey et al. (1994).

**Table 2. Mixing of Aged, Recycled Carbonate and Apatite-Rich Sediment and Primitive Mantle**

<b>Estimated Carbonate and Apatite-Rich Sediment @ 2 Ga<sup>(1)</sup></b>					
$^{143}\text{Nd}/^{144}\text{Nd}$	$^{176}\text{Hf}/^{177}\text{Hf}$	Sm/Nd	Lu/Hf	Nd (ppm)	Hf (ppm)
0.509941	0.281490	0.25	1.4	10.13	0.17
<b>Calculated Carbonate and Apatite-Rich Sediment after 2 Ga of Aging</b>					
$^{143}\text{Nd}/^{144}\text{Nd}$	$^{176}\text{Hf}/^{177}\text{Hf}$				
0.511972	0.289299				
<b>Present Primitive Mantle</b>					
$^{143}\text{Nd}/^{144}\text{Nd}$	$^{176}\text{Hf}/^{177}\text{Hf}$	Nd (ppm) <sup>(2)</sup>	Hf (ppm) <sup>(2)</sup>		
0.512638	0.282843	1.19	0.27		
<b>Mixture of 3% 2 Ga Recycled Carbonate and Apatite-Rich Sediment and 97% Primitive Mantle</b>					
$^{143}\text{Nd}/^{144}\text{Nd}$	$^{176}\text{Hf}/^{177}\text{Hf}$	epsilon Nd	epsilon Hf		
0.512499	0.282967	-2.71	4.40		

(1) Isotopic ratios are assumed to be primitive mantle values at 2Ga, and trace element abundances are from carbonate section at Guatemala (Table 1 of Plank and Langmuir, 1998).

(2) from Hofmann (1988).

**Table 3. Input Parameters for Peridotite Melting Model**

		Mineral Proportions															
		Olivine	orthopyroxene	clinopyroxene	garnet												
Source Mode <sup>(1)</sup>		0.53	0.04	0.38	0.05												
Melting Reaction <sup>(1)</sup>		0.05	-0.49	1.31	0.13												
		Partition Coefficients															
		olivine <sup>(2)</sup>	orthopyroxene <sup>(3)</sup>	clinopyroxene <sup>(4)</sup>	garnet <sup>(4)</sup>												
La		0	0.002	0.008 <sup>(5)</sup>	0.023 <sup>(5)</sup>												
Zr		0	0.017	0.027	0.411												
Hf		0	0.036	0.049	0.517												
Tb <sup>(6)</sup>		0	0.046	0.119	1.72												
Yb		0	0.092	0.174	5.17												
Y		0	0.060	0.165	2.37												
Sc		0.14 <sup>(7)</sup>	0.27 <sup>(7)</sup>	1.4 <sup>(8)</sup>	5.17 <sup>(9)</sup>												
		source compositions															
		La	Nb	Zr	Tb	Yb	Y	Sc	Sr	Th	Th/La	La/Nb	Sr/Nb	La/Yb	Zr/Yb	Sc/Y	Tb/Yb
		ppm	ppm	ppm	ppm	ppm	ppm	ppm	ppm	ppm							
original source <sup>(10)</sup>		0.67	0.71	10	0.085	0.28	3.9	10.8	28	0.047	0.070	0.95	40	2.4	36	2.8	0.30
Guatemala Carbonate Section <sup>(11)</sup>		14	0.79	5.9	0.47 <sup>(12)</sup>	1.6	32	4.8	1504	0.29	0.020	18.0	1904	9.1	3.8	0.15	0.29
adding 3% sediment into original source		1.1	0.71	10	0.096	0.32	4.7	11	73	0.05	0.050	1.5	102	3.4	31	2.3	0.30

(1) from Table 2 of Salters (1996)

(2)  $D_{\text{olivine/melt}}$  is assumed to be zero, except for Sc.

(3) sample TM 295-5 (2.8GPa and 1540°C) from Salters and Longhi, 1999

(4) sample TM 694-6 (2.8GPa and 1537°C) from Salters and Longhi, 1999

(5)  $D_{\text{La}}^{\text{clinopyroxene/melt}} = D_{\text{Nb}}^{\text{clinopyroxene/melt}}$  and  $D_{\text{La}}^{\text{garnet/melt}} = D_{\text{Nb}}^{\text{garnet/melt}}$  are assumed.

(6)  $D_{\text{Tb}} = (D_{\text{Sm}} + D_{\text{Er}})/2$ .

(7)  $D_{\text{Sc}}^{\text{olivine/melt}}$  and  $D_{\text{Sc}}^{\text{orthopyroxene/melt}}$  are calculated using mineral and melt composition of Sample TM 295-5 (2.8GPa and 1540°C) and Equation 39 of Beattie et al. (1991).

(8)  $D_{\text{Sc}}^{\text{clinopyroxene/melt}}$  ranges from 0.8 to 3.2 (e.g., Hart and Dunn, 1993; Hauri et al., 1994; Blundy and Wood, 1998).

We take  $D_{\text{Sc}}^{\text{clinopyroxene/melt}} = 1.4$  in our modeling.

(9)  $D_{\text{Sc}}^{\text{garnet/melt}} = D_{\text{Yb}}^{\text{garnet/melt}}$  is assumed (e.g., van Westrenen et al., 1999).

(10) Y abundance is taken as the primitive mantle value, and Y/Yb is assumed equal to the ratio in both Makapuu- and Kalihi-stage lavas (13.6+/-0.8).

Other ratios are chosen to fit the trends, and abundances of La, Nb, Tb, Zr and Sc are calculated based on these ratios and abundances of Y and Yb.

(11) from Table 1 of Plank and Langmuir, 1998. Sediment column at this trench is carbonate-rich.

(12) Tb abundance is calculated assuming  $\text{Tb}_{\text{PM}} = (\text{Gd}_{\text{PM}} + \text{Dy}_{\text{PM}})/2$ . Primitive mantle values are from Hofmann (1988).

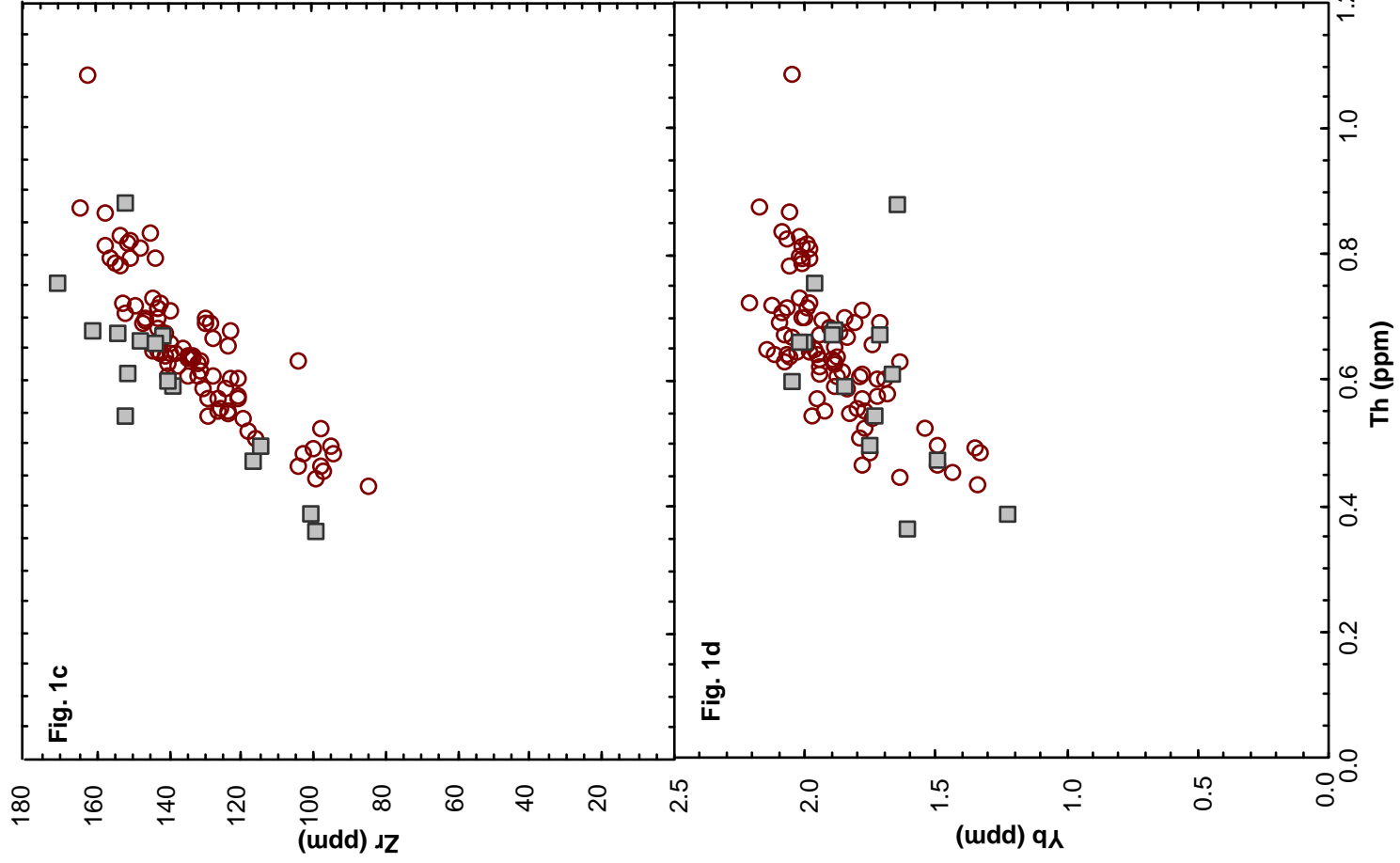
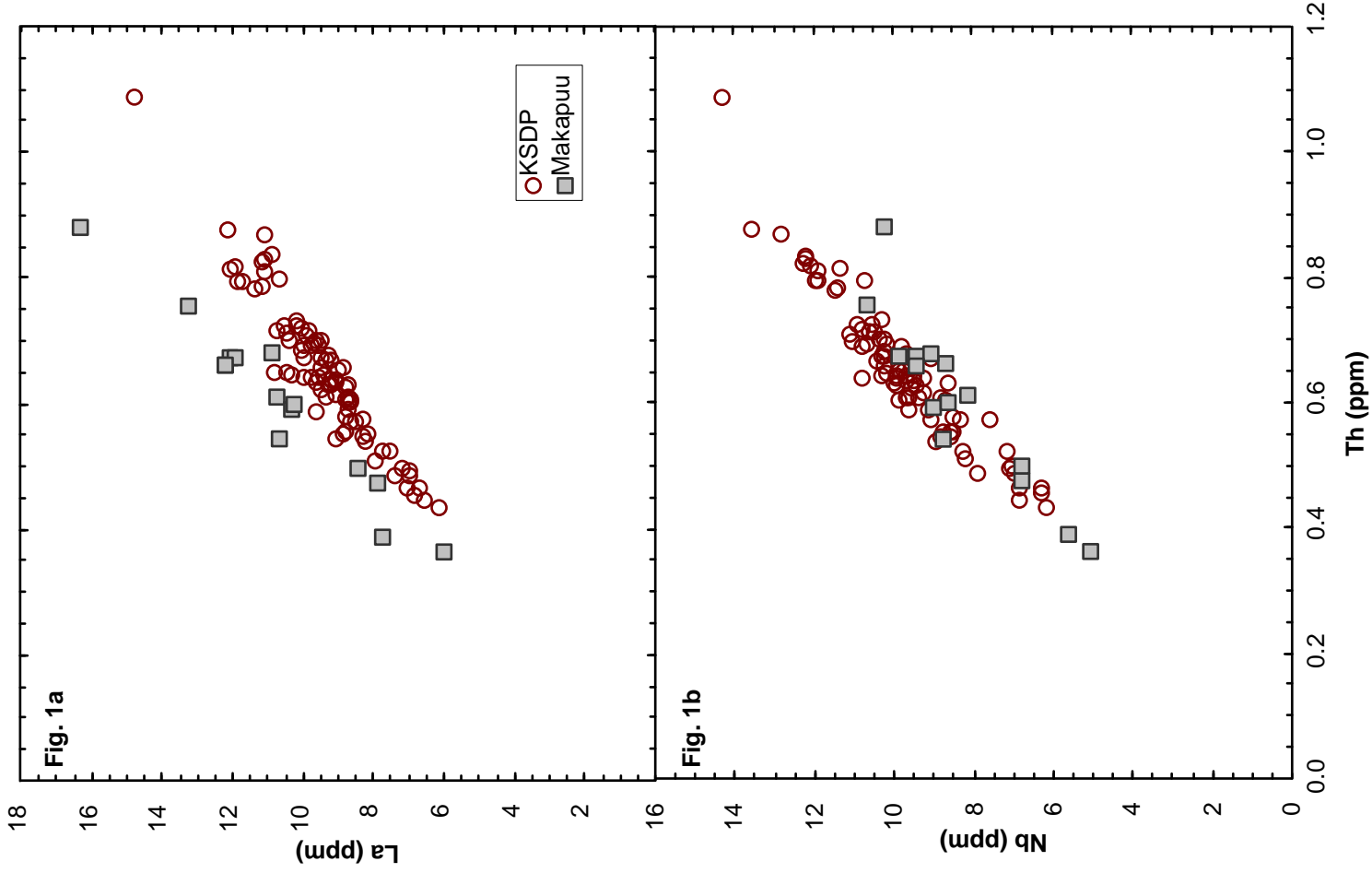
**Table 4. Average Compositions (in %) of Olivine Adjusted Makapuu-Stage Lavas.**

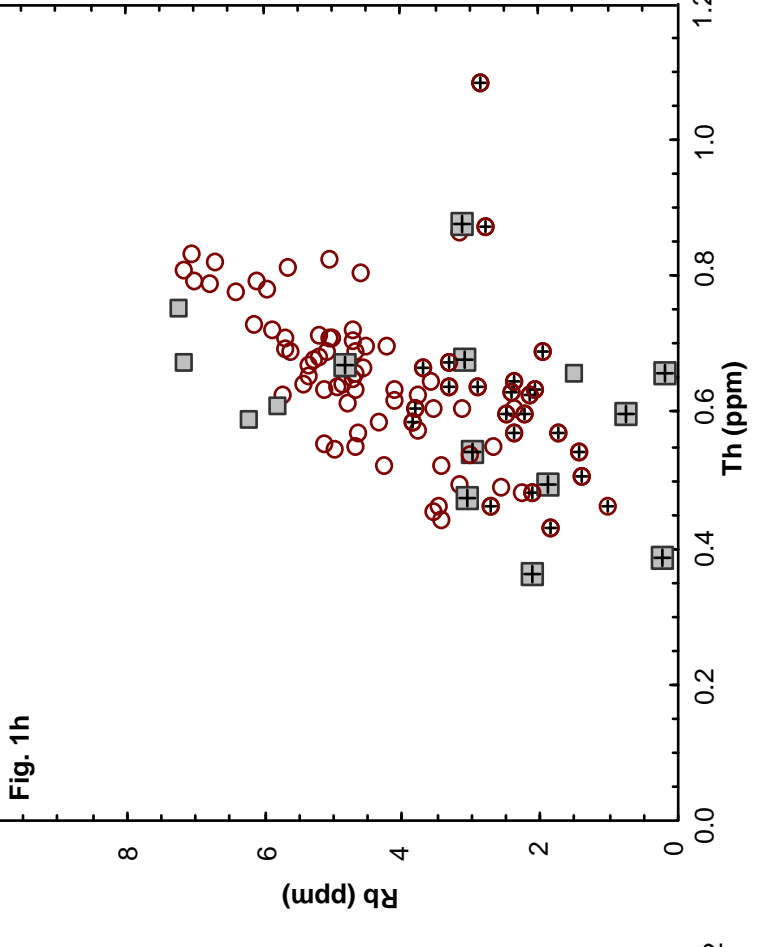
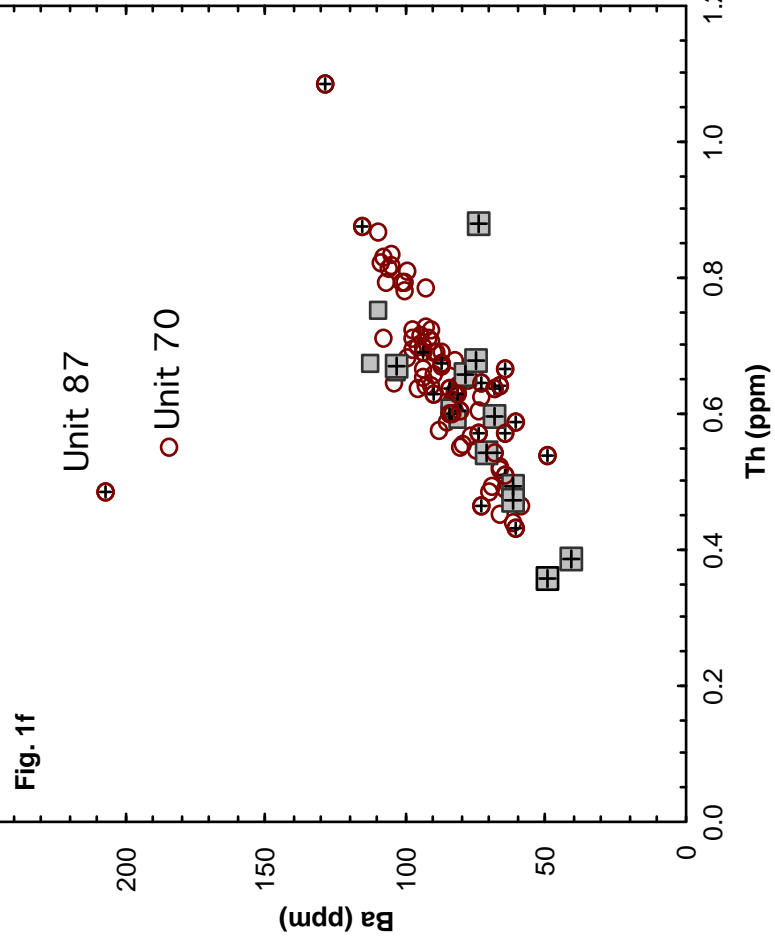
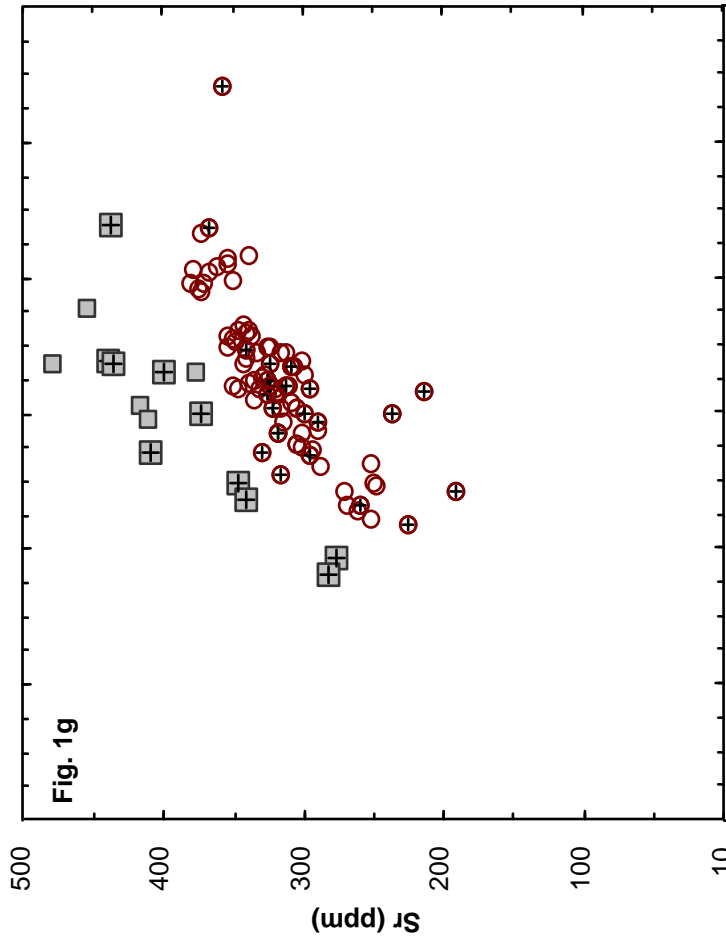
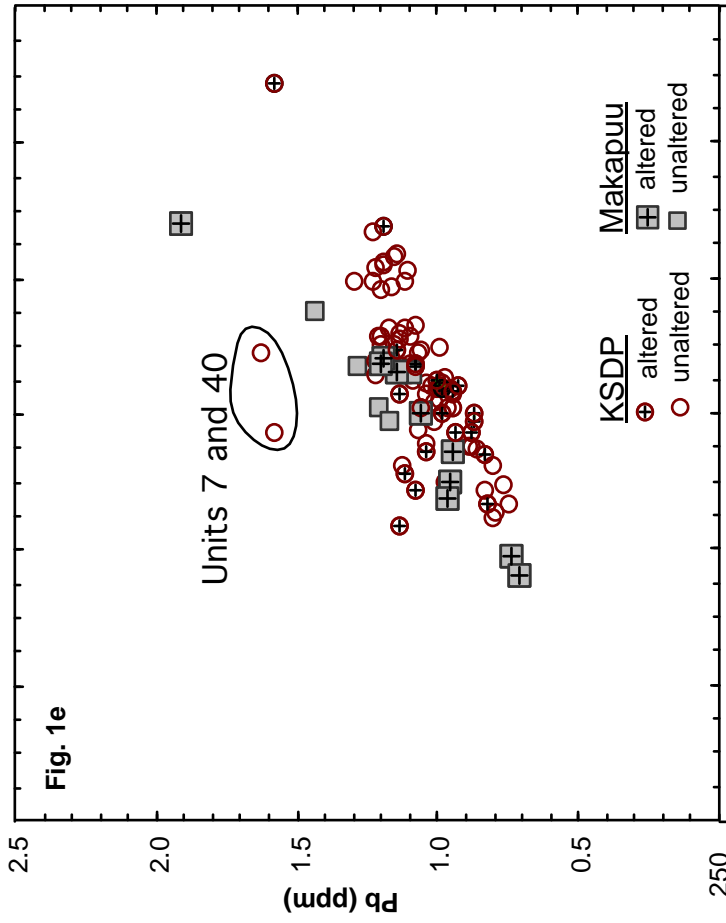
	SiO	TiO <sub>2</sub>	Al <sub>2</sub> O <sub>3</sub>	FeO	MnO	MgO	CaO	Na <sub>2</sub> O	K <sub>2</sub> O	P <sub>2</sub> O <sub>5</sub>
unaltered	50.3	1.67	11.1	10.9	0.13	15.70	7.43	2.29	0.37	0.2
Hauri 's average	49.98	1.65	11.3	10.8	0.14	15.6	7.60	2.28	0.36	0.2

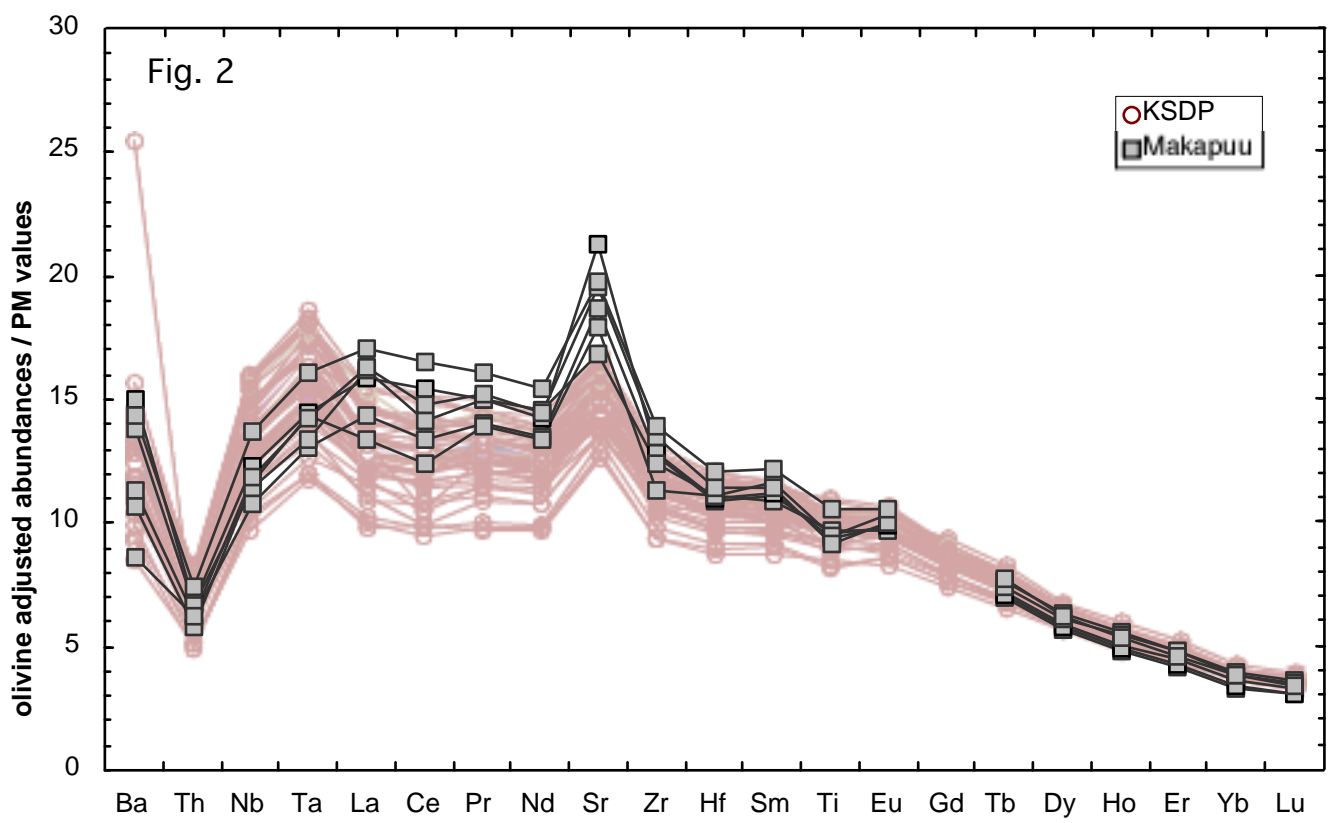
"Unaltered" includes only Makapuu-stage lavas with  $K_2O/P_2O_5 > 1.2$  and  $MgO > 6.5\%$  (Frey et al., 1994).

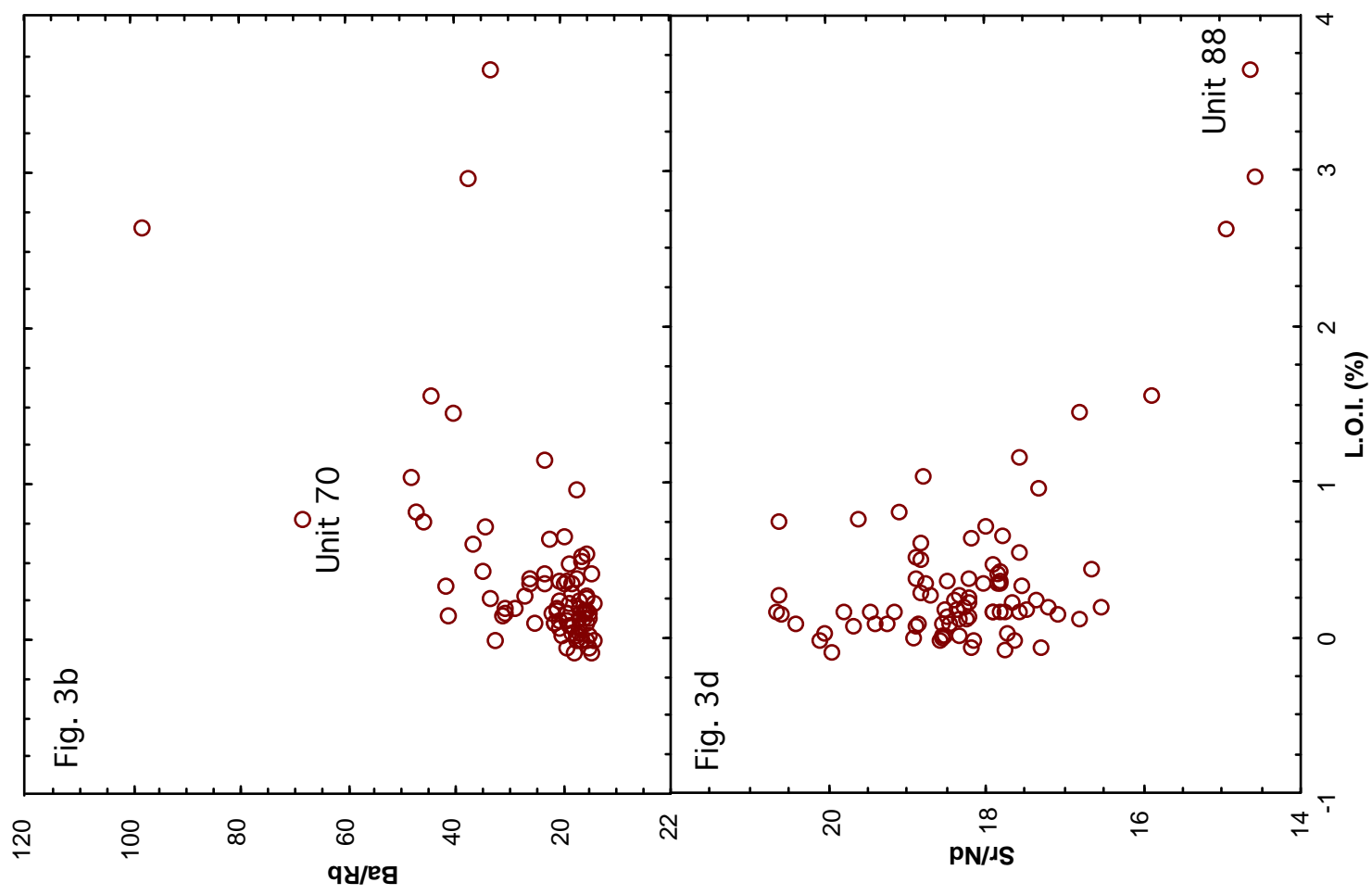
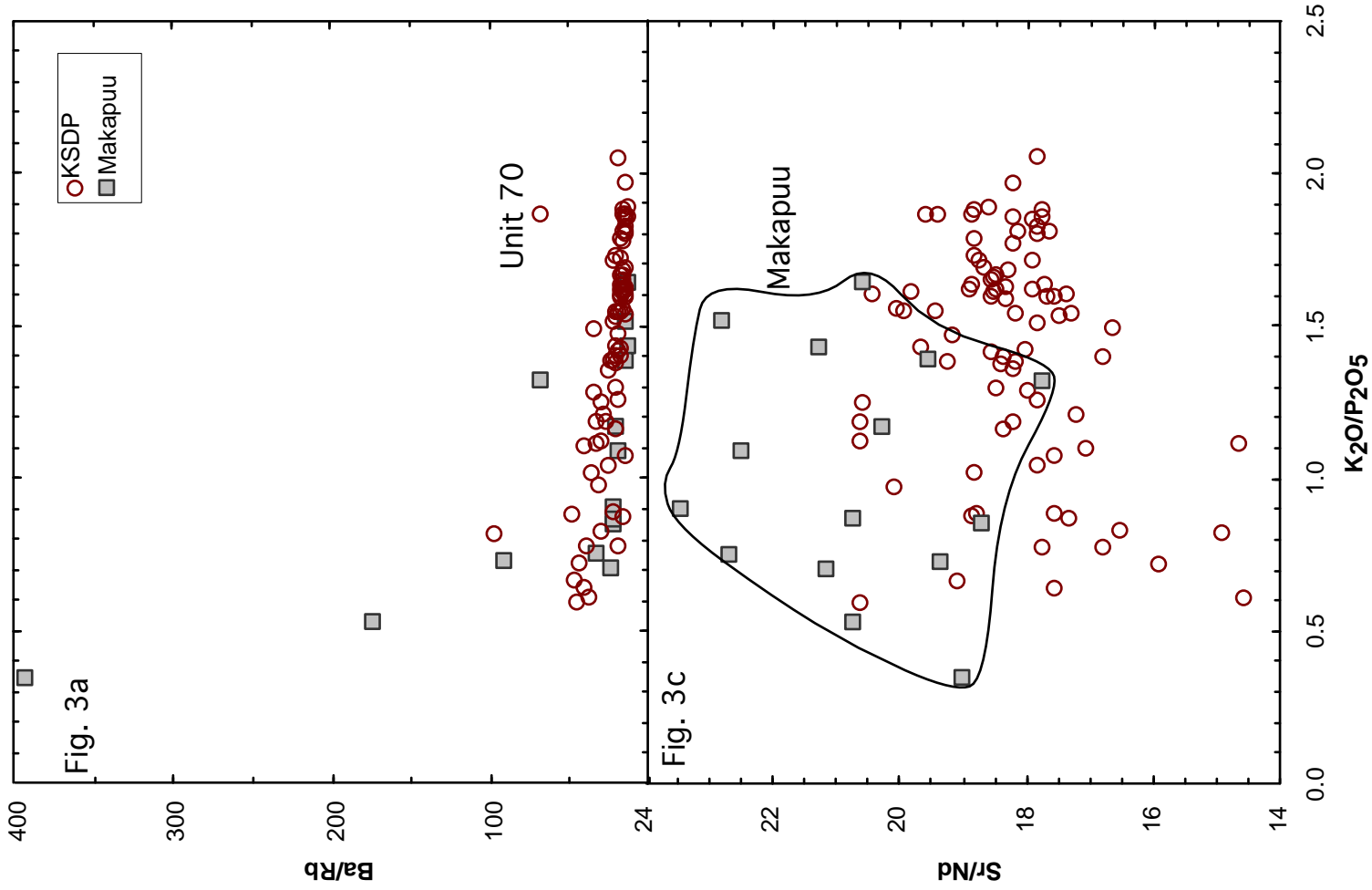
"Hauri's average" is taken from Hauri (1996), and includes Makapuu-stage lavas with  $MgO > 6.5\%$ .

Both groups are adjusted to be in equilibrium with olivine  $Fo_{90.5}$ . These averages are similar; hence, including altered lavas does not have major effect on the average compositions of Makapuu-stage lavas.









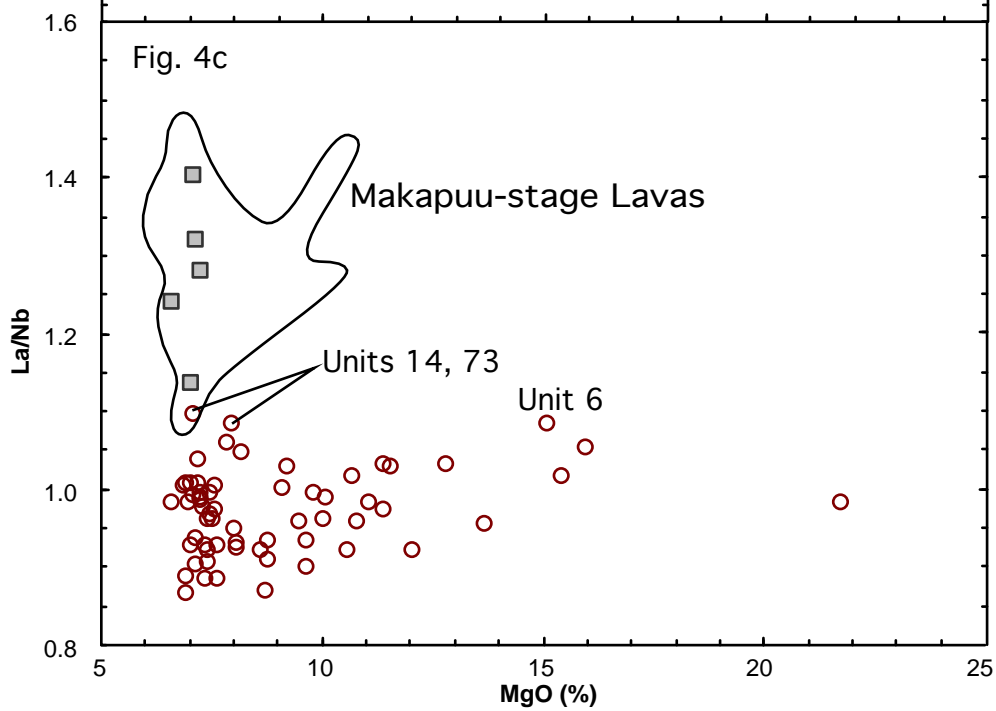
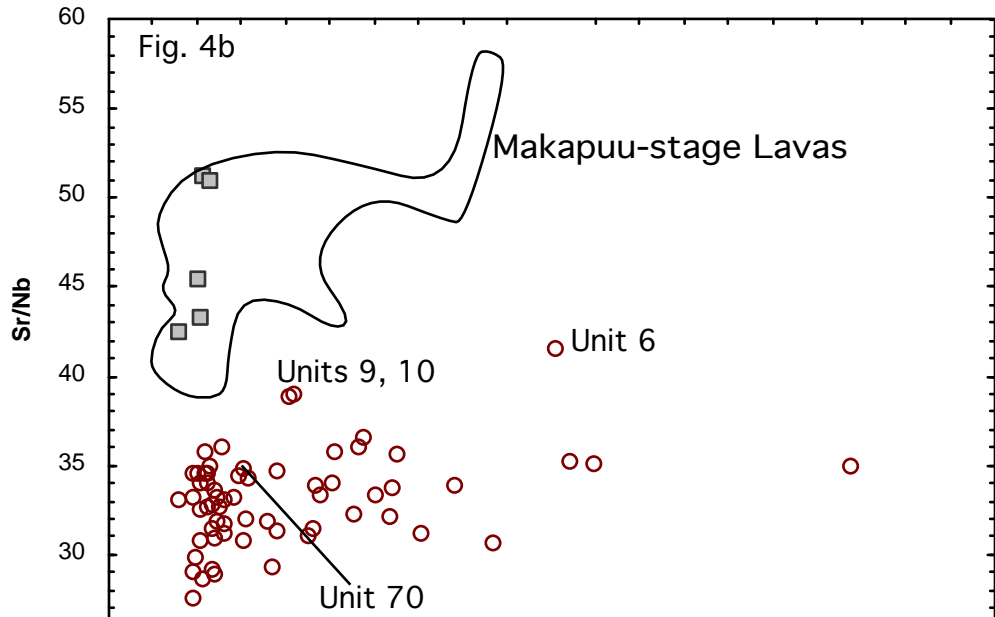
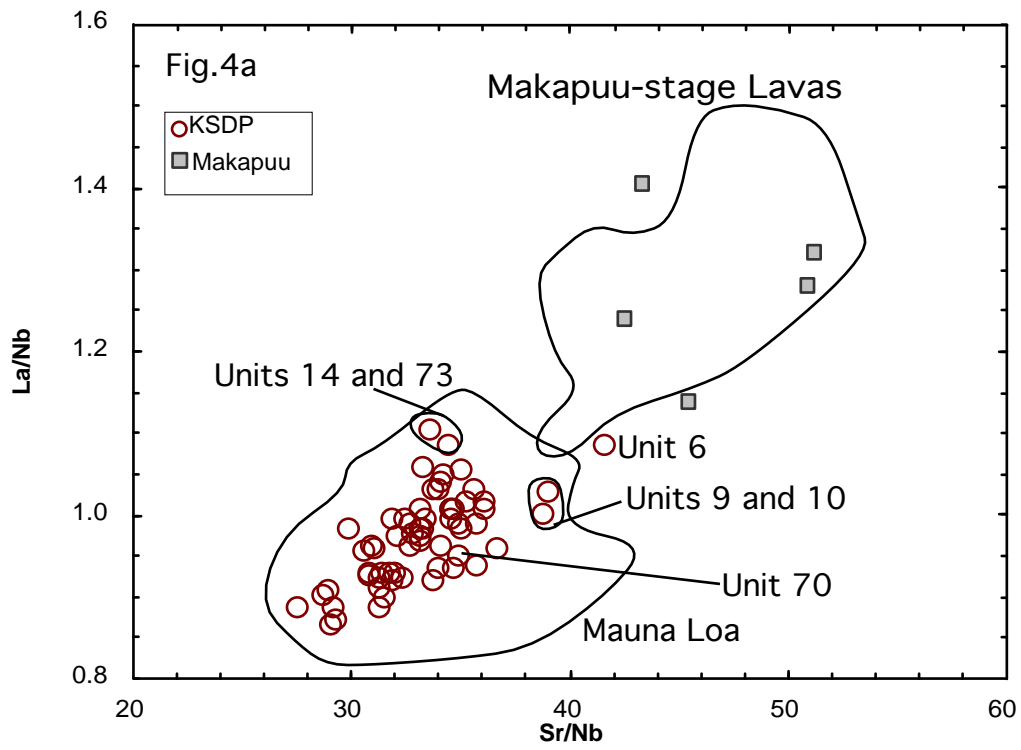
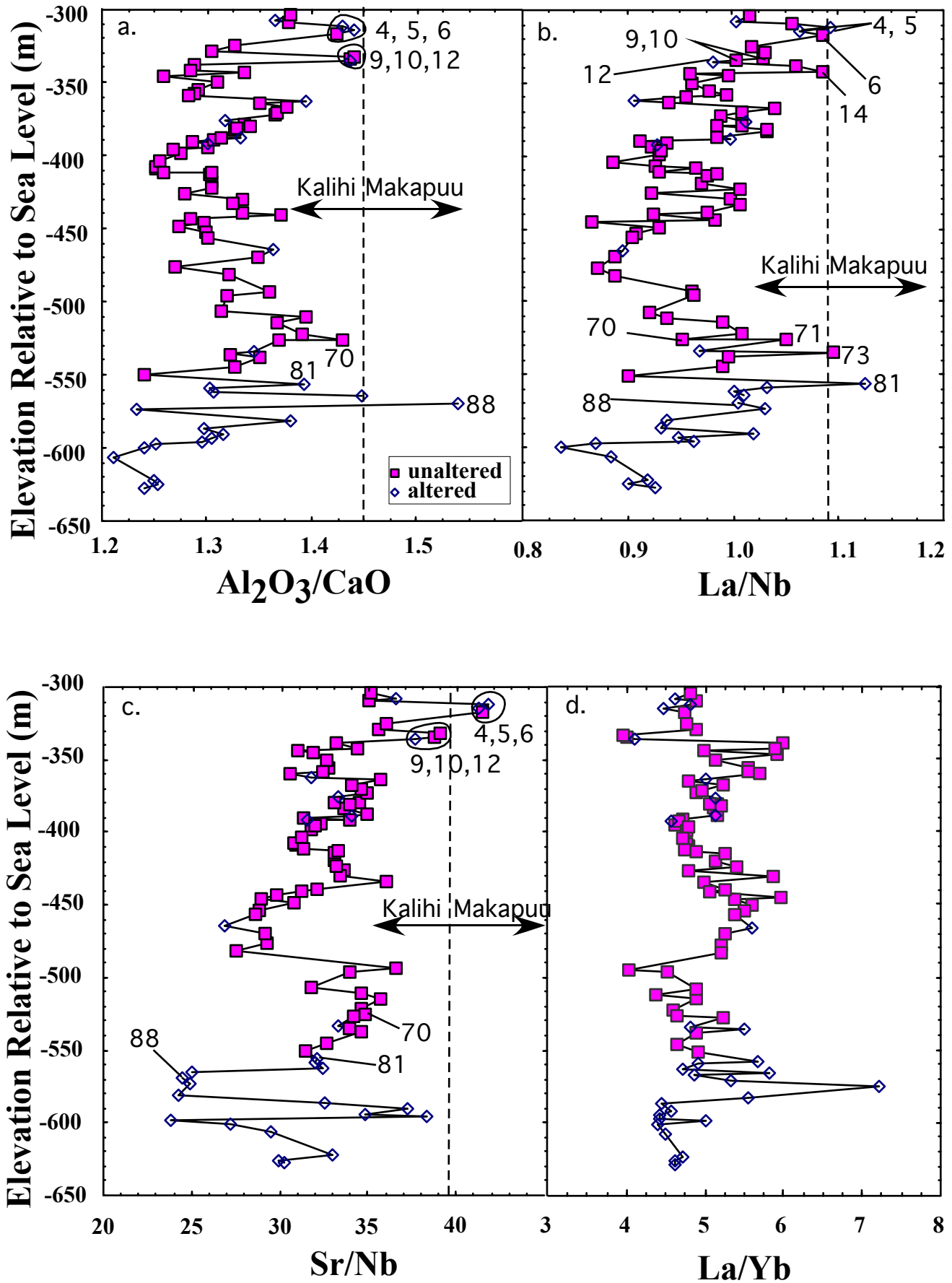
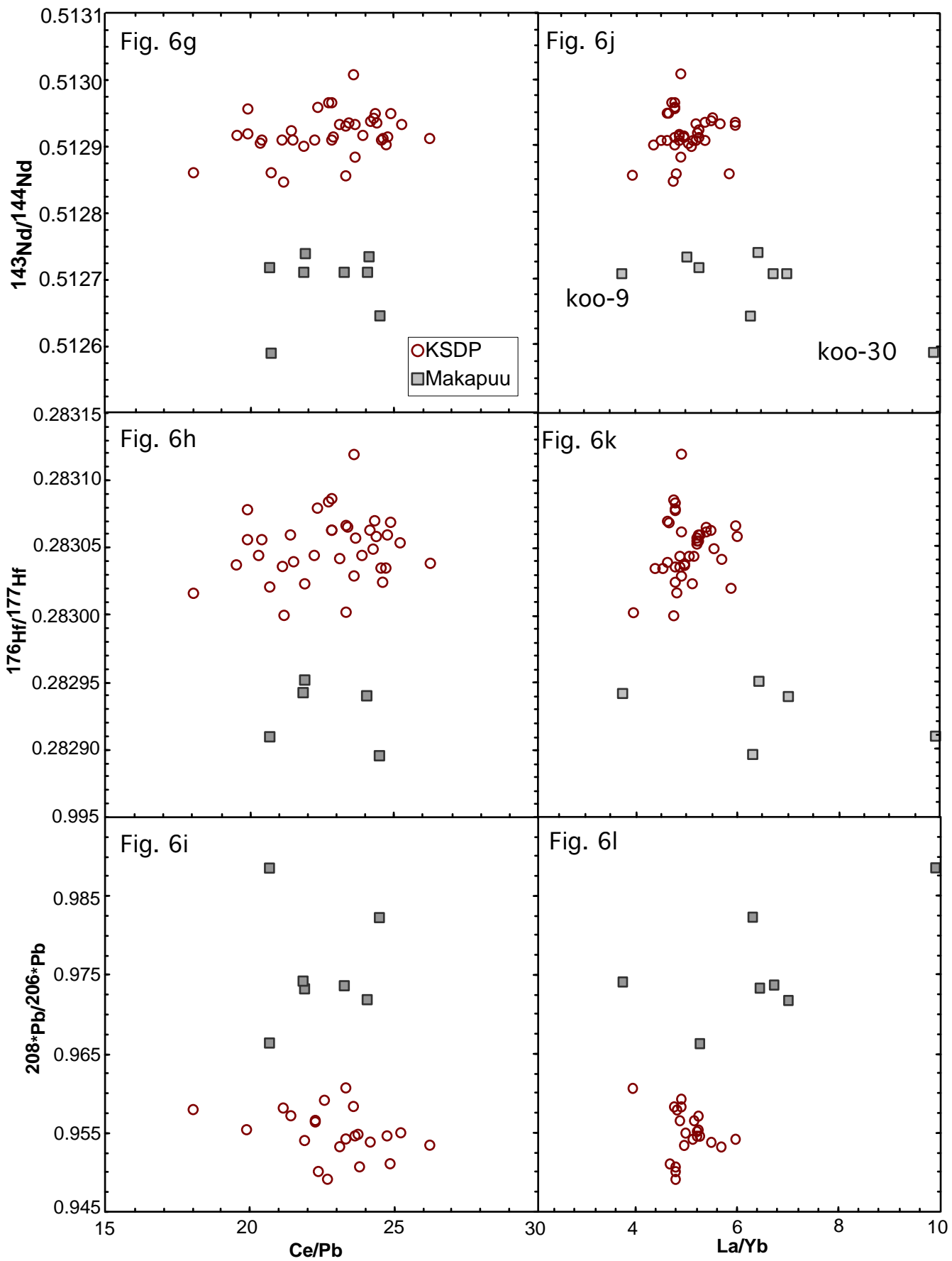
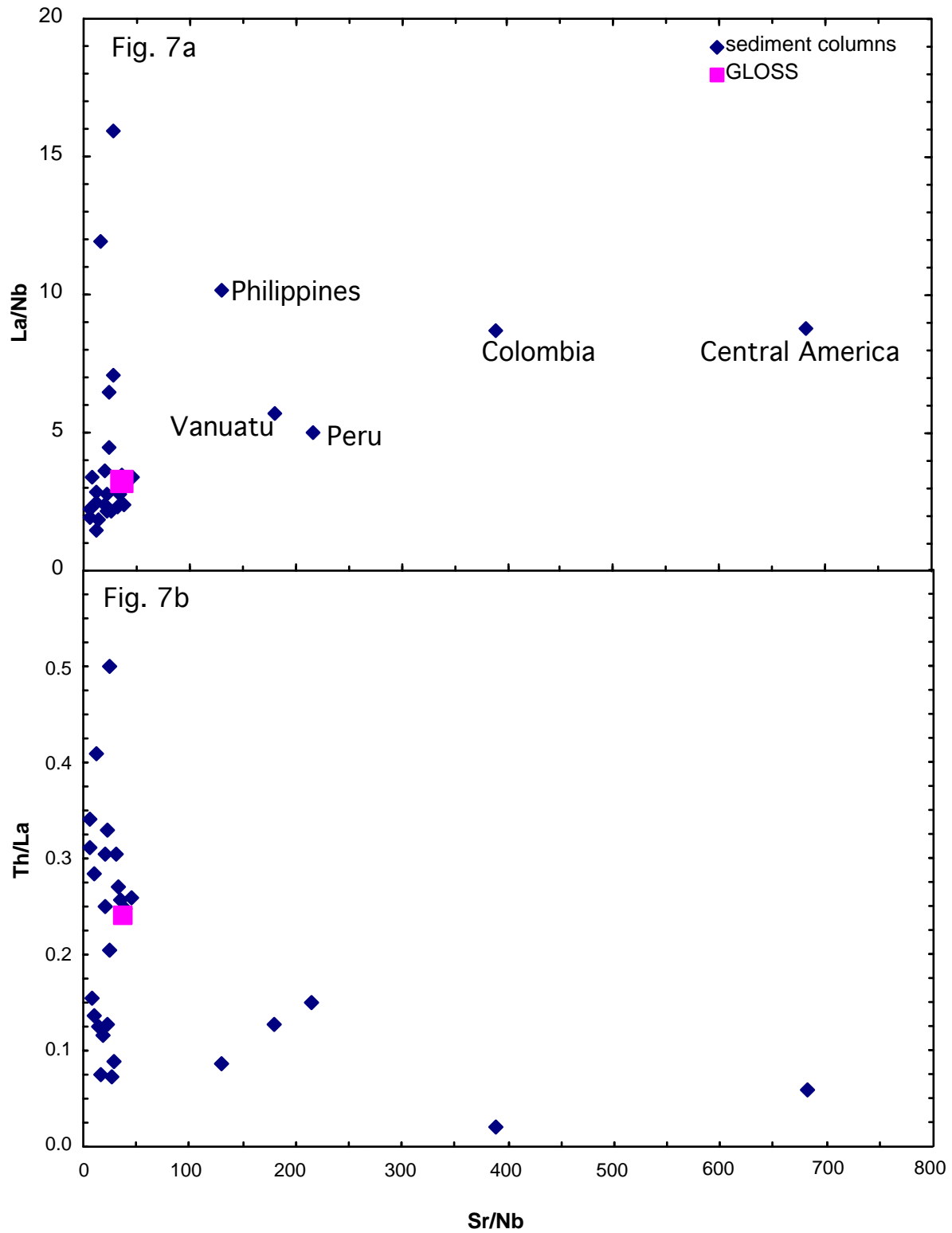


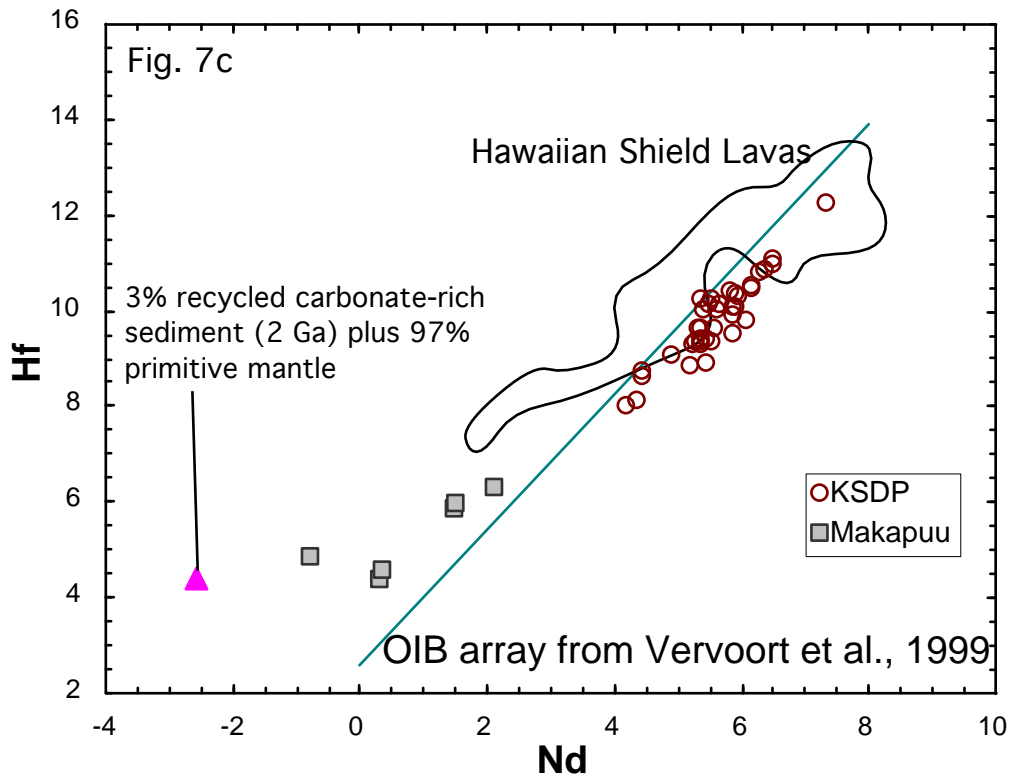
Fig. 5











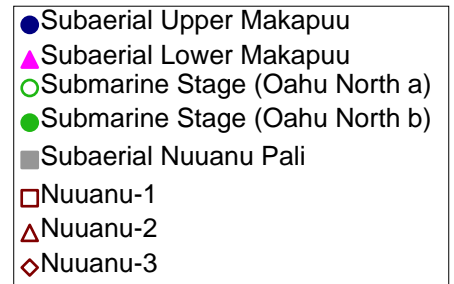
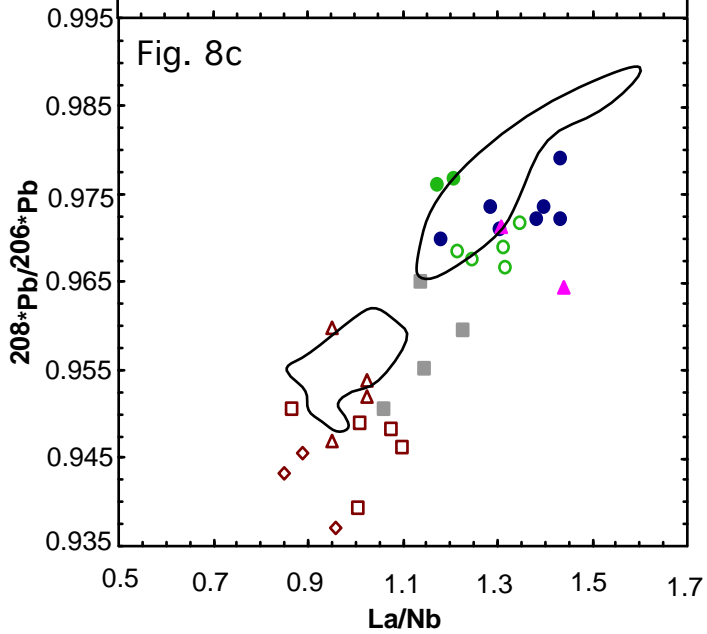
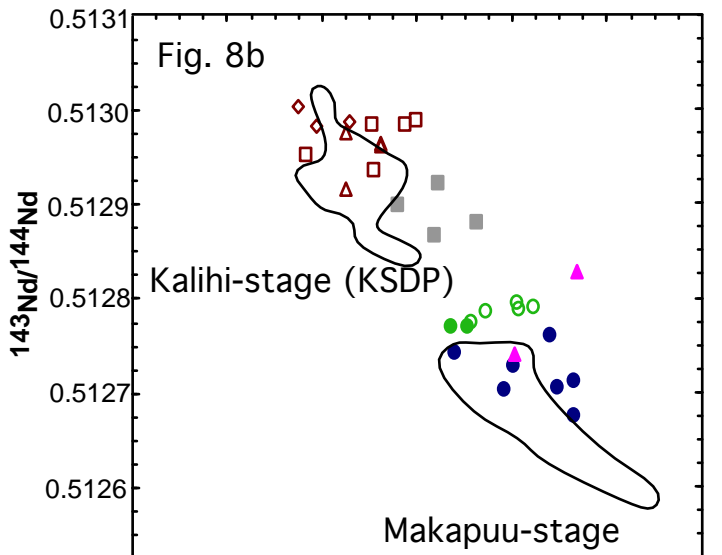
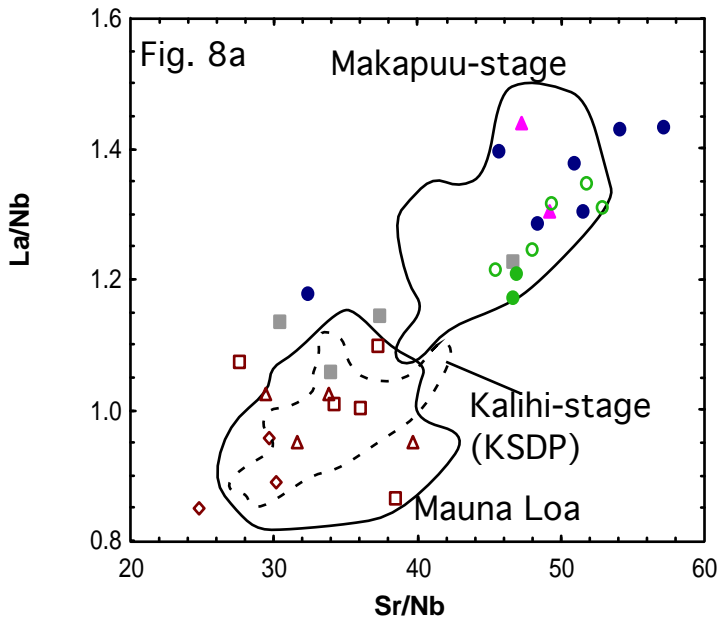
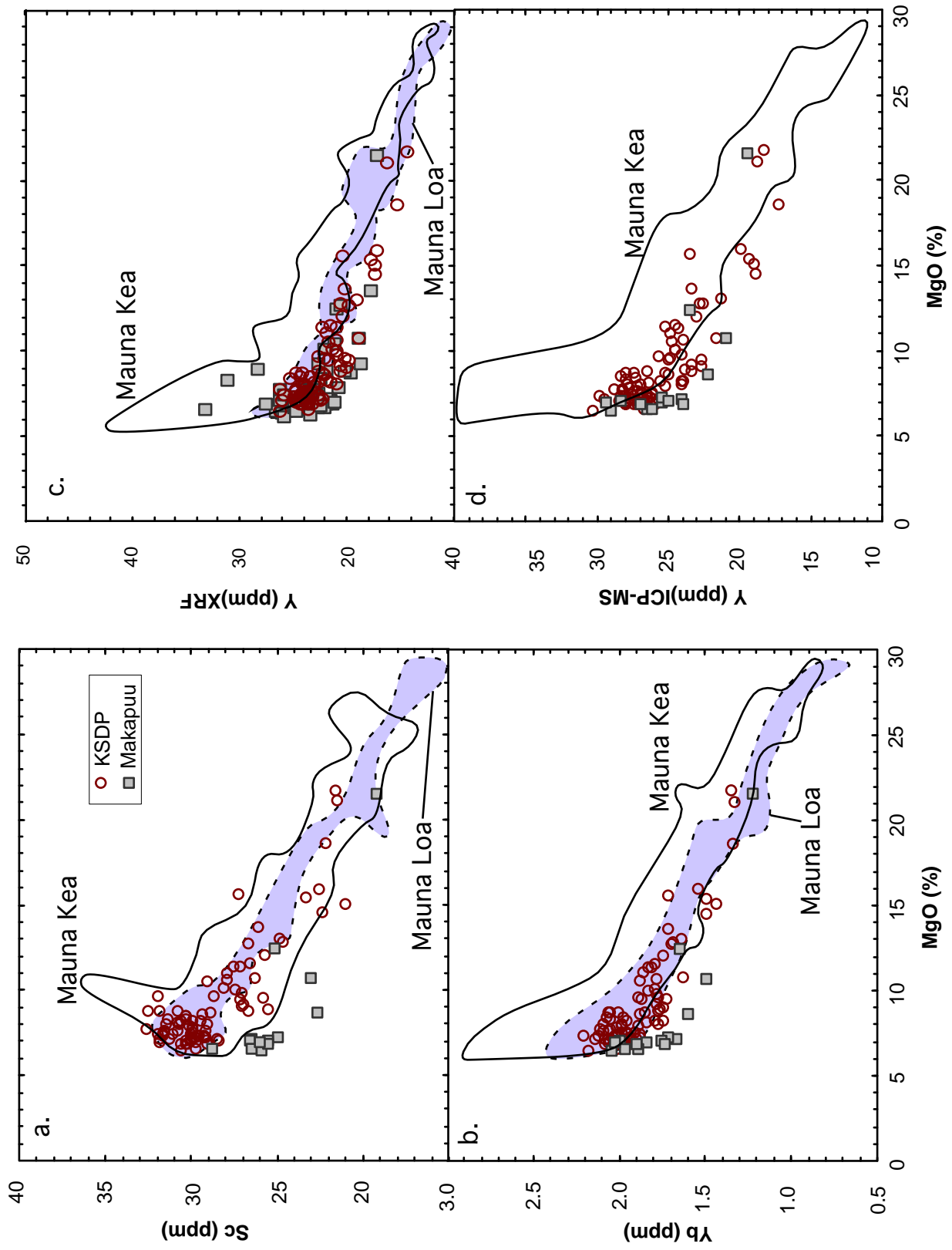
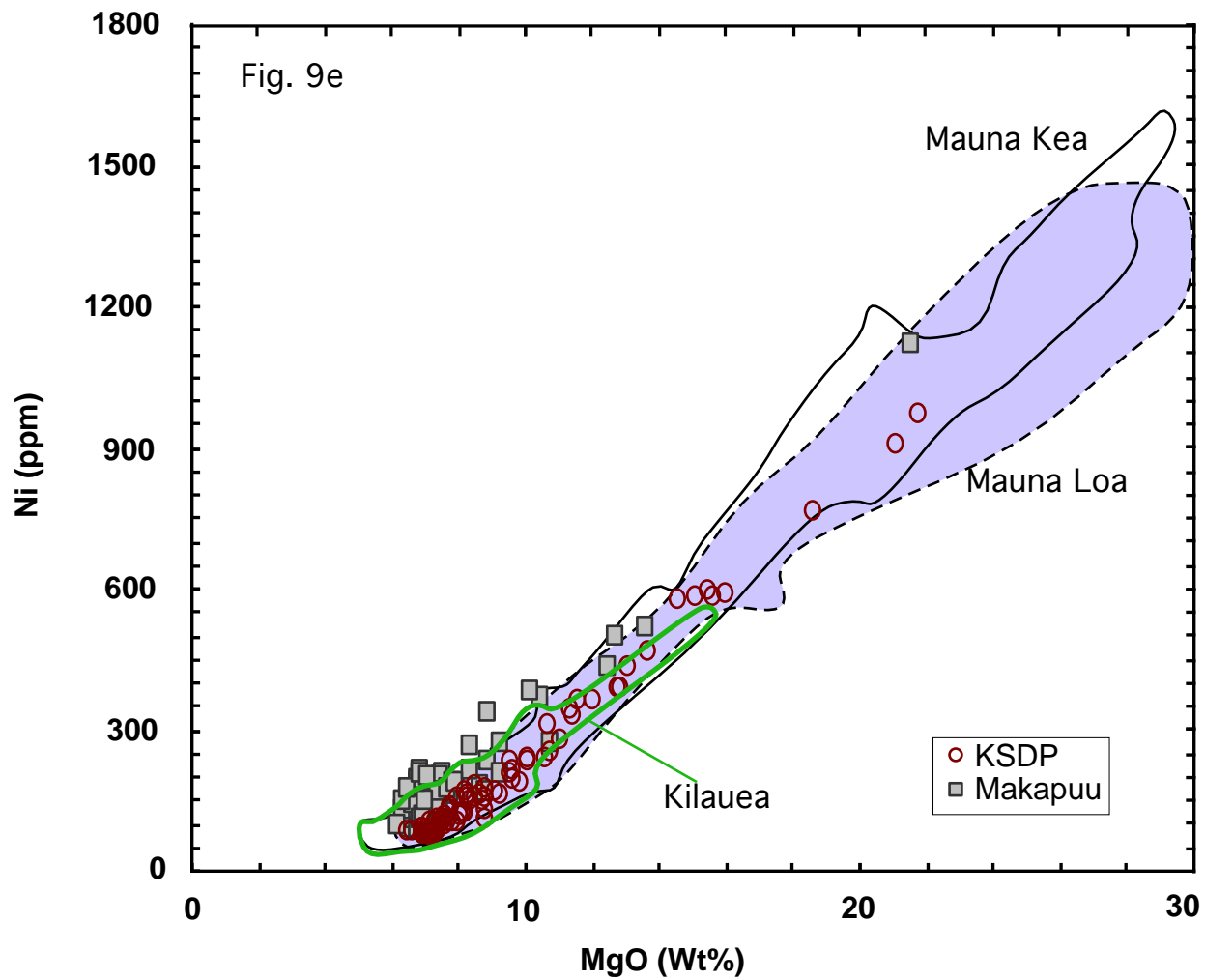


Fig. 9





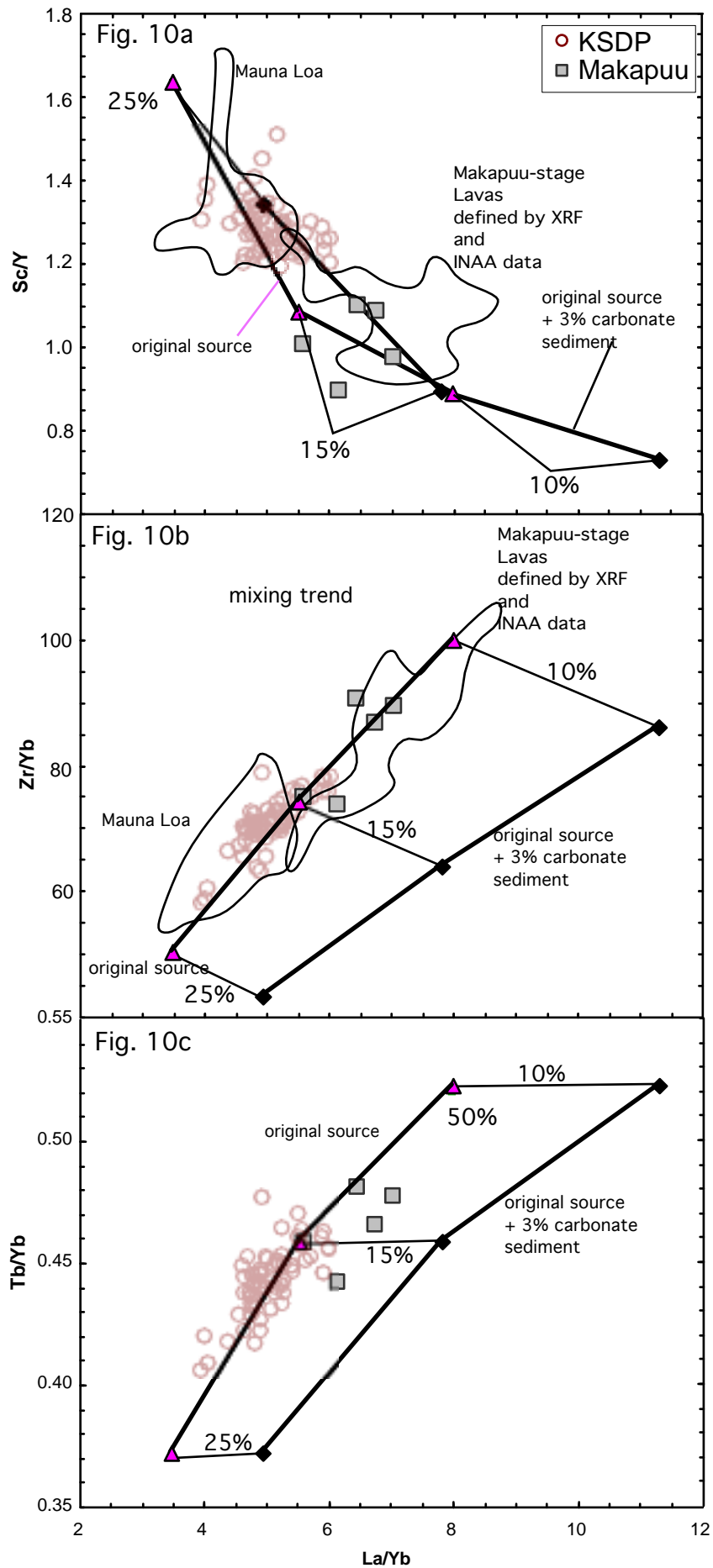
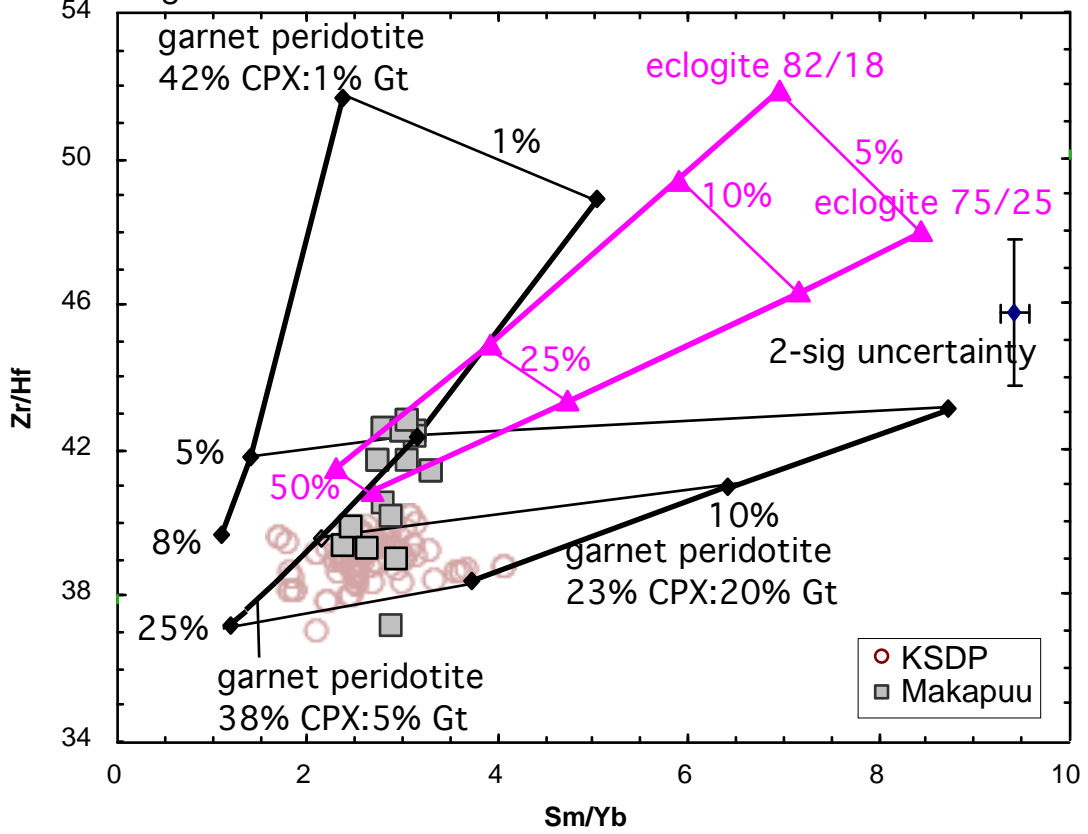
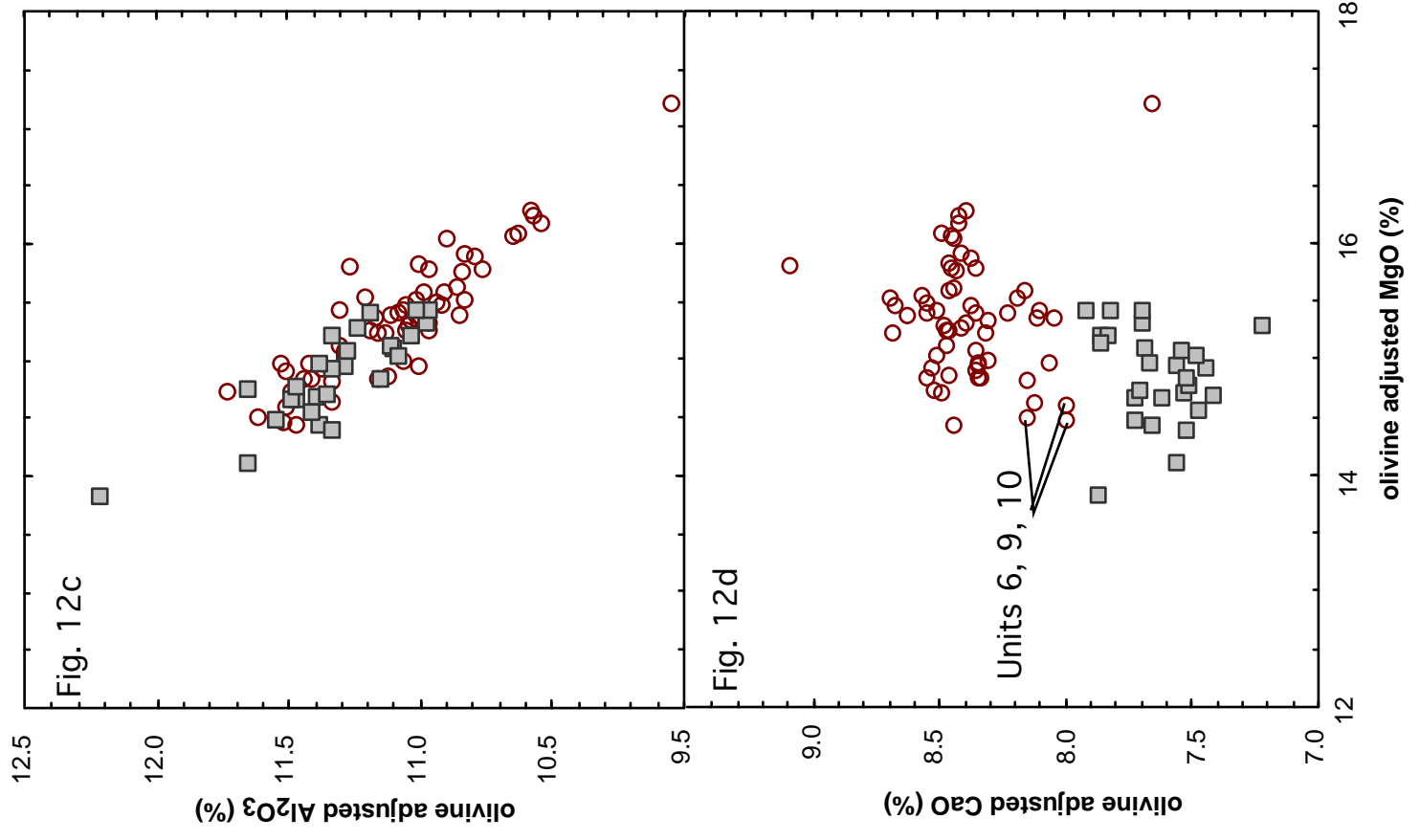
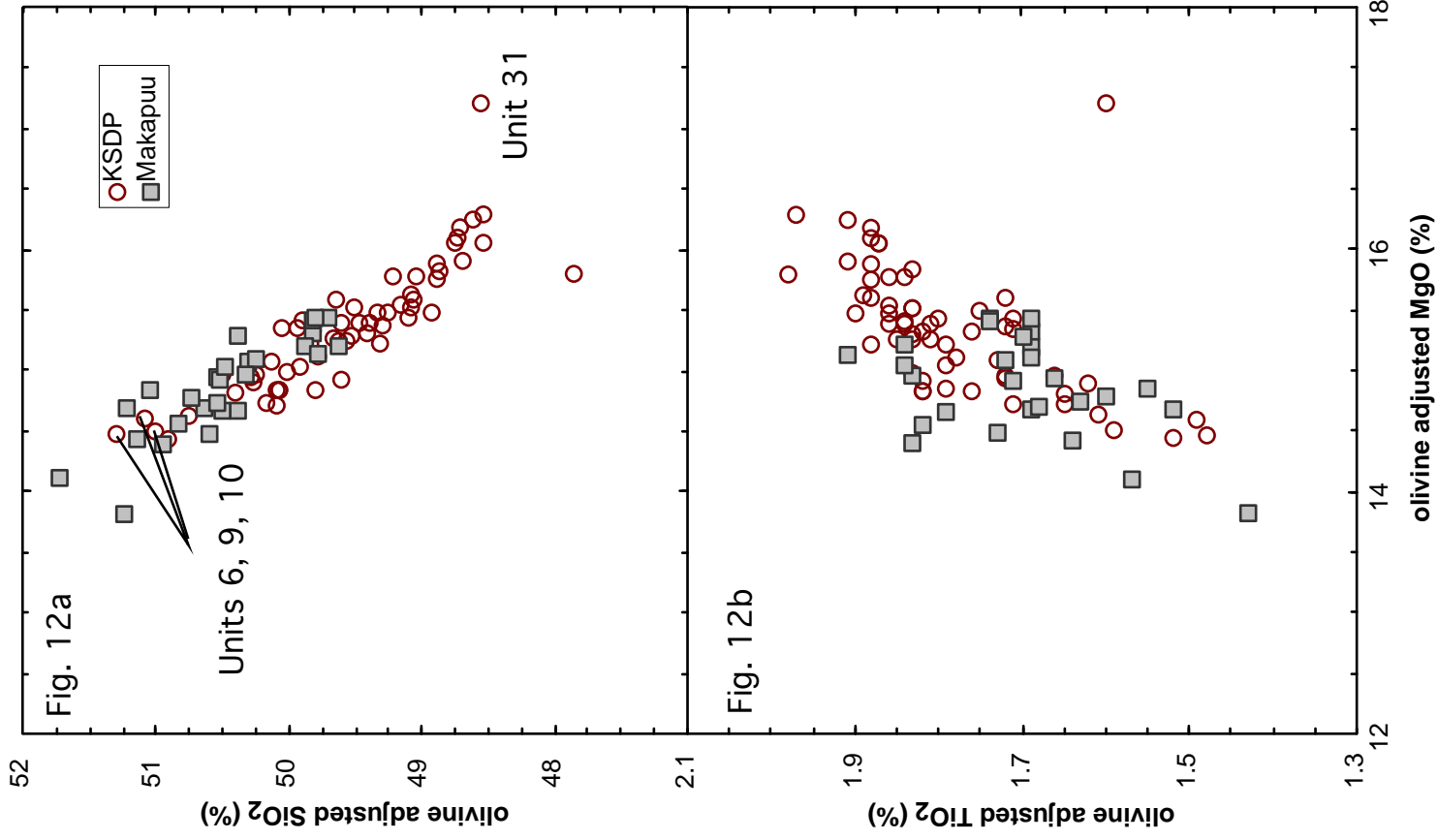
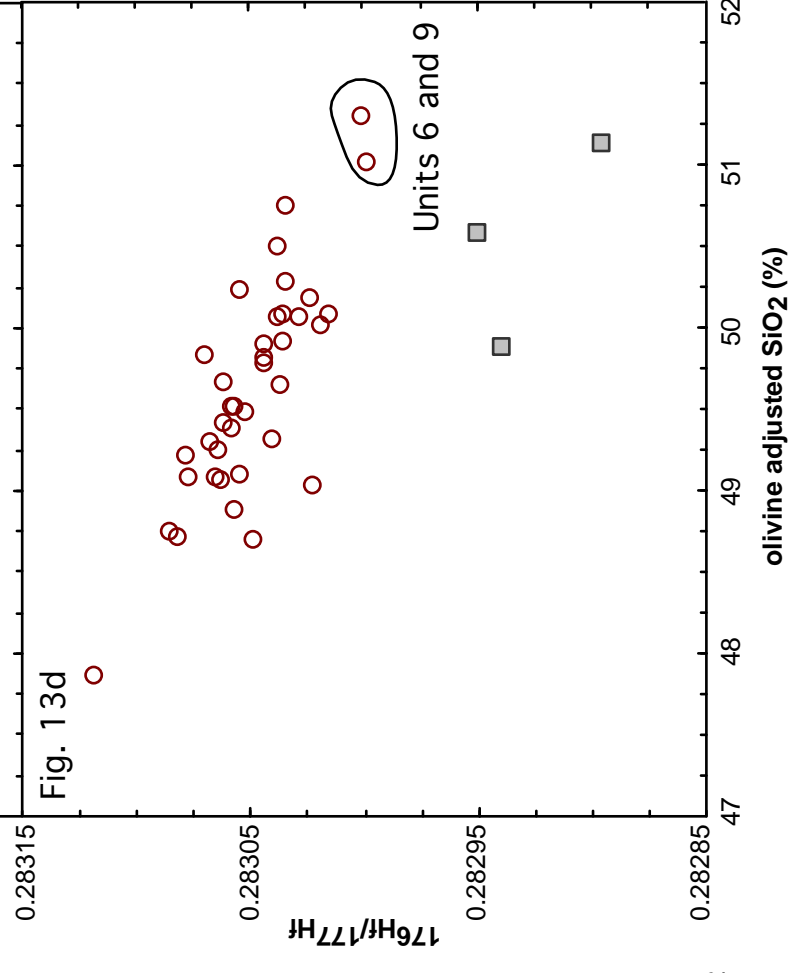
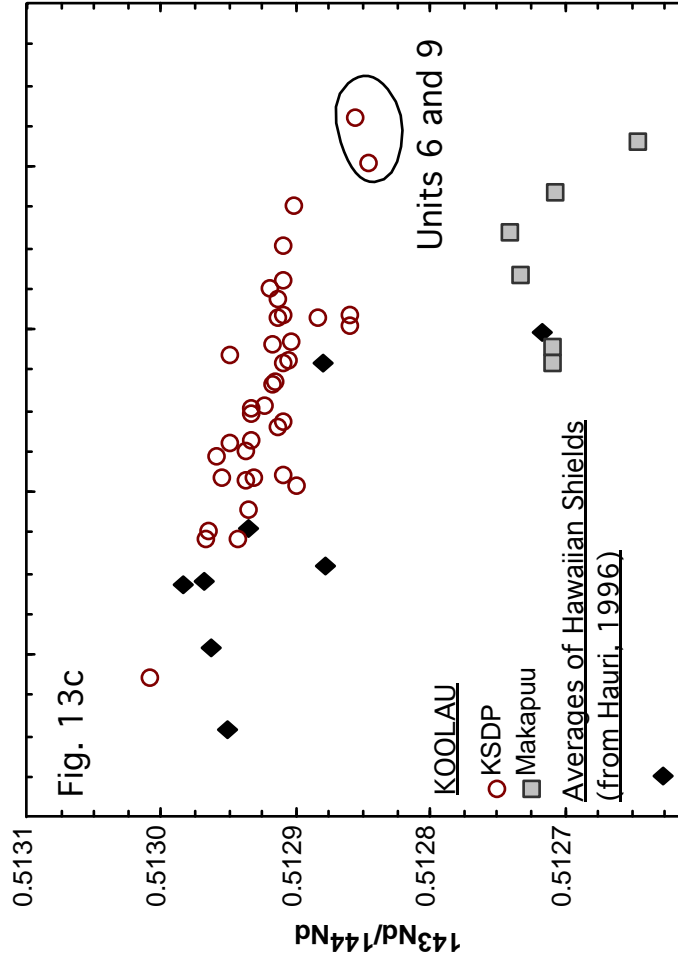
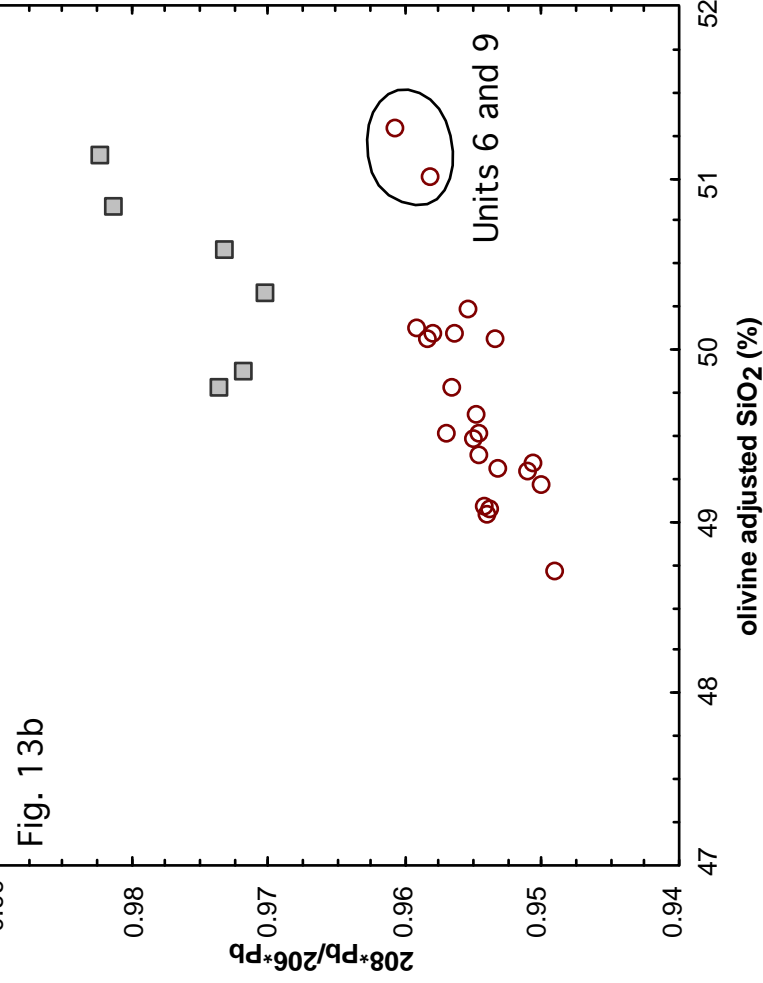
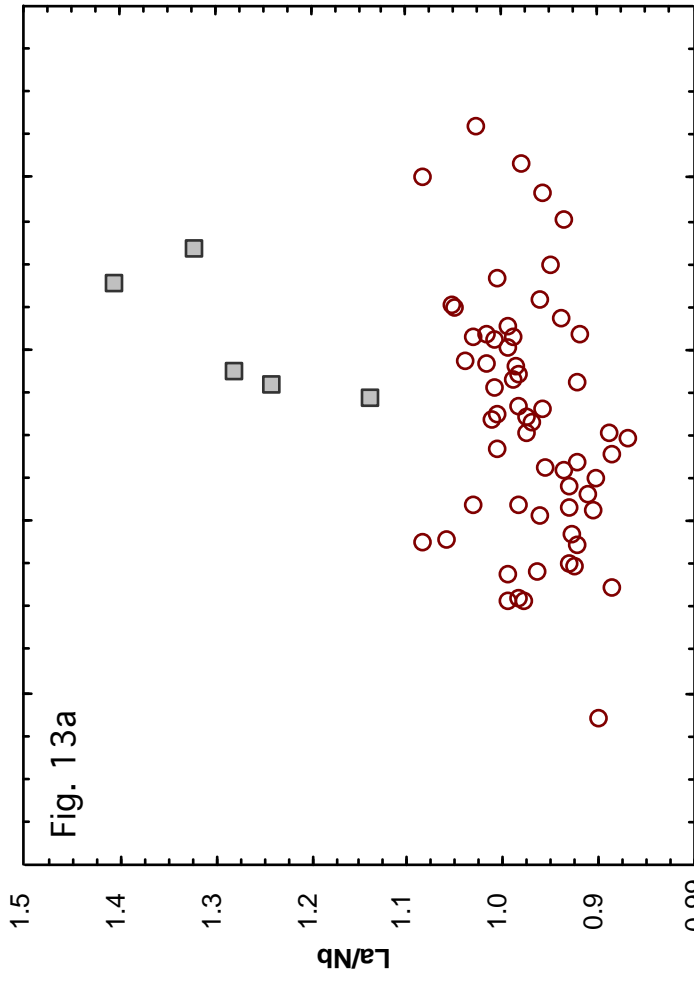


Fig. 11







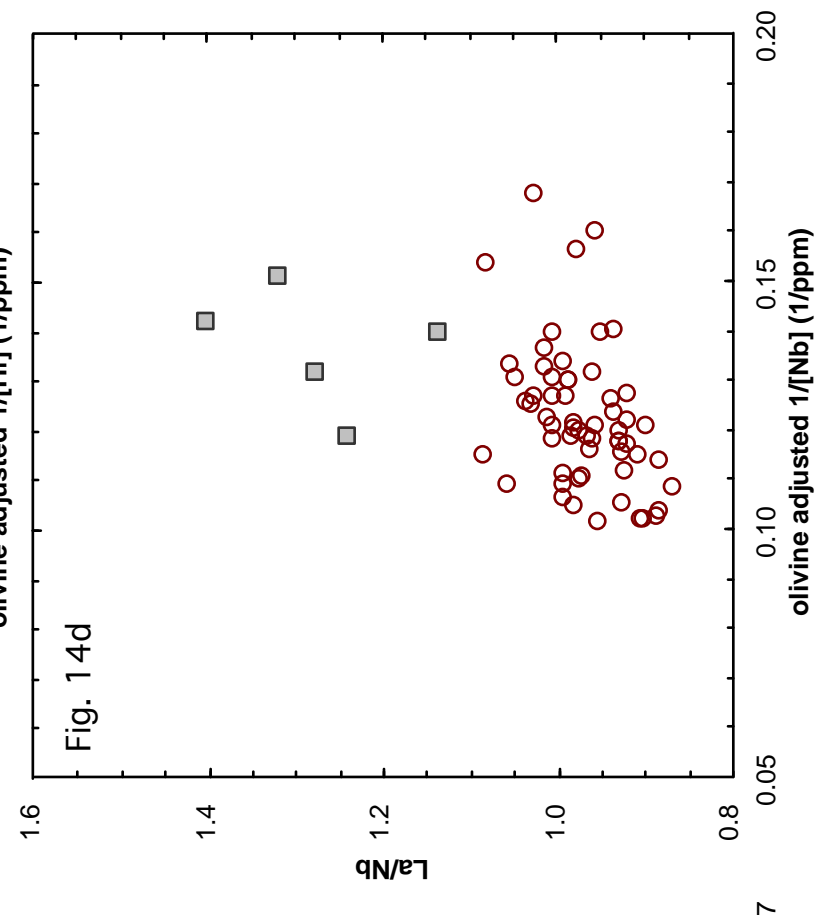
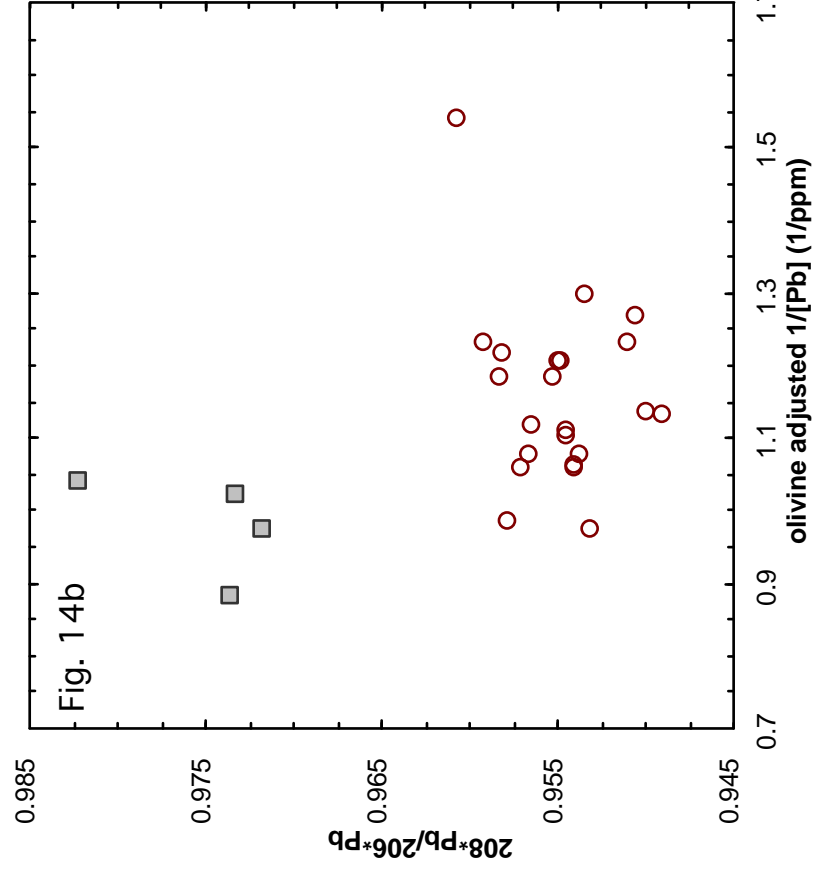
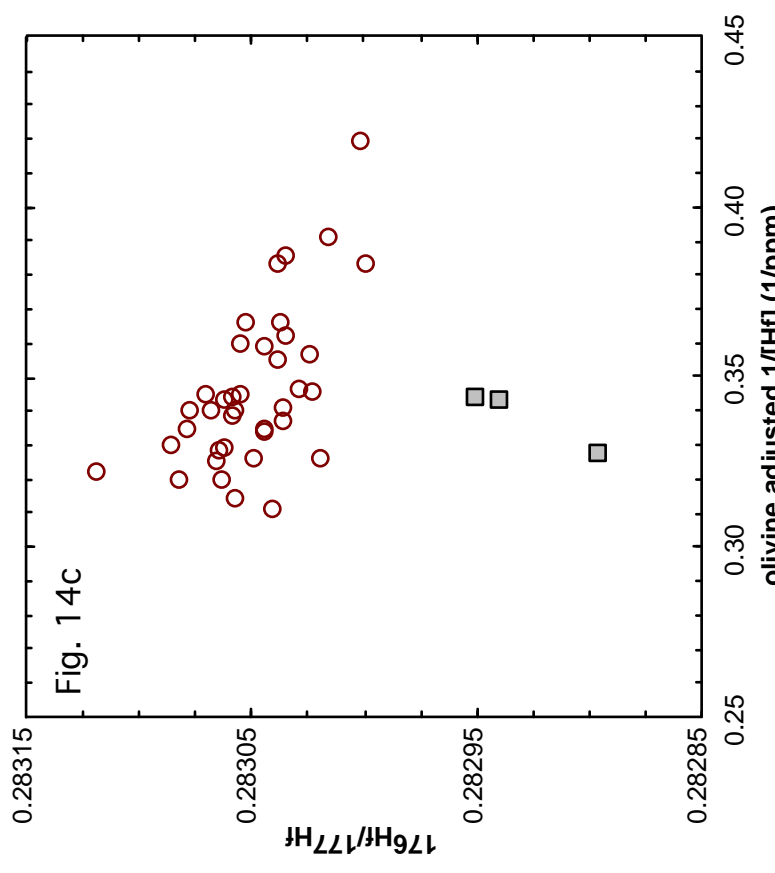
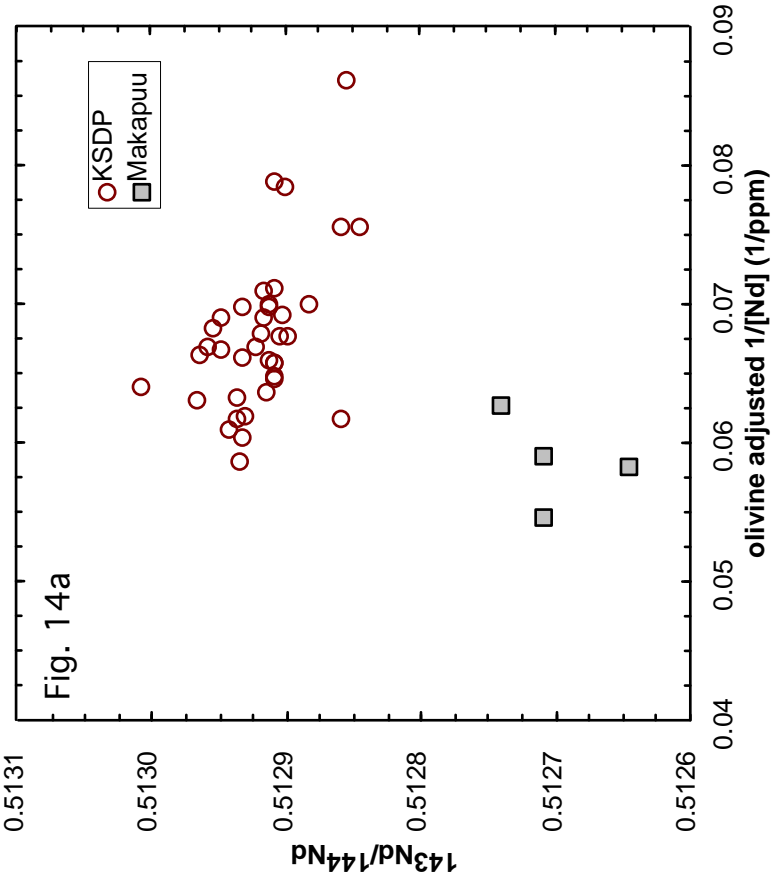


Fig. 15a

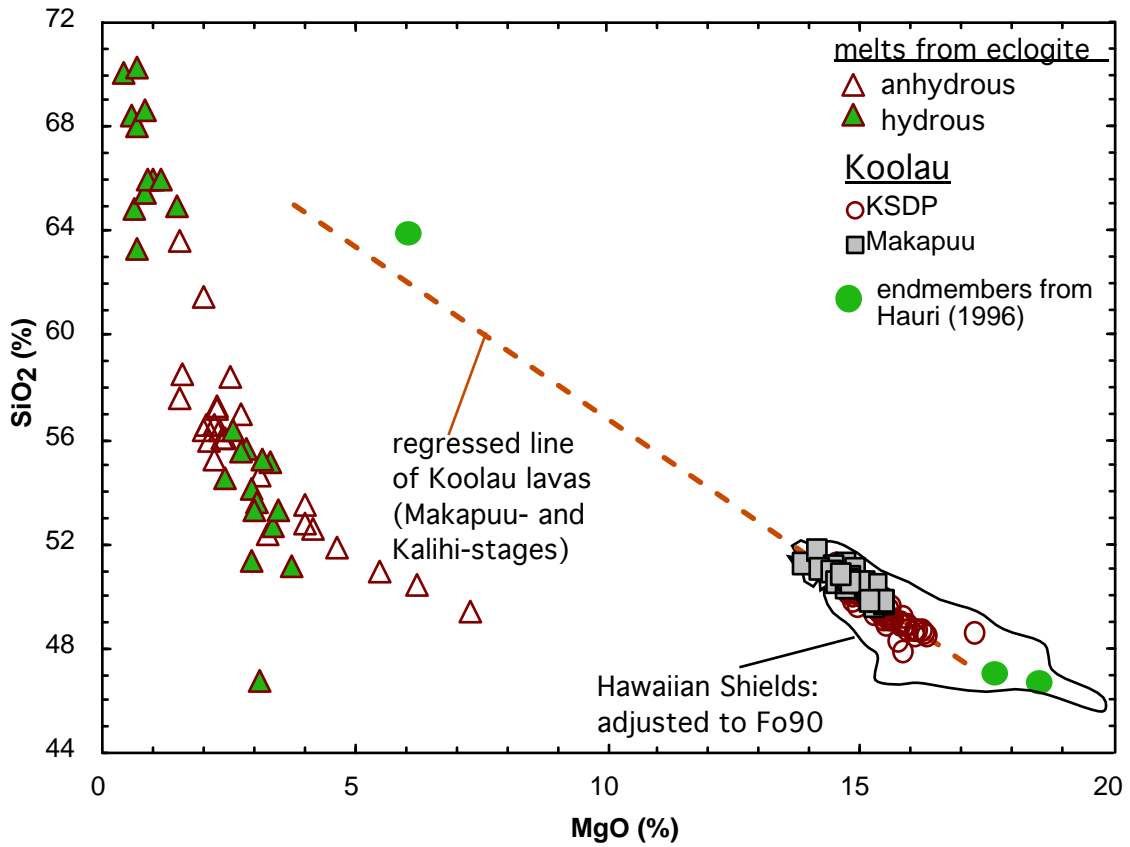


Fig. 15b

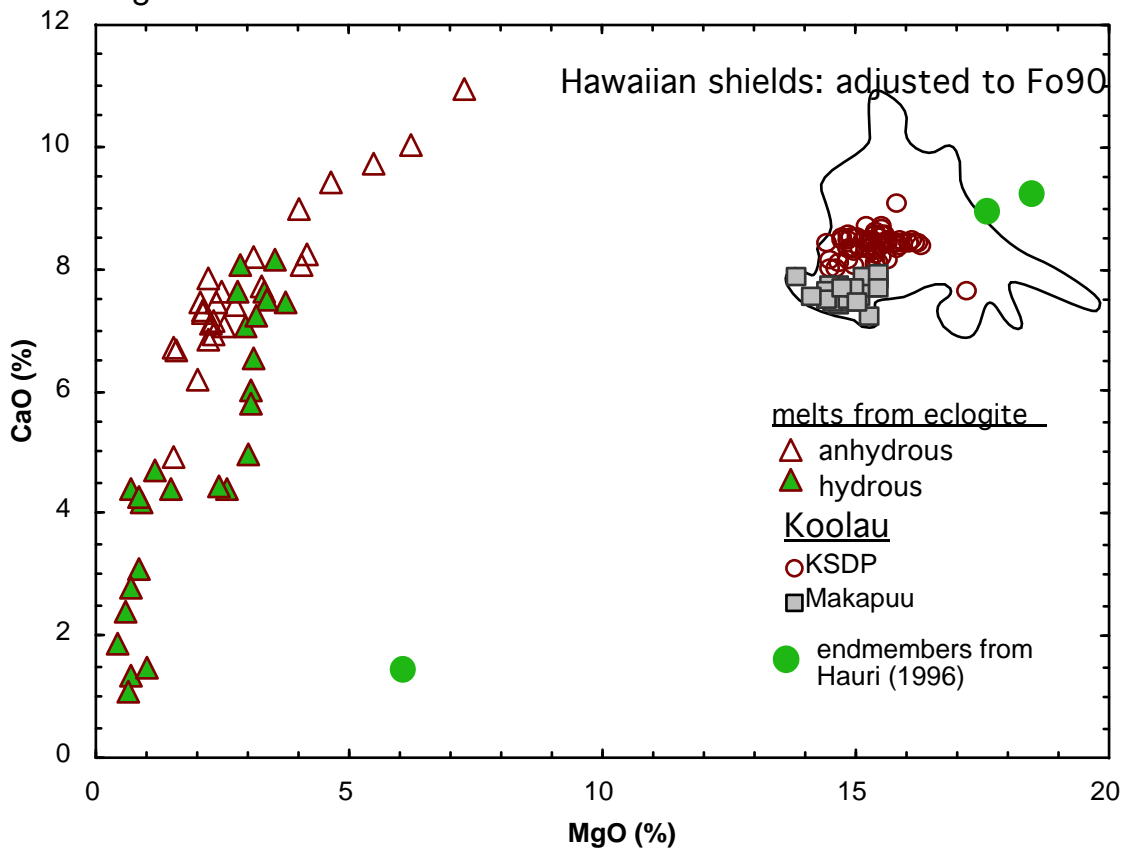


Fig. 16

